Calculation of lepton flavor violating SUSY processes at e^+e^- linear colliders

Diplomarbeit
von
Frank Deppisch

Institut für Theoretische Physik
der
Julius-Maximilians-Universität Würzburg

Oktober 2000

Contents

Chapter 1

Introduction

One of the most promising candidates for an extension of the Standard Model (SM) is the so called Minimal Supersymmetric Standard Model (MSSM). Supersymmetry (SUSY) predicts that each fermion must have a bosonic partner, which would create a plethora of new particles. Although exact supersymmetry predicts the masses of a particle and its SUSY partner to be equal, the masses must differ because the sparticles have not been discovered yet. This means that supersymmetry must be broken. In the MSSM the SUSY breaking is incorporated in the so-called soft-SUSY breaking terms. Supersymmetry breaking is sensitive to the physics beyond the MSSM. One possibility to unravel the origins of this SUSY breaking is the study of Lepton Flavor Violation (LFV) that is induced indirectly to the lepton sector through the effects of supersymmetric breaking in the slepton sector. Many studies have been done for LFV processes at low energies like the decays $\mu \to e\gamma$, $\tau \to \mu\gamma$ with virtual sleptons in loops. Such processes have been useful in establishing experimental bounds on the LFV in the slepton sector.

In this work, we choose an alternative way by studying slepton production at an e^+e^- linear collider. An upcoming e^+e^- linear colliders (Next Linear Collider, NLC) may provide a means to explore the theoretically estimated energy range where these supersymmetric particles can be found. The produced sleptons subsequently decay, producing leptons and neutralinos or charginos. If there is a mixing between the slepton flavors this violation of flavor is induced to the leptons also. The slepton mixing may be present in the left- and/or right-handed sector. Such a difference can be observed by using polarized e^+e^- beams. By choosing the proper polarization, one can significantly enhance the signal. To accomodate this fact we calculate the helicity amplitudes of our processes for general slepton production (charged sleptons and sneutrinos). For our numerical work we specifically choose $e-\tau$ mixing as an example, studying various distributions.

We introduce the slepton mixing (and thus the lepton flavor violation) in two ways. First, by introducing the LFV by hand in a minimal way generating a simple two-flavor mixing model, so we can change its strength and study the principal effects. The second way is to take a specific theoretical model beyond the MSSM that includes LFV. We use two such models. First, the supersymmetrized versions of the Standard Model with right-handed neutrinos and second a grand unified theory, SU(5) SUSY GUT with right-handed neutrinos. These two models will serve as examples for what kind of signals one can expect. We use the minimal Supergravity model as a general framework in the form of three benchmark scenarios [17, 18, 19].

Our main interest will be the signals itself. A detailed study of their background is beyond the scope of this work.

After this introduction, we will present the basic notions of the minimal supersymmetric Standard Model in chapter 2. In chapter 3 we show how Lepton Flavor Violation can be incorporated through the slepton sector. Chapter 4 contains the Feynman rules for Majorana particles and all vertices that are necessary for our calculations. The processes are presented in chapter 5, with the calculation of the amplitudes given in chapter 6 and that of the phase space in chapter 7. Chapter 8 contains the numerical results and their discussion. In chapter 9 we give a brief account of possible background processes for our signals. Chapter 10 closes this work with a summary.

Chapter 2

Supersymmetry

2.1 Why SUSY?

Although the Standard Model is very succesful in describing the presently known experimental phenomena in particle physics, it seems clear that it must be extended at higher energies. One reason for this is the so called "hierarchy problem" resulting from the fact that the ratio between the Planck scale $M_{Pl} \approx 10^{19}$ GeV where gravitational effects become important and the scale of electroweak symmetry breaking, $m_W \approx 10^2$ GeV is very huge: $\frac{M_{Pl}}{m_W} \approx 10^{17}$. This would have a large impact on the Higgs mass m_H because it receives huge quantum corrections from virtual effects of particles which couple to the Higgs, even indirectely. If we calculate such loop corrections, these will depend on the ultraviolet momentum cutoff Λ_{UV} which should be interpreted as the scale where new physics effects enter. If Λ_{UV} is of the order M_{Pl}, these corrections would be enormously larger than the favoured value $m_H \approx 100$ GeV. We could avoid such problems if there are cancellations between various contributions.

Such cancellations can occur systematically if there is some symmetry that relates the various types of particles in the loops to each other. In this case it can be shown that we need a symmmetry between bosons and fermions (for example there is relative minus sign between a one loop fermion and a one loop boson contribution). In fact, such cancellations are unavoidable once we assume that a symmetry that relates bosons and fermions exists. Such a symmetry is called a supersymmetry (SUSY).

In the simplest but phenomenological viable supersymmetric model there exists one supersymmetry generator that turns a bosonic state into a fermionic state, and vice versa. Because it is not possible to relate known Standard Model particles to each other, each known particle must therefore have a superpartner (a sparticle) with the two spins differing by 1/2. The two particles form a so called supermultiplet. To be more exact, in the Minimal Supersymmetric Standard Model (MSSM) there are two types of supermultiplets: A chiral supermultiplet contains a Weyl fermion and a complex scalar. A gauge supermultiplet contains a massless (before symmetry breaking) spin-1 gauge boson and a massless spin-1/2 Weyl fermion (called a gaugino). In both cases the numbers of bosonic and fermionic degrees of freedom are equal.

Exact supersymmetry predicts the masses of a particle and its superpartner to be equal. The sparticles would have already been discovered, therefore supersymmetry must be broken. If supersymmetry is to provide a solution to the hierarchy problem we must introduce a "soft" supersymmetry breaking (SSB) Lagrangian

$$\mathcal{L} = \mathcal{L}_{SUSY} + \mathcal{L}_{SSB}, \tag{2.1}$$

with a supersymmetry breaking scale m_{SSB} ($\approx$ the largest mass scale in $\mathcal{L}_{SSB}$) not larger than about 1 TeV. This is the reason why many theorists expect supersymmetry to be discoverd at the upcoming LHC or a NLC.

2.2 The Minimal Supersymmetric Standard Model

The MSSM is obtained by supersymmetrizing the Standard Model and adding soft-SUSY-breaking terms. The supersymmetric part is almost completely fixed by the underlying Standard Model. The only exception is that we need two Higgs doublets $H_1 = (H_1^0, H_1^-)$, $H_2 = (H_2^+, H_2^0)$ in order to create an anomaly-free model and to give masses to all quarks and charged leptons. The complete particle content of the MSSM is shown in Table 2.1. A feature of the MSSM is that it conserves $(B - L)$, with B the Baryon-number and L the Lepton-number (in principle there could be supersymmetric interactions that violate B or L). This can be seen as a consequence that the MSSM is defined to conserve a discrete, multiplicative quantum number called R-parity (s: spin),

$$R = (-1)^{3(B-L)+2s}. \tag{2.2}$$

The usual Standard Model particles have even R-parity, $R = +1$ while their superpartners have odd R-parity, $R = -1$. A conservation of R-parity has very important consequences:

- The lightest sparticle with $R = -1$ (LSP) is stable
- Sparticles can only be produced in even numbers

Particles	Sparticles		
	gauge eigenstate		mass eigenstate
l_α	$\tilde{l}_{\alpha_L}, \tilde{l}_{\alpha_R}$	Ch. sleptons	$\tilde{l}_i$, $i = 1, ..., 6$
ν_α	$\tilde{\nu}_\alpha$	Sneutrinos	$\tilde{\nu}_i$, $i = 1, ..., 3$
q	$\tilde{q}_L, \tilde{q}_R$	Squarks	$\tilde{q}_i$, $i = 1, ..., 6$
B^0	$\tilde{B}^0$	Bino	$\tilde{\chi}^0_a$, $a = 1, ..., 4$
W^0	$\tilde{W}^0$	Wino	Neutralinos
H^0_1	$\tilde{H}^0_1$	Higgsino	
H^0_2	$\tilde{H}^0_2$	Higgsino	
$W^\pm$	$\tilde{W}^\pm$	Wino	$\tilde{\chi}^\pm_a$, $a = 1, 2$
H^+_1	$\tilde{H}^+_1$	Higgsino	Charginos
H^-_2	$\tilde{H}^-_2$	Higgsino	
g	$\tilde{g}$	Gluino	$\tilde{g}$

Table 2.1: Particle content of the MSSM, α is a generational index, e.g. $l_1 = e, l_2 = \mu, l_3 = \tau$, q represents the quarks, $q = u, d, s, c, d, b$

- Each sparticle other than the lightest supersymmetric particle (LSP) must finally decay into a state with an odd number of LSPs

In the scenarios we studied, the LSP is always the lightest neutralino $\tilde{\chi}^0_1$. Because it is electrically and color neutral it is a good candidate for dark matter in astrophysics.

The problem of the MSSM is that it has more than hundred free parameters. One of these is the SUSY-Higgs mass parameter μ which is the supersymmetric version of the Higgs boson mass in the Standard Model. In the superpotential the appropriate term is written as $\mu H_2 H_1$, where H_1, H_2 are the superfields of the two Higgs doublets. In the usual language, μ appears in (omitting squark interactions) [12]

$$\begin{aligned}\mathcal{L} \supset\ & -\mu(\tilde{H}^+_2 \tilde{H}^-_1 - \tilde{H}^0_2 \tilde{H}^0_1) + c.c. \\ & -|\mu|^2(|H^0_1|^2 + |H^-_1|^2 + |H^0_2|^2 + |H^+_2|^2) \\ & +\mu^*(\tilde{l}^\dagger_R y \tilde{l}_L H^0_2 + \tilde{l}^\dagger_R y \tilde{\nu} H^{+*}_2) + c.c., \end{aligned} \tag{2.3}$$

so μ provides higgsino mass terms, higgs boson (mass)^2 terms and (scalar)^3 couplings, with the lepton 3×3 Yukawa coupling matrix y, the left-, right-handed charged sleptons and sneutrinos, $\tilde{l}_L, \tilde{l}^\dagger_R, \tilde{\nu}$ which are all 3-vectors in flavor space. The rest of the MSSM parameters is introduced by the arbitrariness of the supersymmetry breaking. The soft-supersymmetry-breaking contribution to the Lagrangian (omitting squarks and gluinos) is given by [12]:

$$
\begin{aligned}
\mathcal{L}_{SSB} &= -\frac{1}{2}(M_2\tilde{W}^{\pm}\tilde{W}^{\pm} + M_1\tilde{B}^0\tilde{B}^0) + c.c. \\
&\quad -\tilde{l}_L^{\dagger} m_{\tilde{L}}^2 \tilde{l}_L - \tilde{\bar{l}}_R m_{\tilde{R}}^2 \tilde{\bar{l}}_R^{\dagger} \\
&\quad -\tilde{\bar{l}}_R A \tilde{l}_L H_1 + c.c \\
&\quad -m_{H_1}^2 H_1^{\dagger} H_1 - m_{H_2}^2 H_2^{\dagger} H_2 - (bH_1H_2 + c.c.)
\end{aligned}
\tag{2.4}
$$

M_2 and M_1 are the wino and bino masses, respectively (the adjoint representation gauge indices of the wino fields are omitted). The second line consists of the soft-SUSY breaking contributions to the slepton masses, with the $m_{\tilde{L}}^2, m_{\tilde{R}}^2$ being 3×3 hermitian matrices in family space ($\tilde{l}_L$ and $\tilde{l}_R$ are 3-vectors in family space). The third line contains (scalar)^3 couplings, A being a 3×3 complex matrix. In the last line, we have higgs mass terms, $m_{H_1}^2$ and $m_{H_2}^2$, and the SSB higgs mixing parameter b.

All the matrices and parameters are completely arbitrary (apart from formal constraints like hermiticity on the matrices) within the MSSM. If for example the entries of $m_{\tilde{L}}^2$ are all of comparable size, the induced lepton flavor and CP violation would be disastrously large, so we need some theoretical framework that helps to create a phenomenologically viable model.

2.3 The minimal SUperGRAvity model

One way to calculate the SSB-parameters is to use the mSUGRA framework. Here one assumes that SUSY is broken spontaneously in a hidden particle-sector. Gravitational interactions then automatically mediate SUSY breaking to the visible sector, i.e. to the particles of the MSSM. In the minimal SUGRA framework, the SSB parameters take a particularly simple form, in which the scalar squared masses are flavor diagonal and universal, and the trilinear $A-$couplings are proportional to the corresponding SUSY-couplings (the Yukawa couplings y) at the gravitational scale M_{Pl}:

$$
\begin{aligned}
m_{\tilde{R}}^2 = m_{\tilde{L}}^2 &= m_0^2 \mathbf{1} \\
m_{H_1}^2 = m_{H_2}^2 &= m_0^2 \\
A &= A_0 y,
\end{aligned}
\tag{2.5}
$$

with the common scalar mass m_0 and the common trilinear coupling constant A_0. In practice, one uses the gauge coupling unification scale M_{GUT} as the scale at which the parameters unify, because little is known about physics between M_{Pl} and M_{GUT}.

In addition, the gauge couplings and gaugino mass parameters are assumed to be unified at M_{GUT}. This implies

$$M_1 = M_2 = m_{1/2}, \tag{2.6}$$

with the common gaugino mass $m_{1/2}$. In addition all parameters are chosen to be real, thus avoiding CP violation. The entire spectrum of the model can thus be described by a small number of parameters. The universality at M_{GUT} evades large lepton flavor mixing (but, hopefully, not too small), the subject of our study, and CP-violation. This model also succesfully predicts radiative electroweak gauge symmetry breaking. By requiring that it is compatible to the observed $SU(2) \times U(1) \to U(1)_{EM}$ symmetry breaking, we can trade two free parameters, the absolute value of the SUSY-Higgs mixing parameter $|\mu|$ and the SSB-Higgs mixing parameter b, for the ratio of the Higgs vacuum expectation values, $\tan\beta$,

$$\tan\beta = \frac{\langle H_2^0\rangle}{\langle H_1^0\rangle}, \langle H_2^0\rangle = v\sin\beta, \langle H_1^0\rangle = v\cos\beta, \tag{2.7}$$

$$v^2 = \langle H_2^0\rangle^2 + \langle H_1^0\rangle^2 = \frac{2m_Z^2}{g^2+g'^2}. \tag{2.8}$$

This does not determine the sign of μ. The mSUGRA model then has four continous and one discrete free parameter (in addition to the Standard Model parameters):

$$m_0, m_{1/2}, A_0, \tan\beta, \mathrm{sign}(\mu)$$

For our numerical work, we use three mSUGRA benchmark scenarios, [17, 18, 19] with the input parameters given in Table 8.1. These parameters should be viewed as the initial conditions at the unification scale for the MSSM renormalization group equations, which govern the energy-scale dependence of all the MSSM parameters. The RGEs of the MSSM (see for example [12]) do not radiatively induce lepton flavor mixing, so we need extensions of the MSSM that include such behaviour.

2.4 Sparticle mixings

2.4.1 Neutralinos

The higgsinos and electroweak gauginos of the MSSM mix with each other because of the effects of electroweak symmetry breaking. The neutral higgsinos $(\tilde{H}_1^0, \tilde{H}_2^0)$ and the neutral gauginos $(\tilde{B}, \tilde{W}^0)$ combine to form four neutral mass eigenstates called neutralinos.

In the gauge-eigenstate basis $\psi^0 = (\tilde{B}, \tilde{W}^0, \tilde{H}_1^0, \tilde{H}_2^0)^T$, the neutralino mass term has the form

$$\mathcal{L} = -\frac{1}{2}(\psi^0)^T Y \psi^0 + c.c. \tag{2.9}$$

where the neutralino mass matrix is given by [14]

$$Y = \begin{pmatrix} M_1 & 0 & -m_Z s_W c_\beta & m_Z s_W s_\beta \\ 0 & M_2 & m_Z c_W c_\beta & -m_Z c_W s_\beta \\ -m_Z s_W c_\beta & m_Z c_W c_\beta & 0 & -\mu \\ m_Z s_W s_\beta & -m_Z c_W s_\beta & -\mu & 0 \end{pmatrix}. \tag{2.10}$$

The M_1, M_2 entries are from the SSB Lagrangian (2.4), the μ terms come directly from the SUSY Lagrangian (2.3) and the terms proportional to m_Z are from Higgs-higgsino-gaugino couplings once the higgs scalars get vacuum expectation values. The mass-eigenstates are given by

$$\chi_i^0 = N_{ij}\psi_j^0, \qquad i, j = 1, \ldots, 4, \tag{2.11}$$

where N is a unitary matrix satisfying:

$$N^* Y N^{-1} = \mathrm{diag}(m_{\tilde{\chi}_1^0}, m_{\tilde{\chi}_2^0}, m_{\tilde{\chi}_3^0}, m_{\tilde{\chi}_4^0}), \tag{2.12}$$

One can choose N such that the eigenvalues are real and non-negative [14]. By convention, these are labelled with ascending mass value: $m_{\tilde{\chi}_1^0} < m_{\tilde{\chi}_2^0} < m_{\tilde{\chi}_3^0} < m_{\tilde{\chi}_4^0}$. The easiest way to determine N is to take the absolute square of (2.12):

$$\begin{aligned} \mathrm{diag}(m^2_{\tilde{\chi}_1^0}, \ldots) &= N^* Y N^{-1} N Y^* (N^{-1})^* \\ &= N(Y^* Y) N^{-1}, \end{aligned} \tag{2.13}$$

which is just the standard diagonalization of $Y^* Y$. The proper Majorana spinors for the neutralinos are

$$\tilde{\chi}_i^0 = \begin{pmatrix} \chi_i^0 \\ \bar{\chi}_i^0 \end{pmatrix} \tag{2.14}$$

2.4.2 Charginos

Like the neutral higgsinos and gauginos, the charged higgsinos $(\tilde{H}_2^+, \tilde{H}_1^-)$ and winos $(\tilde{W}^+, \tilde{W}^-)$ mix to form two mass eigenstates with charge ±1 called charginos. In the gauge eigenstate basis $\psi = (\tilde{W}^+, \tilde{H}_2^+, \tilde{W}^-, \tilde{H}_1^-)^T$ the chargino mass term has the form

$$\mathcal{L} = -\frac{1}{2}(\psi)^T C \psi^+ + c.c., \tag{2.15}$$

with the mass matrix in 2×2 block form [14]

$$C = \begin{pmatrix} 0 & X^T \\ X & 0 \end{pmatrix}; \quad X = \begin{pmatrix} M_2 & \sqrt{2} m_W s_\beta \\ \sqrt{2} m_W c_\beta & \mu \end{pmatrix}, \tag{2.16}$$

with eqivalent sources in the Lagrangian as in the neutralino case. The mass eigenstates are related to the gauge eigenstates by two different, unitary 2×2 matrices O_1 and O_2:

$$\begin{pmatrix} \chi_1^+ \\ \chi_2^+ \end{pmatrix} = O_2 \begin{pmatrix} \tilde{W}^+ \\ \tilde{H}_2^+ \end{pmatrix}; \quad \begin{pmatrix} \chi_1^- \\ \chi_2^- \end{pmatrix} = O_1 \begin{pmatrix} \tilde{W}^- \\ \tilde{H}_1^- \end{pmatrix} \tag{2.17}$$

These matrices are to be chosen such that (mass labels again in ascending order)

$$O_1{}^* X O_2{}^{-1} = \mathrm{diag}(m_{\tilde{\chi}_1^\pm}, m_{\tilde{\chi}_2^\pm}), \quad m_{\tilde{\chi}_1^\pm} < m_{\tilde{\chi}_2^\pm} \tag{2.18}$$

Again, the matrices O_1 and O_2 can be chosen that the mass eigenvalues are real and non-negative. The Dirac spinors of the charginos are built from the particle-aniparticle two-component spinors,

$$\tilde{\chi}_i^+ = \begin{pmatrix} \chi_i^+ \\ \bar{\chi}_i^- \end{pmatrix}. \tag{2.19}$$

2.4.3 Charged Sleptons

In principle, any scalars with the same electric charge, R-parity and color quantum numbers can mix with each other. This means that the mass eigenstates of the sleptons should be obtained by diagonalizing a 6×6 matrix for the charged sleptons $(\tilde{l}_{\alpha_L}, \tilde{l}_{\alpha_R})$=$(\tilde{e}_L, \tilde{\mu}_L, \tilde{\tau}_L, \tilde{e}_R, \tilde{\mu}_R, \tilde{\tau}_R)$ and a 3×3 matrix for the sneutrinos $\tilde{\nu}_\alpha$=$(\tilde{\nu}_e, \tilde{\nu}_\mu, \tilde{\nu}_\tau)_L$.

The charged slepton (mass)^2 matrix has the following form (in the above gauge eigenstate basis) [13]

$$M^2 = \begin{pmatrix} m_L^2 & (m_{LR}^2)^T \\ m_{LR}^2 & m_R^2 \end{pmatrix} \tag{2.20}$$

where m_L^2, m_R^2 are 3×3 hermitian matrices and m_{LR}^2 is a 3×3 matrix. The elements are given by

$$
\begin{aligned}
(m_L^2)_{ij} &= (m_{\tilde{L}}^2)_{ij} + \delta_{ij}(m_{l_i}^2 + m_Z^2\cos(2\beta)(-\frac{1}{2} + \sin^2\theta_W)) && (2.21)\\
(m_R^2)_{ij} &= (m_{\tilde{R}}^2)_{ij} + \delta_{ij}(m_{l_i}^2 - m_Z^2\cos(2\beta)\sin^2\theta_W) && (2.22)\\
(m_{LR}^2)_{ij} &= A_{ij} v\cos\beta - \delta_{ij} m_i \mu \tan\beta. && (2.23)
\end{aligned}
$$

The contributions $m_{\tilde{L}}^2, m_{\tilde{R}}^2$ are the mass terms from the SSB lagragian (2.4), while the lepton masses m_{l_i} are just the SUSY prediction, $m_{\tilde{l}_i} = m_{l_i}$. The terms proportional to m_Z^2 originate from so called D-terms generally given by

$$\Delta_\Phi = m_Z^2(T_{3_\Phi} - Q_{EM_\Phi}\sin^2\theta_W)\cos 2\beta, \qquad (2.24)$$

with T_{3_Φ} and Q_{EM_Φ} the third component of the weak isospin and the electric charge of the supermultiplet to which the relevant particle belongs (for the right-handed sector this is the anti-supermultiplet, $Q_{EM_{\bar{l}}} = +1$). They arise from (slepton)^2(higgs)^2 quartic interactions once the higgses get vacuum expectation values. Such higgs VEVs are also the source of the left-right mixing terms in m_{LR}^2: $Av\cos\beta$ arises from soft (scalar)^3 couplings in (2.4) while the term proportional to μ comes from (2.3).

The parameters are subject to RGE running and must be calculated by the renormalization group equations of the relevant models once the mSUGRA limit is applied. In general the mass matrix is not diagonal. It is diagonalized by a 6×6 orthogonal matrix U,

$$UM^2U^T = \mathrm{diag}(m_{\tilde{l}_1}^2, ..., m_{\tilde{l}_j}^2, ..., m_{\tilde{l}_6}^2), \qquad (2.25)$$

with the charged slepton eigenmasses $m_{\tilde{l}_j}^2, j = 1, ..., 6$. The slepton mass-eigenstates are expressed in terms of the gauge eigenstates by

$$\tilde{l}_j = U_{j\alpha}\tilde{l}_{\alpha_L} + U_{j\alpha+3}\tilde{l}_{\alpha_R}. \qquad (2.26)$$

2.4.4 Sneutrinos

The sneutrino (mass)^2 matrix in the gauge eigenstate basis $\tilde{\nu}_\alpha=(\tilde{\nu}_e, \tilde{\nu}_\mu, \tilde{\nu}_\tau)_L$ is given by

$$(m_{\tilde{\nu}}^2)_{ij} = (m_{\tilde{L}}^2)_{ij} + \frac{1}{2}\delta_{ij} m_Z^2\cos 2\beta; \quad i,j = 1,2,3. \qquad (2.27)$$

The two contributions are analogous to the charged slepton case (we explicitly neglect the neutrino masses). The mass matrix is diagonalized by an orthogonal 3×3 matrix U^ν:

$$U^\nu m_{\tilde{\nu}}^2 (U^\nu)^T = \mathrm{diag}(m_{\tilde{\nu}_1}^2, m_{\tilde{\nu}_2}^2, m_{\tilde{\nu}_3}^2) \qquad (2.28)$$

The mass eigenstates $\tilde{\nu}_i$ are related to the gauge eigenstates by

$$\begin{pmatrix} \tilde{\nu}_1 \\ \tilde{\nu}_2 \\ \tilde{\nu}_3 \end{pmatrix} = U^{\nu} \begin{pmatrix} \tilde{\nu}_e \\ \tilde{\nu}_\mu \\ \tilde{\nu}_\tau \end{pmatrix} . \tag{2.29}$$

In the course of this work we consider extensions of the MSSM (chapter 3) with right handed sneutrinos as partners to right handed neutrinos which are introduced via a Majorana mass term. In principle such a Majorana term induces left-right sneutrino mixing and also sneutrino-antisneutrino mixing [10], so we would have a nontrivial 12×12 sneutrino mass matrix. The size of these mixings is proportional to the inverse of the Majorana mass scale M and can be neglected if M is large, just like the right-handed sneutrinos which are extremely heavy in this limit.

Chapter 3

Lepton flavor violation

Up to now, the MSSM does not contain LFV due to the mSUGRA framework in combination with the flavor-diagonal RGEs of the MSSM. We introduce LFV in two ways, first by manually changing the sneutrino mass matrix (i.e. making it non-diagonal), and secondly by using theoretical extensions of the MSSM whose RGEs radiatively induce LFV in the slepton sector.

3.1 Minimal LFV for sneutrinos

In this model, we introduce $\tilde{\nu}_e - \tilde{\nu}_\tau$ mixing by choosing the following mass matrix for the sneutrinos extending the mSUGRA,

$$m_{\tilde{\nu}}^2 = \begin{pmatrix} M_1^2 & 0 & \delta a^2 \\ 0 & M_1^2 & 0 \\ \delta a^2 & 0 & (M_3 + \delta M)^2 \end{pmatrix}, \tag{3.1}$$

where M_1^2, M_3^2 are the values of the lepton flavor conserving mSUGRA, in which case the mass matrix is always diagonal and degenerate in the first two generations. δa^2 and δM are small additional parameters that describe the lepton flavor violation between $\tilde{\nu}_e - \tilde{\nu}_\tau$. The diagonalization of the $\tilde{\nu}_e - \tilde{\nu}_\tau$ submatrix is given by ($c_\phi = \cos\phi$, $s_\phi = \sin\phi$)

$$\mathrm{diag}(m_{\tilde{\nu}_e}^2, (m_{\tilde{\nu}_\tau} + \delta m)^2) = \begin{pmatrix} c_\phi & -s_\phi \\ s_\phi & c_\phi \end{pmatrix} \begin{pmatrix} M_1^2 & \delta a^2 \\ \delta a^2 & (M_3 + \delta M)^2 \end{pmatrix} \begin{pmatrix} c_\phi & -s_\phi \\ s_\phi & c_\phi \end{pmatrix}^T. \tag{3.2}$$

$m_{\tilde{\nu}_e}$ and $m_{\tilde{\nu}_\tau}$ are the masses of the electron-sneutrino and tau-sneutrino in the lepton flavor conserving mSUGRA. The mixing can equally be described by the parameters ϕ and δm. The sneutrino mixing matrix is given by

$$U^\nu = \begin{pmatrix} \cos\phi & 0 & -\sin\phi \\ 0 & 1 & 0 \\ \sin\phi & 0 & \cos\phi \end{pmatrix}. \tag{3.3}$$

The lepton flavor conserving case is recovered in the limit $\phi \to 0, \delta m \to 0$. This model serves as a playground for the study of lepton flavor violation. It is minimal in the sense that it only describes a two-flavor mixing.

3.2 MSSM with right-handed neutrinos

One model that induces non-diagonal mass terms is the supersymmetrized version of the Standard Model+right-handed neutrinos that is also used to produce nonvanishing neutrino-masses and -mixings (exactly this feature will induce the slepton flavor mixing). In this model, the neutrino mass term is given by [10]

$$-\left(\overline{\nu_L}, \overline{\nu_R^C}\right) \begin{pmatrix} 0 & m_\nu^{D^T} \\ m_\nu^D & M \end{pmatrix} \begin{pmatrix} \nu_L \\ \nu_R \end{pmatrix}, \tag{3.4}$$

where ν_L, ν_R are vectors and m_ν^D, M are matrices in flavor space. Small neutrino mass differences (as indicated by the various neutrino oscillation experiments) can be obtained naturally by the see-saw mechanism: If the Majorana mass term M is much larger than the neutrino Dirac term m_ν^D, the light-neutrino mass matrix (i.e. of the left-handed neutrinos) is given by, [11]

$$\begin{aligned} m_\nu &= m_\nu^{D^T} M^{-1} m_\nu^D & (3.5) \\ &\equiv V \mathrm{diag}(m_{\nu_e}, m_{\nu_\mu}, m_{\nu_\tau}) V^T, & (3.6) \end{aligned}$$

with the light-neutrino mixing matrix V and the neutrino eigenmasses m_{ν_e}, m_{ν_μ}, m_{ν_τ}. We make the simplifying assumption of a diagonal Majorana mass matrix, $M_{ij} = M_i \delta_{ij}$. In this case the only diagonalization matrix needed is the above light-neutrino mixing matrix, and the neutrino eigenmasses can be written in terms of the Majorana masses M_i and the neutrino Yukawa couplings y_i^ν as

$$m_{\nu_i} = \frac{(y_i^\nu v \sin\beta)^2}{M_i}. \tag{3.7}$$

Now we are in a position to calculate the renormalization group equations for the SSB parameters $m_{\tilde{L}}^2, m_{\tilde{R}}^2$ and A that are needed to calculate the slepton mass matrices. We obtain the one-loop corrections in the leading-logarithm approximation going from the scale M_{GUT} (imposing the mSUGRA universality) down to Majorana mass scale(s) M_k, [11]:

$$
\begin{aligned}
(\delta m^2_{\tilde{L}})_{ij} &= -\frac{1}{8\pi^2}(3m_0^2 + A_0^2)V^*_{ik}(y^\nu_k)^2 V_{jk} \ln\left(\frac{M_{GUT}}{M_k}\right) && (3.8)\\
(\delta m^2_{\tilde{R}})_{ij} &= 0 && (3.9)\\
(\delta A)_{ij} &= -\frac{3A_0}{8\pi^2} y^E_i V^*_{ik}(y^\nu_k)^2 V_{jk} \ln\left(\frac{M_{GUT}}{M_k}\right), && (3.10)
\end{aligned}
$$

with the charged lepton Yukawa couplings $y^E_i = m_{l_i}/(v\cos\beta)$ and the neutrino Yukawa couplings $y^\nu_i = \sqrt{m_{\nu_i} M_i}/(v\sin\beta)$. These are only the contributions due to the addition of right-handed neutrinos, originating from loops with virtual left-handed neutrinos. In order to get the full correction, we also add the usual MSSM-contributions:

$$
\begin{aligned}
(m^2_{\tilde{L}})_{ij} &= m_0^2\delta_{ij} + (\delta m^2_{\tilde{L}})^{MSSM}_{ij} + (\delta m^2_{\tilde{L}})_{ij} && (3.11)\\
(m^2_{\tilde{R}})_{ij} &= m_0^2\delta_{ij} + (\delta m^2_{\tilde{R}})^{MSSM}_{ij} + (\delta m^2_{\tilde{R}})_{ij} && (3.12)\\
(A)_{ij} &= A_0\delta_{ij} + (\delta A)^{MSSM}_{ij} + (\delta A)_{ij} && (3.13)
\end{aligned}
$$

The $(\delta X)^{MSSM}$ are calculated using the MSSM RGEs. This is an approximation because the RGEs of a model should be solved as a whole, but in our case we can use the superior RGE solutions for the MSSM given in [17, 18, 19] (higher loop contributions). The model presented here is an example where LFV is induced to the left-handed sector only. We will refer to this model as ν_RX, where X denotes the mSUGRA scenario.

The neutrino mixing matrix V and the neutrino mass eigenvalues can be obtained from the neutrino oscillation experiments [24]. The atmospheric neutrino data can be explained by $\nu_\mu - \nu_\tau$ oscillation with the following mass squared difference and mixing angle:

$$\Delta m^2_{23} = (10^{-3} - 10^{-2})\ \mathrm{eV}^2, \quad \sin^2\theta_{23} > 0.8, \qquad (3.14)$$

while the solar neutrino data can be explained by $\nu_e - \nu_\mu$ oscillation in the so called LargeMSW parameter range:

$$\Delta m^2_{12} = (8\times 10^{-6} - 3\times 10^{-4})\ \mathrm{eV}^2, \quad \sin^2\theta_{12} > 0.5 \qquad (3.15)$$

We choose the following parametrization for V ($s_i = \sin\theta_i, c_i = \cos\theta_i$):

$$V = \begin{pmatrix} c_2 c_3 & c_2 s_3 & s_2 \\ -c_1 s_3 - s_1 s_2 c_3 & c_1 c_3 - s_1 s_2 s_3 & s_1 c_2 \\ s_1 s_3 - c_1 s_2 c_3 & -s_1 c_3 - c_1 s_2 s_3 & c_1 c_2 \end{pmatrix}, \qquad (3.16)$$

with the mixing angles

$$\theta_1 = \pi/4, \quad \theta_2 = 0.05, \quad \theta_3 = \pi/4. \tag{3.17}$$

For the neutrino masses, we choose (the absolute mass values are not fixed by the oscillation experiments, only the mass differences)

$$m_{\nu_e} = 0, \quad m_{\nu_\mu} = 0.003 \text{ eV}, \quad m_{\nu_\tau} = 0.07 \text{ eV}, \tag{3.18}$$

and for the Majorana mass parameters we assume

$$M_1 = M_2 = M_3 = 10^{14} \text{ GeV}. \tag{3.19}$$

3.3 SU(5) SUSY GUT with right-handed neutrinos

Next, we consider a Grand Unified Theory, putting quarks U_i, D_i (i: color label), right-handed charged leptons E^c and right-handed neutrinos N^c (written as superfields, combining particle and sparticle) in representations of the gauge group $SU(5)$ (flavor indices are suppressed):

$$\mathbf{10} \;:\; (\psi)_{\alpha\beta} = \frac{1}{\sqrt{2}} \begin{pmatrix} 0 & U_3^c & -U_2^c & U_1 & D_1 \\ -U_3^c & 0 & U_1^c & U_2 & D_2 \\ U_2^c & -U_1^c & 0 & U_3 & D_3 \\ -U_1 & -U_2 & -U_3 & 0 & E^c \\ -D_1 & -D_2 & -D_3 & -E^c & 0 \end{pmatrix} \tag{3.20}$$

$$\mathbf{5}^* \;:\; \phi^\alpha = \begin{pmatrix} D_1^c & D_2^c & D_3^c & E & -N \end{pmatrix} \tag{3.21}$$

$$\mathbf{1} \;:\; \bar{N} \tag{3.22}$$

In this model, the "beyond MSSM"-corrections (leading-log, one-loop) are [11]

$$(\delta m^2_{\tilde{L}})_{ij} = -\frac{1}{8\pi^2}(3m_0^2 + A_0^2) V^*_{ik} (y^\nu_k)^2 V_{jk} \ln\left(\frac{M_{Pl}}{M_k}\right) \tag{3.23}$$

$$(\delta m^2_{\tilde{R}})_{ij} = -\frac{3}{8\pi^2}(3m_0^2 + A_0^2) V^{KM}_{3i} (y^U_3)^2 V^{KM*}_{3j} \ln\left(\frac{M_{Pl}}{M_{GUT}}\right) \tag{3.24}$$

$$(\delta A)_{ij} = -\frac{3A_0}{8\pi^2}\left(y^E_i V^*_{ik} (y^\nu_k)^2 V_{jk} \ln\left(\frac{M_{Pl}}{M_k}\right) + 3 y^E_j V^{KM}_{3i} (y^U_3)^2 V^{KM*}_{3j} \ln\left(\frac{M_{Pl}}{M_{GUT}}\right)\right), \tag{3.25}$$

where V^{KM} is the Kobayashi-Maskawa matrix and the top-quark Yukawa coupling, $y_3^U = m_t/(v \sin\beta)$ (all other up-quark Yukawa couplings are neglected). Here we actually start the RGEs from the Plank scale downwards because now we know the behaviour between M_{GUT} and M_{Pl}, which is described by the GUT model. In this model, the lepton-flavor violation is induced to both the left- and right-handed sector. We will refer to it as SU(5)ν_RX.

Chapter 4

Feynman rules

4.1 Majorana particles

The charged slepton production can occur through the t-channel exchange of neutralinos (see next chapter), which are totally uncharged spin-1/2 particles. The rules for such Majorana particles are taken from [20]. They are listed here only for reference purposes. In fact, applying these rules to our process we will see that the neutralinos can technically be treated as normal Dirac particles.

External lines All external fermions are denoted by a solid line with an arrow. For Dirac fermions, the direction of the arrow is set by convention and indicates the flow of some quantum number (e.g. the charge). For Majorana fermions, the direction of the arrow is arbitrary (they do not carry a conserved additive quantum number). The particular choice of the direction dictates which Feyman rules are used, for example what sort of propagator or vertex.

Corresponding to each external fermion line, one attaches a u or v spinor. For Majorana fermions this appears ambigous as there is no distinction between particle and antiparticle. One can choose an arbitrary direction for the arrow on a given Majorana line. For simplicity, we adopt the usual correspondence between the arrows and the u, v-spinors for Dirac particles. In general, the u and v spinors for either Dirac or Majorana fermions are related via

$$u(p,s) = C\bar{v}^T(p,s), \quad v(p,s) = C\bar{u}^T(p,s) \tag{4.1}$$

where C is the charge conjugation matrix satisfying $C^\dagger = C^{-1}, C^T = -C$.

Internal lines For internal Majorana fermion lines (i.e. propagators) there are three possibilities of arranging the arrows:

- $\beta \to\to \alpha$ $\left(i\frac{\not{p}+M}{p^2-M^2+i\epsilon}\right)_{\alpha\beta}$
- $\beta \to\leftarrow \alpha$ $\left(i\frac{C^{-1}(\not{p}+M)}{p^2-M^2+i\epsilon}\right)_{\alpha\beta}$
- $\beta \leftarrow\to \alpha$ $\left(-i\frac{(\not{p}+M)C}{p^2-M^2+i\epsilon}\right)_{\alpha\beta}$

The momentum flow is from left to right. The latter two are fermion-number violating propagators with "clashing" arrows.

Vertices with Majorana particles In our calculation, we need boson-Majorana-Dirac vertices. In general these are (c: boson, λ: Majorana fermion, ψ: Dirac fermion) [20]:

1. 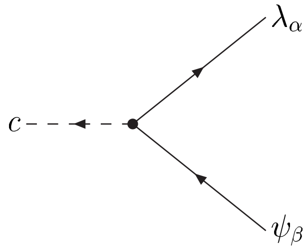

$ik^m(\Gamma_m)_{\alpha\beta}$

2. 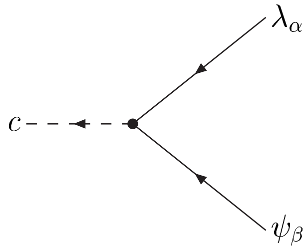

$-ik^m(C^{-1}\Gamma_m)_{\alpha\beta}$

3. 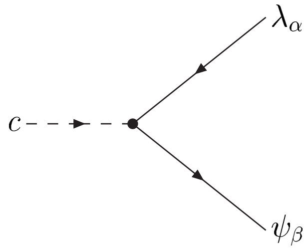

$ik^{m*}(\Gamma_m^T)_{\alpha\beta}$

4. 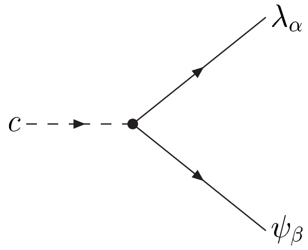

$ik^{m*}((\Gamma_m C)^T)_{\alpha\beta}$

where k^m are coupling coefficients and $\Gamma_m = 1, i\gamma_5, \gamma_\mu\gamma_5, \gamma_\mu, \sigma_{\mu\nu} = \frac{1}{2}i[\gamma_\mu, \gamma_\nu]$ are combinations of the gamma matrices.

4.2 Vertices

Here, we list all vertices used in our processes. They are taken from [14, 20].

Standard model vertices

- 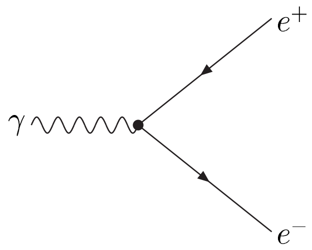

$+ie\gamma^\mu$

- 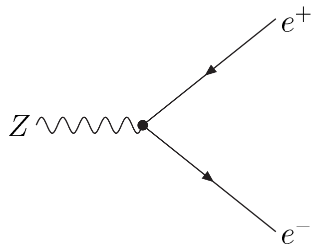

$-i\frac{g}{2\cos\theta_W}\gamma^\mu(g_V - g_A\gamma_5)$

with the coupling strength $g = \frac{e}{\sin\theta_W}$ and $g_V = -\frac{1}{2} + 2\sin^2\theta_W,\ g_A = -\frac{1}{2}$. θ_W is the Weinberg angle.

MSSM vertices

Slepton-slepton-gauge boson The definition of the momentum flow of the scalar particles is crucial for these vertices. We choose the momentum direction to be equal with the particle arrow and opposite to the antiparticle arrow, so the momenta always flow out of the vertex in the following cases.

- 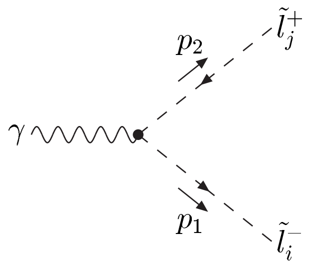

$+ie\delta_{ij}(p_1 - p_2)^\mu$

- 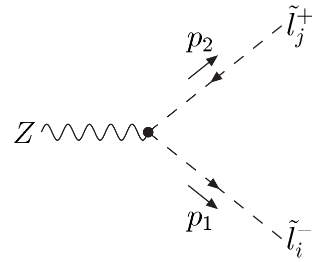

  $-i\frac{g}{\cos\theta_W} z_{ij}(p_1 - p_2)^\mu$

- 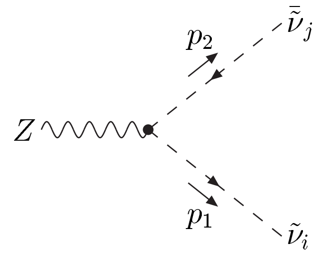

  $-i\frac{g}{2\cos\theta_W} \delta_{ij}(p_1 - p_2)^\mu$

with $z_{ij} = -\frac{1}{2}\sum_{n=1}^{3} U_{in}U_{jn} + \sin^2\theta_W\delta_{ij}$. U is the charged slepton mixing matrix.

Charged lepton-charged slepton-neutralino

- 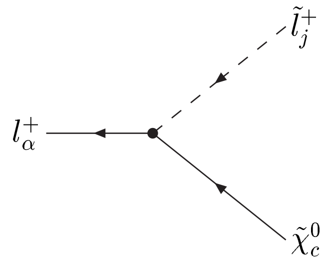

  $-\frac{i}{\sqrt{2}} e\left\{a_{j\alpha,c}(1-\gamma_5) + b_{j\alpha,c}(1+\gamma_5)\right\}$

with

$$a_{j\alpha,c} = \frac{N_{c1}^*}{\cos\theta_W} U_{j\alpha+3} + \frac{m_\alpha N_{c3}^*}{2m_W \sin\theta_W \cos\beta} U_{j\alpha} \tag{4.2}$$

$$b_{j\alpha,c} = \frac{m_\alpha N_{c3}}{2m_W \sin\theta_W \cos\beta} U_{j\alpha+3} - \frac{N_{c1}\tan\theta_W + N_{c2}}{2\sin\theta_W} U_{j\alpha} \tag{4.3}$$

N is the neutralino mixing matrix. Here we have to take care about the terms proportional to the lepton mass m_α. Although of the order of $\frac{m_\alpha}{m_W}$ they can be numerically important for large $\tan\beta$ due to the appearence of $\cos\beta$ in the denominator. As a consequence, we do not neglect the tau mass in these terms.

Charged lepton-sneutrino-chargino

- 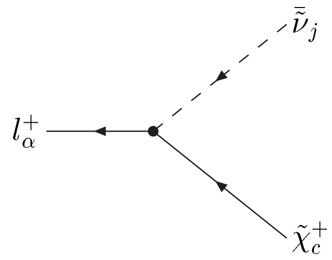

$-\frac{i}{\sqrt{2}} e \left\{ a^\nu_{j\alpha,c}(1-\gamma_5) + b^\nu_{j\alpha,c}(1+\gamma_5) \right\}$

Here the factors are given by

$$a^\nu_{j\alpha,c} = -\frac{m_\alpha (O_1)_{c2}}{2 m_W \cos\beta \sin\theta_W} U^\nu_{j\alpha} \tag{4.4}$$

$$b^\nu_{j\alpha,c} = \frac{(O_2)_{c1}}{\sqrt{2}} U^\nu_{j\alpha} \tag{4.5}$$

O_1, O_2 are the chargino mixing matrices. For the last two vertices, the versions with all arrows reversed can easily be read off the generic results 1. and 3. from the list in 4.1. The vertex factor for the reversed case is generically given by

$$-\frac{i}{\sqrt{2}} e \left\{ a^*(1+\gamma_5) + b^*(1-\gamma_5) \right\},$$

i.e. conjugating the factors a, b and switching the sign in front of γ_5. For the calculation of sneutrino widths we also need the following vertex:

Neutrino-sneutrino-chargino

- 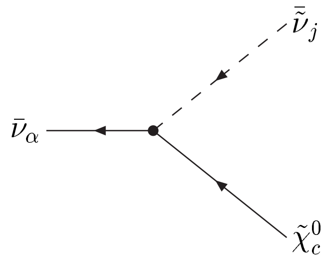

$-\frac{i}{\sqrt{2}} e \left\{ a^{\nu\nu}_{j\alpha,c}(1-\gamma_5) + b^{\nu\nu}_{j\alpha,c}(1+\gamma_5) \right\}$

with

$$a^{\nu\nu}_{j\alpha,c} = 0 \tag{4.6}$$

$$b^{\nu\nu}_{j\alpha,c} = \frac{N_{c1}\tan\theta_W - N_{c2}}{2\sin\theta_W} U^\nu_{j\alpha} \tag{4.7}$$

Chapter 5

The processes

5.1 Charged slepton-pair production

We consider charged slepton-pair production and subsequent decay to leptons and neutralinos:

$$e^+e^- \to \tilde{l}_j^+\tilde{l}_i^- \quad \tilde{l}_j^+ \to l_\beta^+\tilde{\chi}_b^0,\ \tilde{l}_i^- \to l_\alpha^-\tilde{\chi}_a^0 \tag{5.1}$$

where $i, j = 1, ..., 6$ are mass-eigenstate indices for the sleptons, $\alpha, \beta = 1, 2, 3$ flavor indices, and $a, b = 1, ..., 4$ are neutralino labels.

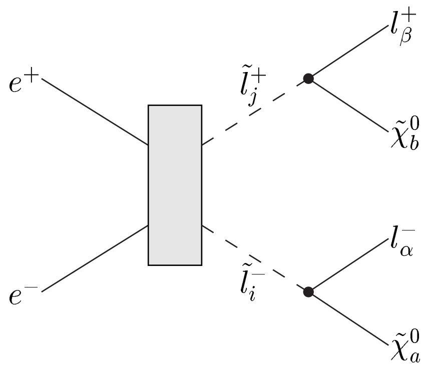

The charged slepton-pair production occurs via photon and Z-boson s-channel exchange, and via t-channel exchange of neutralinos. The lowest-order Feynman diagrams are shown below. Because we specifically allow lepton flavor violation, we must sum over all six intermediate slepton states.

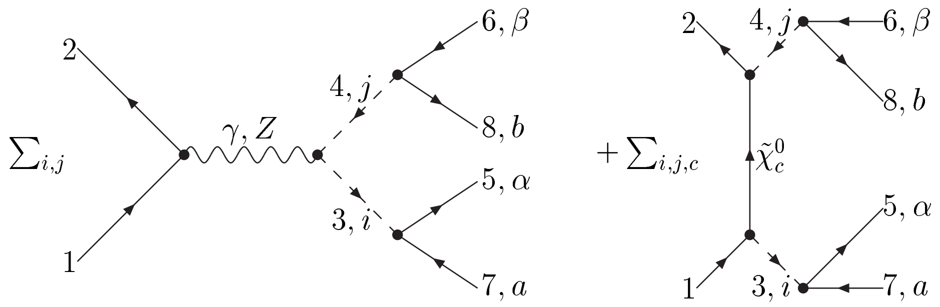

Because of the scalar nature of the intermediate particles, the amplitude completely factors in a production part and two decay parts:

$$M = \sum_{i,j} (M^s_{ij} + \underbrace{\sum_c M^c_{ij}}_{M^t_{ij}}) M^-_i M^+_j \frac{i}{p_3^2 - m_i^2 + i m_i \Gamma_i} \frac{-i}{p_4^2 - m_j^2 + i m_j \Gamma_j}. \qquad (5.2)$$

The notation is as follows:

- M^s_{ij}: s-channel production amplitude
- $M^t_{ij} = \sum_c M^c_{ij}$: t-channel production amplitude summed over all neutralino species
- $M^{+(-)}_{j(i)}$: decay amplitude of the positive (negative) slepton
- The last two terms are the slepton propagators with the slepton masses m_i, m_j, the slepton widths Γ_i, Γ_j and their invariant masses p_3^2, p_4^2

Using the Feynman rules of the previous chapter, the amplitudes are given by:

s-channel production

$$M^s_{ij} = M^\gamma + M^Z = \bar{v}_2 \gamma_\mu \left(\frac{e^2 \delta_{ij}}{s} + \frac{g^2 z_{ij}}{2 \cos^2 \theta_W} \frac{1}{s - m_Z^2} (g_V - g_A \gamma_5) \right) (p_3 - p_4)^\mu u_1 \qquad (5.3)$$

For the Z-propagator, we use two approximations. First, we neglect the Z width, because the beam energies are well beyond the Z mass in order to produce two sleptons on-shell (the lightest slepton we come across has $m \approx 90$ GeV, so the beam energy must always be larger than ≈ 180 GeV). Second, we approximate the propagator by ($q = p_1 + p_2$)

$$-i \frac{g_{\mu\nu} - q_\mu q_\nu / m_Z^2}{q^2 - m_Z^2} \approx \frac{-i g_{\mu\nu}}{q^2 - m_Z^2}. \qquad (5.4)$$

This is possible because the propagator is sandwiched between two massless spinors:

$$\begin{aligned}
& \bar{v}_2\gamma_\mu(g_V - g_A\gamma_5)\frac{q_\mu q_\nu}{m_Z^2}u_1(p_3-p_4)^\nu \\
= \; & \bar{v}_2(\not{p}_2+\not{p}_1)(g_V - g_A\gamma_5)u_1\frac{(p_1+p_2)\cdot(p_3-p_4)}{m_Z^2} \\
= \; & \bar{v}_2(g_V + g_A\gamma_5)\not{p}_1 u_1\frac{(p_1+p_2)\cdot(p_3-p_4)}{m_Z^2} \\
= \; & 0,
\end{aligned}$$

because of the Dirac equations $\bar{v}_2\not{p}_2 = 0$, $\not{p}_1 u_1 = 0$ for massless particles.

t-channel production

$$\begin{aligned}
M_{ij}^c = \; - \; & \frac{e^2/2}{t-M_c^2}\bar{v}_2\left\{a_{j1,c}(1-\gamma_5)+b_{j1,c}(1+\gamma_5)\right\}(\not{q}+M_c) \\
& \times\left\{a_{i1,c}^*(1+\gamma_5)+b_{i1,c}^*(1-\gamma_5)\right\}u_1
\end{aligned} \tag{5.5}$$

Decays

$$M_i^- = -\frac{e}{\sqrt{2}}\bar{u}_5\left\{a_{i\alpha,a}(1-\gamma_5)+b_{i\alpha,a}(1+\gamma_5)\right\}v_7 \tag{5.6}$$

$$M_j^+ = -\frac{e}{\sqrt{2}}\bar{u}_8\left\{a_{j\beta,b}^*(1+\gamma_5)+b_{j\beta,b}^*(1-\gamma_5)\right\}v_6 \tag{5.7}$$

The final results calculated as helicity amplitudes can be found in section 6.3. For the squared amplitude, we get from (5.2)

$$\begin{aligned}
|M|^2 = \; & \sum_{i,j}\sum_{k,l}\left\{(M_{ij}^s M_{kl}^{s*} + M_{ij}^t M_{kl}^{t*} + M_{ij}^s M_{kl}^{t*} + M_{ij}^t M_{kl}^{s*})\right. \\
& \times A_{ik}(p_3^2)A_{jl}(p_4^2) \\
& \left.\times\,(M_i^- M_k^{-*})(M_j^+ M_l^{+*})\right\},
\end{aligned} \tag{5.8}$$

with the propagator terms

$$A_{ij}(p^2) = \frac{1}{p^2-m_i^2+im_i\Gamma_i}\frac{1}{p^2-m_j^2-im_j\Gamma_j}. \tag{5.9}$$

In the case of long-lived sleptons ($\Gamma_i, \Gamma_j \to 0$) we take only the singular parts of the propagators (see appendix A for derivation):

$$A_{ij}(p^2) = \frac{1}{1+i\frac{\Delta m^2}{2\overline{m\Gamma}}}\frac{\pi}{2\overline{m\Gamma}}(\delta(p^2-m_i^2)+\delta(p^2-m_j^2)), \tag{5.10}$$

with the mean squared mass, squared mass difference and mean Breit-Wigner-width, respectively defined as

$$\overline{m^2} = \frac{1}{2}(m_i^2 + m_j^2); \quad \Delta m^2 = m_i^2 - m_j^2; \quad \overline{m\Gamma} = \frac{1}{2}(m_i\Gamma_i + m_j\Gamma_j). \tag{5.11}$$

In addition to the above amplitude, one must also consider the neutralino-crossed amplitude $\tilde{\chi}_a^0 \leftrightarrow \tilde{\chi}_b^0$ (with a relative minus sign between the crossed and uncrossed amplitudes in the case of identical particles $a = b$), because the neutralinos (which are Majorana particles) are their own anti-particles. But using the narrow-width-approximation for the slepton propagators we can neglect the cross-interference term:

$$|M|^2 = (1/2)(|M_a^b|^2 + |M_b^a|^2 \pm \underbrace{2ReM_a^b M_b^{a*}}_{\approx 0}), \tag{5.12}$$

where M_a^b is the uncrossed amplitude and M_b^a is the crossed amplitude. The statistical factor $1/2$ and the minus sign are needed in the case of identical particles. A physical argument for this approximation would be the fact, that the intermediate sleptons have a very long lifetime, and by the time they decay, the neutralinos do not have a sufficient overlap to produce interference effects.

A more analytical argumentation is, that the narrow-width approximated propagators put the invariant masses of the sleptons on-shell, regardless of the outgoing particles. Therefore we have in the uncrossed and crossed amplitudes the following momenta in the denominators of the propagators:

$$p_4^2 = (p_6 + p_8)^2 = m_4^2; \quad p_4^2 = (p_6 + p_7)^2 = m_4^2 \tag{5.13}$$
$$p_3^2 = (p_5 + p_7)^2 = m_3^2; \quad p_3^2 = (p_5 + p_8)^2 = m_3^2 \tag{5.14}$$

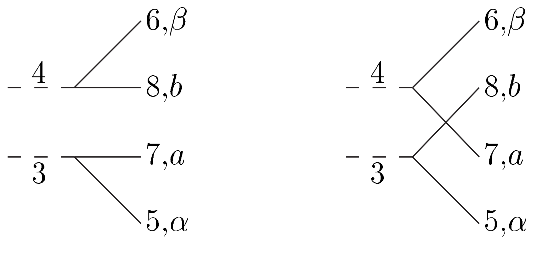

In the cross-interference terms, both versions of the propagator will appear, so all the equations must be fullfilled simultaneously, leading to

$$m_8^2 - m_7^2 = 2p_6 \cdot (p_7 - p_8); \quad m_7^2 - m_8^2 = 2p_5 \cdot (p_8 - p_7), \tag{5.15}$$

or equivalently,

$$(p_6 - p_5) \cdot (p_7 - p_8) = 0. \tag{5.16}$$

This is an additional constraint on the momentum-space (and independent from the momentum-conservation constraints) in order to get a nonvanishing contribution from the interference term in the "zero"-width approximation, thus creating a hypersurface in phase space. The volume of this surface is zero, so it yields no contribution to the total cross-section. If we allow a finite width, i.e. expanding the propagator to higher terms in Γ, this hypersurface becomes smeared out and we arrive at a finite region of phase space where cross-interference is non-negligible.

5.2 Sneutrino-pair production

The second process we consider is sneutrino-pair production with subsequent decay to leptons and charginos:

$$e^+e^- \to \bar{\tilde{\nu}}_j \tilde{\nu}_i, \quad \bar{\tilde{\nu}}_j \to l^+_\beta \tilde{\chi}^-_b\,,\ \tilde{\nu}_i \to l^-_\alpha \tilde{\chi}^+_a \tag{5.17}$$

$i, j = 1, 2, 3$ are mass eigenstate indices for the sneutrinos and $a, b = 1, 2$ are chargino labels. This process is completely analogous to the slepton process regarding the amplitude and phase-space calculation. The sneutrino production occurs via Z-boson s-channel exchange (there is no photon exchange because sneutrinos are uncharged), and via t-channel exchange of charginos. Again, we sum over all intermediate sneutrino flavors, as indicated by the tree-level Feynman diagrams:

$\sum_{i,j}$ 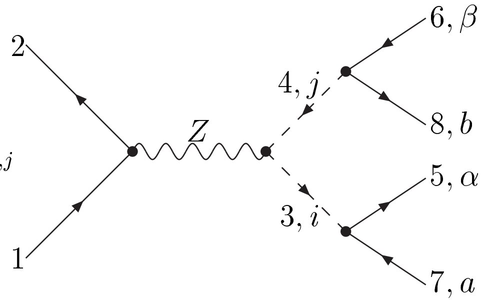 $+\sum_{i,j,c}$ 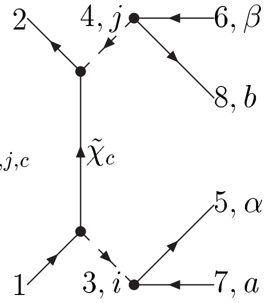

The construction of the amplitude and the narrow-width approximation works exactly the same as in the charged slepton process. In contrast to the slepton production, there is, even in principle, no crossing of the final charginos.

For this process it is quite easy to obtain an analytical result for the intermediate sneutrino sum using the minimal $\tilde{\nu}_e - \tilde{\nu}_\tau$ mixing of section 3.1. Looking at the sneutrino vertex factors (4.4)(4.5) we observe that the mixing matrix elements $U^{\nu}_{i\alpha}$ can be factorized. For the process $e^+e^- \to e^-\tau^+\tilde{\chi}^+_b\tilde{\chi}^-_a$, i.e. $\alpha = 1, \beta = 3$, this yields:

$$\begin{aligned} M^s_{ij} &\propto \delta_{ij} \\ M^t_{ij} &\propto U_{i1}U_{j1} \\ M^-_i &\propto U_{i1} \\ M^+_j &\propto U_{j3}, \end{aligned}$$

where we have dropped the ν on the mixing matrix U. In the charged slepton case, the dependence is more complicated due to the left-right mixing. As an appoximation, we assume that the sneutrinos are almost degenerate, $m_i \approx m_j \approx \bar{m}$, and have equal width, $\Gamma_i \approx \Gamma_j \approx \Gamma$. The narrow-width approximated propagator (A.5) can then be written as ($\Delta m^2 \approx 2\bar{m}\Delta m$):

$$A_{ij}(p^2) = \underbrace{\frac{1}{1 + i\frac{\Delta m}{\Gamma}}}_{C_{ij}} \frac{\pi}{2\bar{m}\Gamma}\delta(p^2 - \bar{m}^2) \tag{5.18}$$

The squared amplitude (5.8) can be written as

$$\begin{aligned} |M|^2 &= |M^t|^2 \sum_{ij}\sum_{kl} U_{j1}U_{i1}U_{k1}U_{l1}C_{ik}C_{jl}U_{i1}U_{k1}U_{j3}U_{l3} \\ &\quad + |M^s|^2 \sum_{ij}\sum_{kl} \delta_{ij}\delta_{kl}C_{ik}C_{jl}U_{i1}U_{k1}U_{j3}U_{l3} \\ &\quad + 2\mathrm{Re}\left(M^s M^{t*} \sum_{ij}\sum_{kl} \delta_{ij}U_{k1}U_{l1}C_{ik}C_{jl}U_{i1}U_{k1}U_{j3}U_{l3}\right) \\ &= |M^t|^2 \sum_{ij}\sum_{kl} U_{j1}U^2_{i1}U^2_{k1}U_{l1}U_{j3}U_{l3}C_{ik}C_{jl} \\ &\quad + |M^s|^2 \sum_{ik} U_{i1}U_{k1}U_{i3}U_{k3}C^2_{ik} \\ &\quad + 2\mathrm{Re}\left(M^s M^{t*} \sum_{ikl} U^2_{k1}U_{l1}U_{i1}U_{i3}U_{l3}C_{ik}C_{il}\right), \end{aligned}$$

where $|M^t|^2, |M^s|^2, M^s M^{t*}$ are the appropriate flavor conserving amplitudes for the process $e^+e^- \to e^+e^-\tilde{\chi}^+_b\tilde{\chi}^-_c$, including production, decay and the slepton propagators (without the interference term C_{ij}) $\frac{\pi}{2\bar{m}\Gamma}\delta(p^2 - \bar{m}^2)$. Using the mixing matrix (3.3) it is straightforward to calculate the sums analytically ($x = \frac{\Delta m}{\Gamma}$):

$$|M|^2 = \underbrace{\frac{x^2(4 + 3x^2 + x^2\cos 4\phi)\sin^2 2\phi}{8(1 + x^2)^2}}_{f_t} |M^t|^2$$

$$+ \quad \underbrace{\frac{x^2(3+x^2)\sin^2 2\phi}{2(1+x^2)^2}}_{f_s}|M^s|^2$$

$$+ \quad 2\mathrm{Re}\left(\underbrace{\frac{x^2(3+x^2-2ix\cos 2\phi)\sin^2 2\phi}{4(1+x^2)^2}}_{f_{st}}M^s M^{t*}\right) \tag{5.19}$$

Figure 5.1 shows the ϕ dependence for a fixed $x = 2$, while Figure 5.2 shows the x behaviour for fixed $\phi = \pi/4$ (maximal mixing). The ϕ behaviour for the s-channel is simply $(\sin\phi\cos\phi)^2 = 1/4\sin^2 2\phi$ because one decay vertex must be lepton flavor violating, yielding $\sin\phi$ and one is conserving yielding $\cos\phi$ from the mixing matrix U. There is no LFV in the production. For the t-channel it is more complicated because, in principle, all vertices can be lepton flavor violating. The lowest order (small mixing) contribution still yields $\sin^2 2\phi$ but for large mixing (around the maxima $\phi = \pi/4, 3\pi/4$), higher order contributions are significant. In the mass difference plot one can see

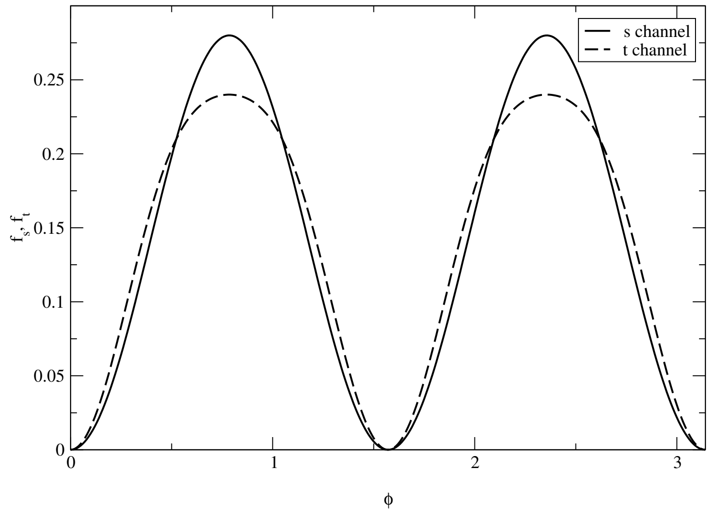

Figure 5.1: Squared amplitudes as function of the mixing angle ϕ for $x = 2$ (arbitrary units)

the decoherent region $|x| \gg 1$ (large mass difference). Here only the diagonal terms of C_{ij} with $i = j$ contribute. In the interference region $|x| < 1$, off-diagonal terms play an important role leading to destructive interference. In the intermediate region $|x| \approx 1$ (i.e. $\Delta m \approx \Gamma$), higher loop contributions will be important [13], so the exact shape of the kink is not exactly the same as in Figure 5.2. The position $x = 0$ and the limiting behaviour $|x| \gg 1$ are not affected by such loop contributions.

We can see that the total amplitude is proportional to $\sin^2 2\phi$ with only higher order contributions in $\sin^2 2\phi$, thus the total cross-section approximately scales with the strength of the flavor mixing. The cross-section will be reduced if the mass differences of the propagating sleptons are comparable to their width.

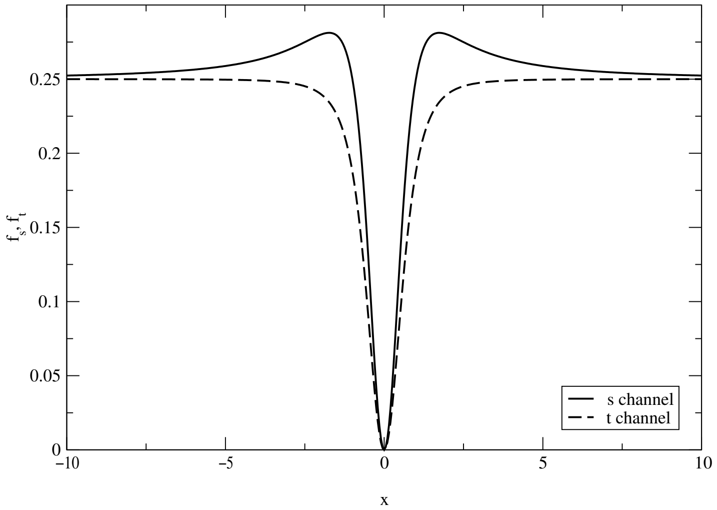

Figure 5.2: Squared amplitudes as function of $x = \frac{\Delta m}{\Gamma}$ for $\phi = \pi/4$ (arbitrary units)

Chapter 6

Calculation of the amplitude

In this section we calculate the amplitudes of the production and decay processes using the helicity method. This means that we do not sum over the helicities of external particles. Helicity amplitudes are necessary when using polarized beams and performing polarization dependent measurements of final particles. We use a method suited for our purposes presented in [6].

6.1 Method of calculation

In order to calculate helicity amplitudes, we need proper helicity eigenspinors $u(\vec{p}, h)$ and $v(\vec{p}, h)$, where $h/2$ is the helicity.

We use the Weyl representation for the Dirac γ-matrices because it simplifies the high energy limit:

$$\gamma_0 = \begin{pmatrix} 0 & 1 \\ 1 & 0 \end{pmatrix}, \quad \gamma^i = \begin{pmatrix} 0 & \sigma^i \\ -\sigma^i & 0 \end{pmatrix}, \quad \gamma_5 = \begin{pmatrix} -1 & 0 \\ 0 & +1 \end{pmatrix}, \tag{6.1}$$

where σ^i are the Pauli-matrices. In this representation the properly normalized helicity spinors are ($E = \sqrt{|\vec{p}|^2 + m^2}$)

$$\begin{aligned} u(\vec{p}, h) &= \begin{pmatrix} \sqrt{E - h|\vec{p}|}\chi(\vec{p}, h) \\ \sqrt{E + h|\vec{p}|}\chi(\vec{p}, h) \end{pmatrix} \\ v(\vec{p}, h) &= \begin{pmatrix} -h\sqrt{E + h|\vec{p}|}\chi(\vec{p}, -h) \\ h\sqrt{E - h|\vec{p}|}\chi(\vec{p}, -h) \end{pmatrix} \end{aligned} \tag{6.2}$$

with the Pauli spinors ($\vec{p} = (|\vec{p}|, \theta, \phi)$ in polar coordinates)

$$\begin{aligned} \chi(\vec{p}, +1) &= \begin{pmatrix} e^{-i\phi/2}\cos\theta/2 \\ e^{i\phi/2}\sin\theta/2 \end{pmatrix} \\ \chi(\vec{p}, -1) &= \begin{pmatrix} -e^{-i\phi/2}\sin\theta/2 \\ e^{i\phi/2}\cos\theta/2 \end{pmatrix} \end{aligned} \tag{6.3}$$

In an actual calculation we must evaluate the following amplitude

$$M(h_1, h_2) = \bar{w}_1(\vec{p}_1, h_1) Q w_2(\vec{p}_2, h_2), \quad w_i = u, v \tag{6.4}$$

where Q is a 4×4 matrix consisting of contractions of some 4-vectors (e.g. momenta) with the Dirac matrices. The helicity amplitudes can now be calculated by brute force. For special cases, the amplitude can be simplified further analytically. For example our production amplitudes (electron-positron pair annihilation) can be written as

$$M = \bar{v}(\vec{p}_{e^+}, h_{e^+}) Q u(\vec{p}_{e^-}, h_{e^-}). \tag{6.5}$$

In the center-of-mass frame with the particle moving in $+z$ and antiparticle moving in $-z$ direction and using the high energy limit $m \ll E$, thus neglecting terms proportional to $E - |\vec{p}|$, the spinors have the form:

$$\begin{array}{ccc} \bar{v}(-z,+1) = \sqrt{2E}\begin{pmatrix} 0 & 0 & i & 0 \end{pmatrix} & , & \bar{v}(-z,-1) = \sqrt{2E}\begin{pmatrix} 0 & i & 0 & 0 \end{pmatrix} \\ u(+z,+1) = \sqrt{2E}\begin{pmatrix} 0 \\ 0 \\ 1 \\ 0 \end{pmatrix} & , & u(+z,-1) = \sqrt{2E}\begin{pmatrix} 0 \\ 1 \\ 0 \\ 0 \end{pmatrix} \end{array}$$

In this limit each helicity amplitude corresponds to one matrix element of Q $(M(h_{e^-}, h_{e^+}))$:

$$\begin{aligned} M(+,+) &= i\sqrt{s}Q_{33} \\ M(-,+) &= i\sqrt{s}Q_{32} \\ M(+,-) &= i\sqrt{s}Q_{23} \\ M(-,-) &= i\sqrt{s}Q_{22}, \end{aligned} \tag{6.6}$$

with the beam energy $\sqrt{s} = 2E$.

6.2 Generic calculation

In this section we explicitly calculate the amplitudes using the helicity method.

6.2.1 s-channel

The s-channel amplitudes have the generic form

$$M_s = \bar{v}_2(A \not{k} + B \not{k}(g_V - g_A\gamma_5))u_1, \tag{6.7}$$

where A, B are complex numbers. The task is now to calculate the four inner matrix elements of

$$\begin{aligned} Q &= A \not{k} + B \not{k}(g_V - g_A\gamma_5) \\ &= (A + Bg_V) \not{k} + Bg_A\gamma_5 \not{k}. \end{aligned}$$

This can be done by using the explicit form of the matrices $\not{k}$ and γ_5 in the Weyl representation (we only need the inner matrix elements)

$$\begin{aligned} Q = (A + Bg_V) &\begin{pmatrix} \dots & \dots & \dots & \dots \\ \dots & 0 & -k_x - ik_y & \dots \\ \dots & k_x - ik_y & 0 & \dots \\ \dots & \dots & \dots & \dots \end{pmatrix} \\ +Bg_A &\begin{pmatrix} \dots & \dots & \dots & \dots \\ \dots & 0 & k_x + ik_y & \dots \\ \dots & k_x - ik_y & 0 & \dots \\ \dots & \dots & \dots & \dots \end{pmatrix} \end{aligned}$$

The helicity amplitudes $M^s(h_1, h_2)$ are:

$$\begin{aligned} M^s(+,+) &= i\sqrt{s}Q_{33} = 0 \\ M^s(-,-) &= i\sqrt{s}Q_{22} = 0 \\ M^s(+,-) &= i\sqrt{s}Q_{23} = i\sqrt{s}(-A + B(g_A - g_V))(k_x + ik_y) \\ M^s(-,+) &= i\sqrt{s}Q_{32} = i\sqrt{s}(A + B(g_A + g_V))(k_x - ik_y) \end{aligned} \tag{6.8}$$

6.2.2 t-channel

The t-channel amplitudes can be written as

$$M_t = \bar{v}_2(A - B\gamma_5)(\not{q} + M)(C + D\gamma_5)u_1, \tag{6.9}$$

with complex numbers A, B, C, D. The matrix is now

$$\begin{aligned} Q &= (A - B\gamma_5)(\not{q} + M)(C + D\gamma_5) \\ &= (AC + BD) \not{q} - (AD + BC)\gamma_5 \not{q} \\ &\quad +(AD - BC)M\gamma_5 + (AC - BD)M. \end{aligned}$$

The helicity amplitudes $M^t(h_1, h_2)$ are:

$$\begin{aligned} M^t(+,+) &= +i\sqrt{s}M(A - B)(C + D) \\ M^t(-,-) &= +i\sqrt{s}M(A + B)(C - D) \\ M^t(+,-) &= -i\sqrt{s}(A + B)(C + D)(q_x + iq_y) \\ M^t(-,+) &= +i\sqrt{s}(A - B)(C - D)(q_x - iq_y) \end{aligned} \tag{6.10}$$

6.2.3 Decays

The decay amplitudes can be calculated in the same way as the production ones. The only difference is the position of the u and v spinors:

$$M_d = \bar{u}_1(A - B\gamma_5)v_2 \tag{6.11}$$

The decay amplitudes are evaluated in the rest frame of the decaying particle. Because the decaying particle is a scalar, there is no preferred direction in space and the decay is spherically symmetric. Thus we can choose as the directions of the final particles (which are produced back to back) the $\pm$z-axis, respectively. The calculation is then analogous to the production (see discussion following (6.5)), with the exception that we do not assume either particle to be massless. We obtain

$$\begin{aligned}
M_d(+,+) &= i((A-B)\sqrt{E_1-p_1}\sqrt{E_2-p_2} - (A+B)\sqrt{E_1+p_1}\sqrt{E_2+p_2}) \\
M_d(-,-) &= i((A+B)\sqrt{E_1-p_1}\sqrt{E_2-p_2} - (A-B)\sqrt{E_1+p_1}\sqrt{E_2+p_2}) \\
M_d(+,-) &= 0 \\
M_d(-,+) &= 0. \qquad (6.12)
\end{aligned}$$

6.3 Final results

Here we present the final results for the production and decay amplitudes in the charged slepton case, using the results of the previous section with the vertices of section 4.2.

6.3.1 s-channnel production

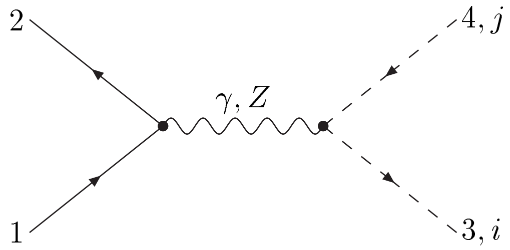

$$M^s_{ij} = M^\gamma + M^Z = \bar{v}_2\gamma_\mu \left(\frac{e^2\delta_{ij}}{s} + \frac{g^2 z_{ij}}{2\cos^2\theta_W} \frac{1}{s - m_Z^2}(g_V - g_A\gamma_5) \right) (p_3 - p_4)^\mu u_1 \tag{6.13}$$

$M^s_{ij}(h_{e^-}, h_{e^+})$:

$$\begin{aligned}
M^s_{ij}(+,+) &= 0 \\
M^s_{ij}(-,-) &= 0 \\
M^s_{ij}(+,-) &= -2ie^2\sqrt{s}\left(\frac{\delta_{ij}}{s} + \frac{1}{\cos^2\theta_W}\frac{z_{ij}}{s-m_Z^2}\right)|\vec{p_3}|\sin\theta_3 \\
M^s_{ij}(-,+) &= +2ie^2\sqrt{s}\left(\frac{\delta_{ij}}{s} + \frac{\sin^2\theta_W - \frac{1}{2}}{\sin^2\theta_W\cos^2\theta_W}\frac{z_{ij}}{s-m_Z^2}\right)|\vec{p_3}|\sin\theta_3 \qquad (6.14)
\end{aligned}$$

with $s = (p_1 + p_2)^2 = 4E^2$. $|\vec{p_3}|$ is given in the center-of-mass frame and can be expressed invariantly in terms of the particle masses and the beam energy (see section 7.1.1).

6.3.2 t-channel production

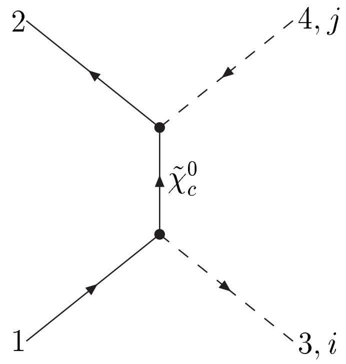

$$\begin{aligned}
M^c_{ij} = \; - \; & \frac{e^2/2}{t-M_c^2}\bar{v}_2\left\{a_{j1,c}(1-\gamma_5) + b_{j1,c}(1+\gamma_5)\right\}(\not{q} + M_c) \\
& \times \left\{a^*_{i1,c}(1+\gamma_5) + b^*_{i1,c}(1-\gamma_5)\right\}u_1 \qquad (6.15)
\end{aligned}$$

$M^c_{ij}(h_{e^-}, h_{e^+})$:

$$\begin{aligned}
M^c_{ij}(+,+) &= -2ie^2\sqrt{s}\frac{b_{j1,c}a^*_{i1,c}}{t-M_c^2}M_c \\
M^c_{ij}(-,-) &= -2ie^2\sqrt{s}\frac{a_{j1,c}b^*_{i1,c}}{t-M_c^2}M_c \\
M^c_{ij}(+,-) &= -2ie^2\sqrt{s}\frac{a_{j1,c}a^*_{i1,c}}{t-M_c^2}|\vec{p_3}|\sin\theta_3 \\
M^c_{ij}(-,+) &= +2ie^2\sqrt{s}\frac{b_{j1,c}b^*_{i1,c}}{t-M_c^2}|\vec{p_3}|\sin\theta_3 \qquad (6.16)
\end{aligned}$$

with $q = p_1 - p_3, t = q^2$. M_c are the neutralino masses.

6.3.3 Decays

Slepton-Decay

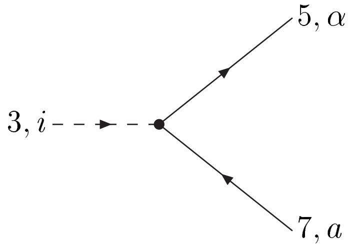

$$M_i^- = -\frac{e}{\sqrt{2}}\bar{u}_5 \left\{a_{i\alpha,a}(1-\gamma_5) + b_{i\alpha,a}(1+\gamma_5)\right\} v_7 \tag{6.17}$$

$M_i^-(h_{5^-}, h_7)$:

$$\begin{aligned} M_i^-(+,+) &= 2iea_{i\alpha,a}\sqrt{|\vec{p}_5|(E_7+|\vec{p}_5|)} \\ M_i^-(-,-) &= 2ieb_{i\alpha,a}\sqrt{|\vec{p}_5|(E_7+|\vec{p}_5|)} \\ M_i^-(+,-) &= 0 \\ M_i^-(-,+) &= 0, \end{aligned} \tag{6.18}$$

where we neglected the mass of the outgoing lepton l_α^-. $|\vec{p}_5|$ and E_7 are given in the rest frame of the decaying particle (see section 7.1.2). Because the helicity of a particle is not Lorentz-invariant unless the particle is massless [2], neither are the helicity amplitudes. In order to obtain a Lorentz-invariant squared amplitude we must sum over the helicity of the massive particle, in this case the outgoing neutralino.

Antislepton-Decay

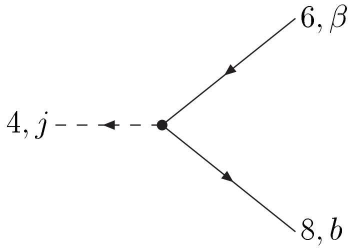

$$M_j^+ = -\frac{e}{\sqrt{2}}\bar{u}_8 \left\{a^*_{j\beta,b}(1+\gamma_5) + b^*_{j\beta,b}(1-\gamma_5)\right\} v_6 \tag{6.19}$$

$M_j^+(h_{6^+}, h_8)$:

$$\begin{aligned} M_j^+(+,+) &= 2ieb^*_{j\beta,b}\sqrt{|\vec{p}_6|(E_8+|\vec{p}_6|)} \\ M_j^+(-,-) &= 2iea^*_{j\beta,b}\sqrt{|\vec{p}_6|(E_8+|\vec{p}_6|)} \\ M_j^+(+,-) &= 0 \\ M_j^+(-,+) &= 0, \end{aligned} \tag{6.20}$$

again neglecting the mass of the lepton l^+_β, and the summation of the squared amplitude over the neutralino helicity is understood.

6.4 Sneutrinos

The sneutrino amplitudes can be easily calculated by substituting

$$\begin{aligned} a_{i\alpha,a} &\to a^\nu_{i\alpha,a} \\ b_{i\alpha,a} &\to b^\nu_{i\alpha,a} \\ z_{ij} &\to \frac{1}{2}\delta_{ij} \end{aligned}$$

in the charged slepton amplitudes, with the indices $i, j = 1, 2, 3$ now labelling the sneutrinos and $a, b = 1, 2$ the charginos. Furthermore we must drop the photon contribution in the s-channel. Here we present only the summed production amplitude $M^{prod}_{ij}(h_{e^-}, h_{e^+}) = M^s_{ij} + \sum_c M^c_{ij}$ for reference:

$$\begin{aligned}
M^{prod}_{ij}(+,+) &= -2ie^2\sqrt{s}\sum_{c=1}^{2}\frac{b^\nu_{j1,c}a^{\nu*}_{i1,c}}{t-M_c^2}M_c \\
M^{prod}_{ij}(-,-) &= -2ie^2\sqrt{s}\sum_{c=1}^{2}\frac{a^\nu_{j1,c}b^{\nu*}_{i1,c}}{t-M_c^2}M_c \\
M^{prod}_{ij}(+,-) &= -2ie^2\sqrt{s}\left(\frac{1}{2\cos^2\theta_W}\frac{\delta_{ij}}{s-m_Z^2}+\sum_{c=1}^{2}\frac{a^\nu_{j1,c}a^{\nu*}_{i1,c}}{t-M_c^2}\right)|\vec{p_3}|\sin\theta_3 \\
M^{prod}_{ij}(-,+) &= +2ie^2\sqrt{s}\left(\frac{\sin^2\theta_W-\frac{1}{2}}{2\sin^2\theta_W\cos^2\theta_W}\frac{\delta_{ij}}{s-m_Z^2}+\sum_{c=1}^{2}\frac{b^\nu_{j1,c}b^{\nu*}_{i1,c}}{t-M_c^2}\right)|\vec{p_3}|\sin\theta_3
\end{aligned}$$

Chapter 7

Calculation of the phase space

The general strategy for the phase space calculation is to decompose the phase space in production and decay parts just like the amplitude. Their only connection are integrals over the invariant masses p_3^2, p_4^2 of the intermediate sleptons which contract with the Dirac deltas of the narrow-width approximated propagators. The number of phase space variables is thus effectively reduced from $3 \times 4 - 4 = 8$ to 6.

7.1 Production and Decay

Here we present the standard formulas for $2 \to 2$ production and $1 \to 2$ decay processes. These will not only be used for some simple calculations like slepton-production cross-sections or the slepton widths, but will also serve as a basis for the decomposed $2 \to 4$ cross-section. They can be found in all standard textbooks on the subject, e.g. [1, 2].

7.1.1 Pair production

Generally, the differential cross-section $d\sigma$ for the process $p_1, p_2 \to p_3, p_4$ with the amplitude M_p can be written as

$$d\sigma = \frac{|M_p|^2}{2\sqrt{\lambda(s, m_1^2, m_2^2)}}(2\pi)^4\delta^{(4)}(p_1 + p_2 - p_3 - p_4)\frac{d^3p_3}{(2\pi)^3 2E_3}\frac{d^3p_4}{(2\pi)^3 2E_4}, \quad (7.1)$$

with $\lambda(a, b, c) = (a - b - c)^2 - 4bc$.

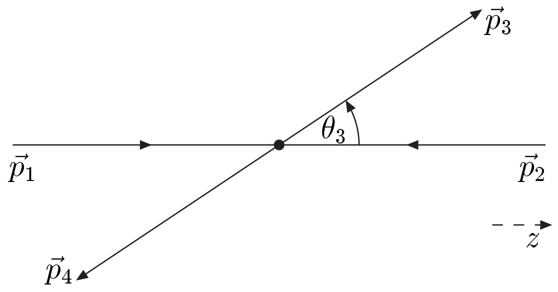

In the center-of-mass frame, with the momenta

$$\begin{aligned} p_1 = (E_1, \vec{p}_1), \qquad & p_2 = (E_2, -\vec{p}_1), \\ p_3 = (E_3, \vec{p}_3), \qquad & p_4 = (E_4, -\vec{p}_3), \end{aligned} \tag{7.2}$$

the cross-section can be written (in terms of $\cos\theta_3, \phi_3$) as

$$d\sigma = \frac{|M|^2}{64\pi^2 s}\frac{|\vec{p}_3|}{|\vec{p}_1|}d\cos\theta_3 d\phi_3, \tag{7.3}$$

with

$$|\vec{p}_3| = \sqrt{\frac{1}{4s}\lambda(s, m_3^2, m_4^2)}, \tag{7.4}$$

$$|\vec{p}_1| = \sqrt{\frac{1}{4s}\lambda(s, m_1^2, m_2^2)} \tag{7.5}$$

$$s = (p_1 + p_2)^2 = (E_1 + E_2)^2 \tag{7.6}$$

7.1.2 Two-body decay

The decay width for the process $p_3 \to p_5, p_7$ with the amplitude M_d is generally written as

$$d\Gamma_3 = \frac{|M_d|^2}{2m_3}(2\pi)^4\delta^{(4)}(p_3 - p_5 - p_7)\frac{d^3p_5}{(2\pi)^3 2E_5}\frac{d^3p_7}{(2\pi)^3 2E_7}. \tag{7.7}$$

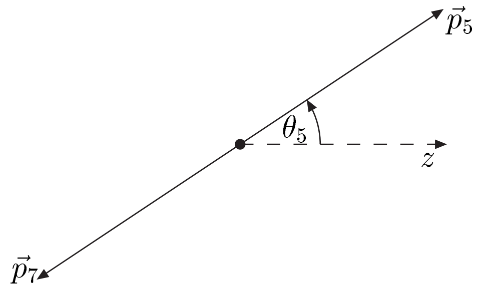

In the rest frame of the decaying particle with

$$\begin{aligned} p_3 &= (m_3, \vec{0}), \\ p_5 &= (E_5, \vec{p}_5), \qquad p_7 = (E_7, -\vec{p}_5), \end{aligned} \tag{7.8}$$

the width becomes (in terms of $\cos\theta_5^*, \phi_5^*, E_5^*$, stars denote the rest frame)

$$d\Gamma_3 = \frac{|M|^2}{32\pi^2 m_3^2}|\vec{p}_5|\delta(E_5^* - \bar{E}_5)d\cos\theta_5^* d\phi_5^* dE_5^*, \tag{7.9}$$

with

$$|\vec{p}_5| = \sqrt{\frac{1}{4m_3^2}\lambda(m_3^2, m_5^2, m_7^2)}, \tag{7.10}$$

$$\bar{E}_5 = \sqrt{m_5^2 + |\vec{p}_5|^2}. \tag{7.11}$$

We have not integrated over E_5^* because we will later transform this differential width to other frames.

7.2 The complete process

Generally, the cross-section for the process $p_1, p_2 \to p_5, p_7, p_6, p_8$ with amplitude M is written as

$$d\sigma = \frac{|M|^2}{2\sqrt{\lambda(s, m_1^2, m_2^2)}}d\Phi, \tag{7.12}$$

with the phase space element

$$d\Phi = (2\pi)^4\delta^{(4)}(p_1+p_2-p_5-p_7-p_6-p_8)\frac{d^3p_5}{(2\pi)^3 2E_5}\frac{d^3p_7}{(2\pi)^3 2E_7}\frac{d^3p_6}{(2\pi)^3 2E_6}\frac{d^3p_8}{(2\pi)^3 2E_8} \tag{7.13}$$

We now decompose the phase space in production and decay parts. This can be done by introducing the momenta

$$p_3 = p_5 + p_7, \quad p_4 = p_6 + p_8. \tag{7.14}$$

Neglecting interference in the final state, these momenta are associated with the intermediate sleptons. After multiplying with the identities

$$1 = \int d^4p_3\delta^{(4)}(p_3 - p_5 - p_7), \quad 1 = \int d^4p_4\delta^{(4)}(p_4 - p_6 - p_8), \tag{7.15}$$

the phase space element (7.13) becomes

$$\begin{aligned} d\Phi &= \int\int (2\pi)^4\delta^{(4)}(p_1 + p_2 - p_3 - p_4) \\ &\quad \times d^4p_3\delta^{(4)}(p_3 - p_5 - p_7)\frac{d^3p_5}{(2\pi)^3 2E_5}\frac{d^3p_7}{(2\pi)^3 2E_7} \\ &\quad \times d^4p_4\delta^{(4)}(p_4 - p_6 - p_8)\frac{d^3p_6}{(2\pi)^3 2E_6}\frac{d^3p_8}{(2\pi)^3 2E_8} \end{aligned} \tag{7.16}$$

Using

$$d^4p_3 = (2\pi)^3 dp_3^2\frac{d^3p_3}{(2\pi)^3 2E_3}, \tag{7.17}$$

and an analogous expression for p_4^2, the fully differential cross-section can finally be written as

$$\begin{aligned} d\sigma &= \frac{|M|^2}{2\sqrt{\lambda(s, m_1^2, m_2^2)}}\underbrace{(2\pi)^4\delta^{(4)}(p_1 + p_2 - p_3 - p_4)\frac{d^3p_3}{(2\pi)^3 2E_3}\frac{d^3p_4}{(2\pi)^3 2E_4}}_{d\Phi_p} \\ &\quad \times \underbrace{(2\pi)^4\delta^{(4)}(p_3 - p_5 - p_7)\frac{d^3p_5}{(2\pi)^3 2E_5}\frac{d^3p_7}{(2\pi)^3 2E_7}}_{d\Phi_3} \\ &\quad \times \underbrace{(2\pi)^4\delta^{(4)}(p_4 - p_6 - p_8)\frac{d^3p_6}{(2\pi)^3 2E_6}\frac{d^3p_8}{(2\pi)^3 2E_8}}_{d\Phi_4} \\ &\quad \times \frac{1}{2\pi}dp_3^2\frac{1}{2\pi}dp_3^2, \end{aligned} \tag{7.18}$$

where we have separated the production and decay parts. Using these decomposed phase space elements, one can write

$$d\sigma = \frac{|M|^2}{2\sqrt{\lambda(s,m_1^2,m_2^2)}} d\Phi_p d\Phi_3 d\Phi_4 \frac{1}{2\pi} dp_3^2 \frac{1}{2\pi} dp_3^2. \tag{7.19}$$

Using the decomposed squared amplitude (5.8)$(M_{ij}^p = M_{ij}^s + M_{ij}^t)$,

$$\begin{aligned} |M|^2 &= \sum_{ijkl} (M_{ij}^p M_{kl}^{p*})(M_i^- M_k^{-*})(M_j^+ M_l^{+*}) C_{ik} \frac{\pi}{2\overline{m\Gamma}_{ik}} C_{jl} \frac{\pi}{2\overline{m\Gamma}_{jl}} \\ &\quad \times (\delta(p_3^2 - m_i^2) + \delta(p_3^2 - m_k^2))(\delta(p_4^2 - m_j^2) + \delta(p_4^2 - m_l^2)), \end{aligned} \tag{7.20}$$

where

$$C_{ik} = \frac{1}{1 + i\frac{\Delta m_{ik}^2}{2\overline{m\Gamma}_{ik}}}, \tag{7.21}$$

the differential cross section can be written as

$$\begin{aligned} d\sigma &= \frac{1}{4} \sum_{ijkl} \sum_{\substack{p_3^2 = m_i^2, m_k^2 \\ p_4^2 = m_j^2, m_l^2}} \underbrace{\frac{M_{ij}^p M_{kl}^{p*}}{2\sqrt{\lambda(s,m_1^2,m_2^2)}} d\Phi_p}_{d\sigma_{ijkl}} \\ &\qquad \times \underbrace{C_{ik} \frac{1}{2\overline{m\Gamma}_{ik}} M_i^- M_k^{-*} d\Phi_3}_{dB_{ik}} \\ &\qquad \times \underbrace{C_{jl} \frac{1}{2\overline{m\Gamma}_{jl}} M_j^+ M_l^{+*} d\Phi_4}_{dB_{jl}}, \end{aligned} \tag{7.22}$$

where we have integrated over p_3^2, p_4^2. With the terms $d\sigma_{ijkl}, dB_{ik}, dB_{jl}$ thus defined, we obtain

$$d\sigma = \frac{1}{4} \sum_{ijkl} \sum_{\substack{p_3^2 = m_i^2, m_k^2 \\ p_4^2 = m_j^2, m_l^2}} d\sigma_{ijkl} dB_{ik} dB_{jl}. \tag{7.23}$$

In the decoherent case (e.g. for large mass differences, thus $C_{ik} \to 0$ if $i \neq k$) only the terms $i = k, j = l$ contribute, yielding

$$d\sigma_{ijkl} \to \frac{|M_{ij}^p|^2}{2\sqrt{\lambda(s,m_1^2,m_2^2)}} d\Phi_p = d\sigma_{ij}(m_i^2, m_j^2) \tag{7.24}$$

$$dB_{ik} \to \frac{1}{2m_i\Gamma_i} |M_i^-|^2 d\Phi_3 = \frac{d\Gamma_i(m_i^2)}{\Gamma_i} \tag{7.25}$$

$$dB_{jl} \to \frac{1}{2m_j\Gamma_j} |M_j^+|^2 d\Phi_4 = \frac{d\Gamma_j(m_j^2)}{\Gamma_j}, \tag{7.26}$$

where $d\sigma_{ij}(m_i^2, m_j^2)$ is the production cross-section for two on-shell sleptons i, j, and $d\Gamma_i(m_i)^2$ is the partial decay-width of an on-shell lepton i (and analogous for $d\Gamma_j(m_j^2)$). Integration over all phase space just yields the well known formula for decoherent production and subsequent decay,

$$\sigma = \sum_{ij} \sigma_{ij} Br_i Br_j, \tag{7.27}$$

with the integrated slepton production cross-section σ_{ij} and the branching ratios Br_i of the sleptons.

7.3 Cross-sections and distributions

7.3.1 Total cross-section

In order to actually calculate the total cross-section, we can choose any parametrization of the phase space because we integrate over all variables. The most convenient choice is to express the production and decay factors in their respective center-of-mass frames, so we can just take the simple results of section 7.1. The only exception is that the on-shell masses of the sleptons, m_3^2, m_4^2, must be replaced by the off-shell invariant masses, p_3^2, p_4^2 (which are now phase space variables), because the intermediate sleptons are virtual particles. We do not use the factorized form of the squared amplitude from the previous section, but use the more condensed and general complete squared amplitude. By carefully comparing (7.3),(7.9) with (7.18), we get

$$\begin{aligned} d\sigma &= \frac{1}{64\pi^2 s} \frac{|\vec{p}_3|}{|\vec{p}_1|} \frac{|\vec{p}_5|}{16\pi^2\sqrt{p_3^2}} \frac{|\vec{p}_6|}{16\pi^2\sqrt{p_4^2}} |M(\theta_3, p_3^2, p_4^2)|^2 d\Omega_3 d\Omega_5^* d\Omega_6^* \frac{1}{2\pi} dp_3^2 \frac{1}{2\pi} dp_4^2 \\ &= \frac{|\vec{p}_3||\vec{p}_5||\vec{p}_6|}{2^{16}\pi^8 s|\vec{p}_1|\sqrt{p_3^2}\sqrt{p_4^2}} |M(\theta_3, p_3^2, p_4^2)|^2 d\Omega_3 d\Omega_5^* d\Omega_6^* dp_3^2 dp_4^2, \end{aligned} \tag{7.28}$$

where $|M(\theta_3, p_3^2, p_4^2)|^2$ is the complete squared amplitude for the process. The momenta are expressed in the respective center-of-mass frames of the production ($|\vec{p}_1|, |\vec{p}_3|$) and the decays ($|\vec{p}_5|, |\vec{p}_6|$). They can be written invariantly as functions of the particle masses, the beam energy and p_3^2, p_4^2. A full list can be found in section 7.4. Thus written, the differential cross-section depends only on θ_3 through the squared amplitude. $d\Omega = d\cos\theta d\phi$ are solid angle elements. The integrals over the solid angles of the decays, $d\Omega_5^*, d\Omega_6^*$ and the production azimuth, $d\phi_3$ are trivial, yielding factors of $4\pi, 4\pi$ and 2π, respectively:

$$d\sigma = \frac{|\vec{p}_3||\vec{p}_5||\vec{p}_6|}{2^{11}\pi^5 s|\vec{p}_1|\sqrt{p_3^2}\sqrt{p_4^2}} |M(\theta_3, p_3^2, p_4^2)|^2 d\cos\theta_3 dp_3^2 dp_4^2 \tag{7.29}$$

In our numerical work, we actually use the method of the previous section, factorizing the squared amplitude and integrate over the intermediate momenta using the delta functions of the propagators. Here we just write

$$\sigma = \int_0^\pi d\theta_3 \sin\theta_3 \int dp_3^2 \int dp_4^2 \frac{|\vec{p}_3||\vec{p}_5||\vec{p}_6|}{2^{11}\pi^5 s|\vec{p}_1|\sqrt{p_3^2}\sqrt{p_4^2}} |M(\theta_3, p_3^2, p_4^2)|^2 \qquad (7.30)$$

7.3.2 Angular distributions

The above result for the differential cross-section, (7.28), expressed in terms of the center-of-mass frame variables is our starting point for the calculation of various distributions. To simplify our discussion, we make the following formal substitution,

$$f(\theta_3) \equiv \int dp_3^2 \int dp_4^2 \frac{|\vec{p}_3||\vec{p}_5||\vec{p}_6|}{2^{16}\pi^8 s|\vec{p}_1|\sqrt{p_3^2}\sqrt{p_4^2}} |M(\theta_3, p_3^2, p_4^2)|^2, \qquad (7.31)$$

thus gathering all terms not relevant for the calculation of distributions with respect to final particles. The differential cross-section is now simply written as

$$d\sigma = f(\theta_3) d\Omega_3 d\Omega_5^* d\Omega_6^*. \qquad (7.32)$$

In order to calculate the angular distributions $\frac{d\sigma}{d\cos\theta_5}, \frac{d\sigma}{d\cos\theta_6}$ of the final leptons with respect to the measurable polar angles θ_5, θ_6 (i.e. measured in relation to the beam pipe), we need to transform the decay distributions given in the rest frames of the decays to the center-of-mass frame of the total process. This can be done in two steps. The first is, to boost the spherically symmetric decay distribution in the direction of the decaying particle with its velocity $v = k/E$. For particle 5, assuming it to be massless, using the results of appendix B, we get

$$\cos\theta_5^* \to \cos\theta_5', \quad \phi_5^* \to \phi_5'$$

with

$$\begin{aligned} \cos\theta_5^* &= \frac{\cos\theta_5' - v_3}{1 - v_3\cos\theta_5'} \\ \phi_5^* &= \phi_5' \end{aligned} \qquad (7.33)$$

where θ_5', ϕ_5' are the angles in the boosted frame (i.e. the z'-axis points in the direction of the velocity vector $\vec{v}_3$). In the boosted frame, the decay is no longer spherically symmetric but more pronounced in the forward boost direction. The decay is still rotationally invariant around the boost direction.

The masslessness of the final particle implies that θ_5' ranges from 0 to π. If it would be massive, its velocity could be smaller than the boost velocity. This would exclude the decay into directions opposite to the boost direction, resulting in a minimal polar angle, $\theta_5' > \theta_5^{min'}$. The transformation of the differentials is now easy to calculate:

$$\begin{aligned} d\cos\theta_5^* &= \frac{d\cos\theta_5^*}{d\cos\theta_5'} d\cos\theta_5' & (7.34)\\ &= \frac{1-v_3^2}{(1-v_3\cos\theta_5')^2} d\cos\theta_5' & (7.35)\\ d\phi_5^* &= d\phi_5', & (7.36)\end{aligned}$$

and the cross section is given by

$$d\sigma = f(\theta_3)\frac{1-v_3^2}{(1-v_3\cos\theta_5')^2} d\Omega_3 d\Omega_5' d\Omega_6^*. \tag{7.37}$$

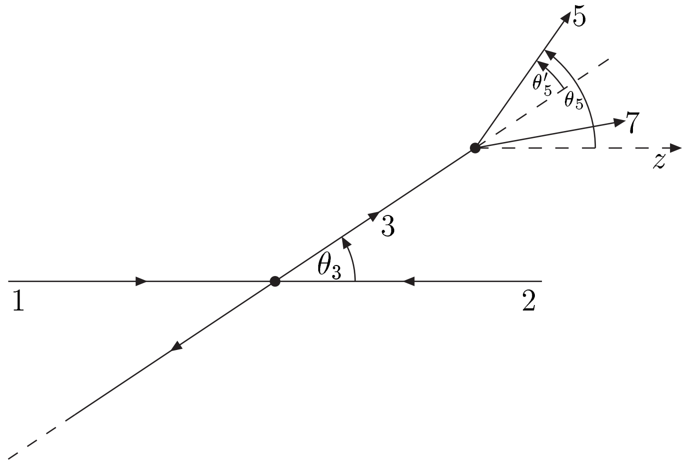

The final step will be to express the θ_5', ϕ_5' in terms of the angles θ_5, ϕ_5 in the beam-pipe frame. We use spherical trigonometry (appendix C.1) to get

$$\cos\theta_5' = \cos\theta_3\cos\theta_5 + \sin\theta_3\sin\theta_5\cos(\phi_5-\phi_3), \tag{7.38}$$

which is the only term we need because ϕ_5^* does not appear and the solid angle element is invariant under such a rotation of frames: $d\Omega_5' = d\Omega_5$. The cross-section becomes

$$d\sigma = 4\pi f(\theta_3)\frac{1-v_3^2}{(1-v_3(\cos\theta_3\cos\theta_5+\sin\theta_3\sin\theta_5\cos(\phi_5-\phi_3)))^2} d\Omega_3 d\Omega_5, \tag{7.39}$$

where we have already integrated over $d\Omega_6^*$. The integration over the production azimuthal angle ϕ_3 can be performed analytically, using (C.3),

$$d\sigma = 4\pi f(\theta_3)\frac{2\pi(1-v_3^2)(1-v_3\cos\theta_3\cos\theta_5)d\cos\theta_3 d\cos\theta_5 d\phi_5}{(1-v_3\cos(\theta_3-\theta_5))^{3/2}(1-v_3\cos(\theta_3+\theta_5))^{3/2}}. \tag{7.40}$$

Here we can see that the cross section is, after the integration over the production azimuth, independent of the final lepton's azimuthal angle ϕ_5. We finally get for the differential cross-section:

$$\frac{d\sigma}{d\cos\theta_5} = 2^4\pi^3\int_0^\pi f(\theta_3)\frac{(1-v_3^2)(1-v_3\sin\theta_3\sin\theta_5)\sin\theta_3 d\theta_3}{(1-v_3\cos(\theta_3-\theta_5))^{3/2}(1-v_3\cos(\theta_3+\theta_5))^{3/2}} \tag{7.41}$$

The distribution for the other lepton, $\frac{d\sigma}{d\cos\theta_6}$, can be calculated analogously by changing the particle indices $3 \to 4$, $5 \to 6$ and using the production distribution of slepton 4, which is simply given by $f(\pi-\theta_4)$ due to momentum conservation at the production level. We obtain:

$$\frac{d\sigma}{d\cos\theta_6} = 2^4\pi^3\int_0^\pi f(\pi-\theta_4)\frac{(1-v_4^2)(1-v_4\sin\theta_4\sin\theta_6)\sin\theta_4 d\theta_4}{(1-v_4\cos(\theta_4-\theta_6))^{3/2}(1-v_4\cos(\theta_4+\theta_6))^{3/2}} \tag{7.42}$$

7.3.3 Energy distributions

We start again with (7.32), now with the energy E_5^* in the rest frame of the slepton decay not integrated over,

$$d\sigma = f(\theta_3)d\Omega_3\delta(E_5^*-\bar{E}_5)dE_5^* d\Omega_5^* d\Omega_6^*, \tag{7.43}$$

where $\bar{E}_5 = \sqrt{m_5^2+|\vec{p}_5|}$, with the momentum given in the rest frame of the decay. E_5^* must be expressed in terms of the energy in the boosted frame, E_5', which is the same as the energy in the beam-pipe frame E_5, since the two frames are connected by a rotation. Using the results of appendix B, we get

$$E_5^* = \frac{E_5}{\gamma_3(1+v_3\cos\theta_5^*)}. \tag{7.44}$$

So the cross-section becomes

$$d\sigma = 4\pi f(\theta_3)\delta\left(\frac{E_5}{\gamma_3(1+v_3\cos\theta_5^*)}-\bar{E}_5\right)\frac{dE_5}{\gamma_3(1+v_3\cos\theta_5^*)}d\Omega_3 d\cos\theta_5^* d\phi_5^*, \tag{7.45}$$

where we have already integrated over $d\Omega_6^*$. Using (C.4), the integration over $\cos\theta_5^*$ and ϕ_5^* yields

$$d\sigma = 8\pi^2 f(\theta_3)\frac{1+v_3(\cos\theta_5^*)_0}{v_3 E_5}dE_5 d\Omega_3, \tag{7.46}$$

where $(\cos\theta_5^*)_0$ is the zero of the argument of the delta function in (7.45),

$$(\cos\theta_5^*)_0 = \frac{E_5-\gamma_3\bar{E}_5}{\gamma_3 v_3\bar{E}_5}. \tag{7.47}$$

The existence of such a zero requires

$$-1 < \frac{E_5-\gamma_3\bar{E}_5}{\gamma_3 v_3\bar{E}_5} < 1, \tag{7.48}$$

otherwise, the integral over $\cos\theta_5^*$ yields zero. We finally get

$$\frac{d\sigma}{dE_5} = 2^4\pi^3\int_0^\pi d\theta_3\frac{f(\theta_3)\sin\theta_3}{\gamma_3 v_3 E_5}\Theta(E_5-E_5^{min})\Theta(E_5^{max}-E_5), \tag{7.49}$$

where $\Theta(x-y)$ is the usual step function

$$\Theta(x-y) = \begin{cases} 0 & \text{if } x < y \\ 1 & \text{if } x \geq y \end{cases}$$

and the energy limits are given by

$$E_5^{min} = \gamma_3\bar{E}_5(1-v_3), \qquad E_5^{max} = \gamma_3\bar{E}_5(1+v_3). \tag{7.50}$$

The energy distribution is flat between the kinematical limits E_5^{min}, E_5^{max}. Using this method also for the second decay, we can easily calculate the double differential cross-section $\frac{d\sigma}{dE_5 dE_6}$. We find

$$\frac{d\sigma}{dE_5 dE_6} = (2\pi)^3\int_0^\pi d\theta_3\frac{d\theta_3 f(\theta_3)\sin\theta_3}{(\gamma_3 v_3 E_5)(\gamma_4 v_4 E_6)}\Xi(E_5,E_6), \tag{7.51}$$

where $\Xi(E_5,E_6)$ is the following combination of step functions

$$\Xi(E_5,E_6) = \Theta(E_5-E_5^{min})\Theta(E_5^{max}-E_5)\Theta(E_6-E_6^{min})\Theta(E_6^{max}-E_6),$$

and the energy limits are given by

$$\begin{aligned} E_5^{min} &= \gamma_3\bar{E}_5(1-v_3), \qquad & E_5^{max} &= \gamma_3\bar{E}_5(1+v_3) \\ E_6^{min} &= \gamma_4\bar{E}_6(1-v_4), \qquad & E_6^{max} &= \gamma_4\bar{E}_6(1+v_4). \end{aligned} \tag{7.52}$$

In order to calculate the missing energy distribution $\frac{d\sigma}{d\not{E}}$, with $\not{E}$ being the energy of the outgoing neutralinos, we must integrate over configurations of the above double differential distribution such that

$$\underbrace{E_5 + E_6}_{\text{leptons}} = \sqrt{s} - \underbrace{(E_7 + E_8)}_{\not{E}}, \tag{7.53}$$

for a fixed $\not{E}$, so we obtain

$$\frac{d\sigma}{d\not{E}} = \int dE_5 \int dE_6 \frac{d\sigma}{dE_5 dE_6}(E_5, E_6)\delta(E_5 + E_6 - \sqrt{s} + \not{E}) \tag{7.54}$$

$$= \int_0^{\sqrt{s}} dE_5 \frac{d\sigma}{dE_5 dE_6}(E_5, \sqrt{s} - \not{E} - E_5). \tag{7.55}$$

7.3.4 Transverse momentum distribution

We start again with (7.32) (already integrated over $d\Omega_6^*$):

$$d\sigma = 4\pi f(\theta_3) d\Omega_3 d\Omega_5^* \delta(E_5^* - \bar{E}_5) dE_5^* \tag{7.56}$$

First, we perform the transformation to the boosted decay-frame,

$$E_5^*, \theta_5^*, \phi_5^* \rightarrow E_5'(= E_5), \theta_5', \phi_5' \tag{7.57}$$

$$E_5^* = \gamma_3 E_5 (1 - v_3 \cos\theta_5') \tag{7.58}$$

$$\cos\theta_5^* = \frac{\cos\theta_5' - v}{1 - v\cos\theta_5'} \tag{7.59}$$

$$\phi_5^* = \phi_5'. \tag{7.60}$$

Here, we have a nontrivial transformation of more than just one variable, so we need the functional determinant in order to calculate the transformation of the volume-element:

$$dE_5^* d\cos\theta_5^* = \left| \begin{pmatrix} \frac{\partial E_5^*}{\partial E_5} & \frac{\partial \cos\theta_5^*}{\partial E_5} \\ \frac{\partial E_5^*}{\partial \cos\theta_5'} & \frac{\partial \cos\theta_5^*}{\partial \cos\theta_5'} \end{pmatrix} \right| dE_5 d\cos\theta_5' \tag{7.61}$$

$$= \frac{\gamma_3(1 - v_3^2)}{1 - v_3\cos\theta_5'} dE_5 d\cos\theta_5'. \tag{7.62}$$

We obtain

$$d\sigma = 4\pi f(\theta_3) d\Omega_3 \delta(\gamma_3 E_5(1 - v_3\cos\theta_5') - \bar{E}_5) \frac{\gamma_3(1 - v_3^2)}{1 - v_3\cos\theta_5'} dE_5 d\cos\theta_5' d\phi_5'. \tag{7.63}$$

The second step is to express the variabels θ_5', ϕ_5' in terms of the variables in the beam-pipe frame θ_5, ϕ_5. Using (C.1), we obtain

$$\begin{aligned}
d\sigma &= 4\pi f(\theta_3) d\Omega_3 \\
&\quad \times \delta(\gamma_3 E_5 (1 - v_3(\cos\theta_3\cos\theta_5 + \sin\theta_3\sin\theta_5\cos(\phi_5 - \phi_3))) - \bar{E}_5) \\
&\quad \times \frac{\gamma_3(1-v_3^2) dE_5 d\cos\theta_5 d\phi_5}{1 - v_3(\cos\theta_3\cos\theta_5 + \sin\theta_3\sin\theta_5\cos(\phi_5 - \phi_3))}. \qquad (7.64)
\end{aligned}$$

Now we can perform the integration over ϕ_3 analytically. Because this is an integral over a function of $\cos(\phi_5 - \phi_3)$ over a complete cycle, $0 \to 2\pi$ of θ_3, the result will not depend on the final particle's azimuthal angle ϕ_5, so we can put it to zero from the beginning. For the integration, we use (C.4) where $g(\phi_3)$ is the argument of the delta function in (7.64) with the derivative

$$|g'(\phi_3)| = \gamma_3 v_3 E_5 \sin\theta_5 \sin\theta_3 |\sin\phi_3|, \qquad (7.65)$$

and the zeros, $g(\phi_{3_i}) = 0$,

$$\begin{aligned}
\phi_{3_1} &= \arccos(\cos\phi_3)_0, \quad \phi_{3_2} = 2\pi - \arccos(\cos\phi_3)_0 \\
\text{with } (\cos\phi_3)_0 &= \frac{\gamma_3 E_5(1 - v_3\cos\theta_5\cos\theta_3) - \bar{E}_5}{\gamma_3 v_3 E_5 \sin\theta_5\sin\theta_3}. \qquad (7.66)
\end{aligned}$$

Thus, the zeros only exist if $-1 < (\cos\phi_3)_0 < 1$, otherwise the cross-section becomes zero. This is just the mathematical expression of the kinematical limits. The contributions from the two zeros yield the same result (they are plugged into $\cos\phi$ and $|\sin\phi|$ which yield the same result for $\phi = \phi_3$ and $\phi = 2\pi - \phi_3$). We finally get (integration over ϕ_5 performed):

$$\frac{d\sigma}{dE_5 d\cos\theta_5} = \int_0^\pi \frac{2^4\pi^2 f(\theta_3)\sin\theta_3 (E_5/\bar{E}_5) d\theta_3}{\sqrt{\gamma_3^2 v_3^2 E_5^2 \sin^2\theta_5 \sin^2\theta_3 - (\gamma_3 E_5 - \gamma_3 v_3 E_5 \cos\theta_5\cos\theta_3 - \bar{E}_5)^2}} \qquad (7.67)$$

if $-1 < (\cos\phi_3)_0 < 1$, otherwise the cross section becomes zero. The distribution with respect to lepton l_β (6) can be calculated analogously with the substitutions $3 \to 4, 5 \to 6$ and $f(\theta_3) \to f(\pi - \theta_4)$.

Using the above double-differential distribution, it is an easy task to calculate the transverse momentum distribution of the particle. We just have to integrate over phase space configurations such that $E_5 \sin\theta_5 = p_{\perp_5}$ (massless particle) for a fixed $p_{\perp_5}$. So we have

$$\begin{aligned}
\frac{d\sigma}{dp_{\perp_5}} &= \int dE_5 \int d\cos\theta_5 \frac{d\sigma}{dE_5 d\cos\theta_5}(E_5, \theta_5)\delta(E_5\sin\theta_5 - p_{\perp_5}) \\
&= \int_{-1}^{+1} \frac{d\cos\theta_5}{\sin\theta_5} \frac{d\sigma}{dE_5 d\cos\theta_5}\left(\frac{p_{\perp_5}}{\sin\theta_5}, \theta_5\right). \qquad (7.68)
\end{aligned}$$

7.4 Summary

Here we present all results in a condensed form for reference purposes.

Total cross-section

$$\sigma = \int dp_3^2 \int dp_4^2 \int_0^\pi d\theta_3 \frac{|\vec{p}_3||\vec{p}_5||\vec{p}_6|}{2^{11}\pi^5 s|\vec{p}_1|\sqrt{p_3^2}\sqrt{p_4^2}} |M(\theta_3, p_3^2, p_4^2)|^2 \sin\theta_3 \tag{7.69}$$

Angular distribution of lepton 5

$$\begin{aligned}\frac{d\sigma}{d\cos\theta_5} = \int dp_3^2 \int dp_4^2 \int_0^\pi d\theta_3 \frac{|\vec{p}_3||\vec{p}_5||\vec{p}_6|}{2^{12}\pi^5 s|\vec{p}_1|\sqrt{p_3^2}\sqrt{p_4^2}} |M(\theta_3, p_3^2, p_4^2)|^2 \\ \times \frac{(1-v_3^2)(1-v_3\cos\theta_3\cos\theta_5)\sin\theta_3}{(1-v_3\cos(\theta_3-\theta_5))^{3/2}(1-v_3\cos(\theta_3+\theta_5))^{3/2}}\end{aligned} \tag{7.70}$$

Angular distribution of lepton 6

$$\begin{aligned}\frac{d\sigma}{d\cos\theta_6} = \int dp_3^2 \int dp_4^2 \int_0^\pi d\theta_4 \frac{|\vec{p}_3||\vec{p}_5||\vec{p}_6|}{2^{12}\pi^5 s|\vec{p}_1|\sqrt{p_3^2}\sqrt{p_4^2}} |M(\pi-\theta_4, p_3^2, p_4^2)|^2 \\ \times \frac{(1-v_4^2)(1-v_4\cos\theta_4\cos\theta_6)\sin\theta_4}{(1-v_4\cos(\theta_4-\theta_6))^{3/2}(1-v_4\cos(\theta_4+\theta_6))^{3/2}}\end{aligned} \tag{7.71}$$

Energy and missing energy distributions

$$\frac{d\sigma}{dE_5 dE_6} = \int dp_3^2 \int dp_4^2 \int_0^\pi d\theta_3 \frac{|\vec{p}_3||\vec{p}_5||\vec{p}_6|}{2^{13}\pi^5 s|\vec{p}_1|\sqrt{p_3^2}\sqrt{p_4^2}} \frac{|M(\theta_3, p_3^2, p_4^2)|^2 \sin\theta_3}{\gamma_3 v_3 E_5^* \gamma_4 v_4 E_6^*} \Xi(E_5, E_6) \tag{7.72}$$

with

$$\begin{aligned}\Xi(E_5,E_6) = \Theta(E_5 - E_5^{min})\Theta(E_5^{max} - E_5)\Theta(E_6 - E_6^{min})\Theta(E_6^{max} - E_6) \\ E_5^{min} = \gamma_3\bar{E}_5(1-v_3), \quad E_5^{max} = \gamma_3\bar{E}_5(1+v_3) \\ E_6^{min} = \gamma_4\bar{E}_6(1-v_4), \quad E_6^{max} = \gamma_4\bar{E}_6(1+v_4)\end{aligned} \tag{7.73}$$

The missing energy distribution ($\not{E}$ is defined as the summed energy of the outgoing neutralinos) is then given by

$$\begin{aligned}\frac{d\sigma}{d\not{E}} &= \int dE_5 \int dE_6 \frac{d\sigma}{dE_5 dE_6}(E_5, E_6)\delta(E_5 + E_6 - \sqrt{s} + \not{E}) \\ &= \int_0^{\sqrt{s}} dE_5 \frac{d\sigma}{dE_5 dE_6}(E_5, \sqrt{s} - \not{E} - E_5)\end{aligned} \tag{7.74}$$

Energy-angular and transverse momentum distributions

$$\begin{aligned}\frac{d\sigma}{dE_5 d\cos\theta_5} &= \int dp_3^2 \int dp_4^2 \int_0^{\pi} d\theta_3 \frac{|\vec{p}_3||\vec{p}_5||\vec{p}_6|}{2^{12}\pi^6 s|\vec{p}_1|\sqrt{p_3^2}\sqrt{p_4^2}} |M(\theta_3, p_3^2, p_4^2)|^2 \\ &\times \frac{\sin\theta_3 (E_5/\bar{E}_5)}{\sqrt{\gamma_3^2 v_3^2 E_5^2 \sin^2\theta_5 \sin^2\theta_3 - (\gamma_3 E_5 - \gamma_3 v_3 E_5 \cos\theta_5 \cos\theta_3 - \bar{E}_5)^2}} \\ &\times \Pi(E_5, \theta_5, \theta_3) \end{aligned} \tag{7.75}$$

with

$$\Pi(E_5, \theta_5, \theta_3) = \Theta\left(1 - \left|\frac{\gamma_3 E_5 (1 - v_3 \cos\theta_5 \cos\theta_3) - \bar{E}_5}{\gamma_3 v_3 E_5 \sin\theta_5 \sin\theta_3}\right|\right) \tag{7.76}$$

The transverse momentum distribution is then given by

$$\begin{aligned}\frac{d\sigma}{dp_{\perp 5}} &= \int dE_5 \int d\cos\theta_5 \frac{d\sigma}{dE_5 d\cos\theta_5}(E_5, \theta_5)\delta(E_5 \sin\theta_5 - p_{\perp 5}) \\ &= \int_{-1}^{+1} \frac{d\cos\theta_5}{\sin\theta_5} \frac{d\sigma}{dE_5 d\cos\theta_5}\left(\frac{p_{\perp 5}}{\sin\theta_5}, \theta_5\right) \end{aligned} \tag{7.77}$$

Constants The following definitions apply in all cases:

$$|\vec{p}_1| = \sqrt{\frac{1}{4s}\lambda(s, m_1^2, m_2^2)} \tag{7.78}$$

$$|\vec{p}_3| = \sqrt{\frac{1}{4s}\lambda(s, p_3^2, p_4^2)},\ E_3 = \sqrt{m_3^2 + |\vec{p}_3|^2},\ E_4 = \sqrt{m_4^2 + |\vec{p}_3|^2} \tag{7.79}$$

$$|\vec{p}_5| = \sqrt{\frac{1}{4p_3^2}\lambda(p_3^2, m_5^2, m_7^2)}, \quad \bar{E}_5 = \sqrt{m_5^2 + |\vec{p}_5|^2} \tag{7.80}$$

$$|\vec{p}_6| = \sqrt{\frac{1}{4p_4^2}\lambda(p_4^2, m_6^2, m_8^2)}, \quad \bar{E}_6 = \sqrt{m_6^2 + |\vec{p}_6|^2} \tag{7.81}$$

$$v_i = \frac{|\vec{p}_3|}{E_i}, \quad \gamma_i = \frac{1}{\sqrt{1 - v_i^2}}, \quad i = 3, 4 \tag{7.82}$$

$$\lambda(a, b, c) = (a - b - c)^2 - 4bc \tag{7.83}$$

The lepton masses m_1, m_2, m_5, m_6 are put to zero. The squared amplitude is given by

$$\begin{aligned}|M(\theta_3, p_3^2, p_4^2)|^2 &= \sum_{i,j}\sum_{k,l}(M_{ij}^s M_{kl}^{s*} + M_{ij}^t M_{kl}^{t*} + M_{ij}^s M_{kl}^{t*} + M_{ij}^t M_{kl}^{s*}) \\ &\times A_{ik}(p_3^2) A_{jl}(p_4^2) \\ &\times (M_i^- M_k^{-*})(M_j^+ M_l^{+*}) \end{aligned} \tag{7.84}$$

with the summations i, j, k, l either over all charged sleptons (1,...,6) or over all sneutrinos (1,2,3). The respective production and decay amplitudes can be found in section 6.3. In our numerical work, the squared propagators A_{mn} are given by (A.5). The squared amplitude is a function of the helicities of the ingoing electron (h_-), ingoing positron (h_+), the outgoing leptons (h_5, h_6) and the outgoing neutralinos/charginos (h_7, h_8). We always sum over the neutralino/chargino helicities. For arbitrarily polarized beams, characterized by the electron and positron polarizations, $P_-, P_+ \in [-1, +1]$, we perform the weighted mean over the initial helicity amplitudes ($h_-, h_+ = -1, +1$):

$$|M(P_-, P_+)|^2_{h_5,h_6} = \frac{1}{4} \sum_{h_-,h_+} (1 + h_- P_-)(1 + h_+ P_+) |M|^2_{h_-,h_+,h_5,h_6} \tag{7.85}$$

In cases where we are not interested in the helicities of the final leptons, we perform the unweighted sum over these helicity states:

$$|M(P_-, P_+)|^2 = \sum_{h_5,h_6} |M(P_-, P_+)|^2_{h_5,h_6} \tag{7.86}$$

Chapter 8

Numerical results

8.1 General calculational scheme

Before we come to the numerical analysis, we would like to present the general method of performing our calculations. The three mSUGRA benchmark-scenarios [17, 18, 19] form the basis of our numerical work. They do not only give us the five input parameters $m_0, m_{1/2}, A_0, \tan\beta, \mathrm{sign}(\mu)$, but also all necessary MSSM parameters at the electroweak scale calculated from the input parameters via the MSSM RGEs.

1. Gaugino-mixings and -masses The first step is to calculate the neutralino and the chargino mixing matrices and mass eigenvalues numerically according to sections 2.4.1 and 2.4.2, respectively, for each of the three mSUGRA scenarios. The neutralino/chargino sector is assumed to be unaffected by whatever extensions we make to include lepton flavor violation.

2. Slepton-mixings and -masses Next, we calculate the charged slepton and sneutrino mixing matrices and masses in the LFV models for all mSUGRA scenarios according to sections 2.4.3 and 2.4.4, respectively.

3. Slepton widths Having obtained the masses, we can now calculate the slepton widths, either with our own decay amplitudes or by using CompHEP [23]. In the minimal LFV model, the $\tilde{\nu}_\tau$ mass is a free parameter, so it may be necessary to include a mass dependent width.

4. The amplitude Now, we have all necessary parameters to calculate the amplitudes and cross-sections. These calculations are performed with Mathematica under the following assumptions:

- The electron and the muon are massless.
- The tau-mass is neglected kinematically, i.e. it is only retained in the vertices.
- Narrow-width approximation of the slepton-propagators.
- No interference of outgoing neutralinos.

Our amplitudes have been calculated for arbitrary lepton flavors α, β and gauginos a, b in the final state. For our numerical analysis, we restrict the processes to

$$\begin{aligned} e^+e^- &\to \tau^+e^-\tilde{\chi}_1^0\tilde{\chi}_1^0 \\ e^+e^- &\to \tau^+e^-\tilde{\chi}_1^+\tilde{\chi}_1^-, \end{aligned}$$

i.e. $\alpha = 1, \beta = 3$; $a, b = 1$ in all cases.

8.2 Standard model parameters

For all calculations, we use the following values of the SM parameters at the electroweak scale, consistent with [17, 18, 19]:

Parameter	Explanation	Value
m_Z	Z-boson mass	91.187 GeV
m_t	top-quark mass	175 GeV
m_τ	τ-lepton mass	1.777 GeV
α_{EM}	EM-coupling constant	7.76×10^{-3}
$\sin^2\theta_W$	θ_W: Weinberg angle	0.2315

Some derived values are

- W-boson mass: $m_W = m_Z \cos\theta_W = 79.94$ GeV
- Electron charge: $e = \sqrt{4\pi\alpha_{EM}} = 0.31$
- Higgs vacuum expectation value: $v = \frac{\sqrt{2}\sin\theta_W \cos\theta_W m_Z}{e} = 175.5$ GeV

In addition, we need the Kobayashi-Maskawa matrix V^{KM} for the SU(5)-model. We use the following parametrization and angles ($s_{12} = \sin\theta_{12}, c_{12} = \cos\theta_{12}$, etc.), [1]

$$V^{KM} = \begin{pmatrix} c_{12} & s_{12} & s_{13} \\ -s_{12}c_{23} - c_{12}s_{23}s_{13} & c_{12}c_{23} - s_{12}s_{23}s_{13} & s_{23} \\ s_{12}s_{23} - c_{12}c_{23}s_{13} & -c_{12}s_{23} - s_{12}c_{23}s_{13} & s_{23} \end{pmatrix}$$

$$s_{12} = 0.221, \quad s_{23} = 0.040, \quad s_{13} = 0.0035 \tag{8.1}$$

where we assumed $c_{13} \approx 1$ and neglected the CP violating phase δ.

8.3 The scenarios

Here we introduce the three benchmark scenarios that build the basis of our numerical work. The five input parameters of these mSUGRA scenarios are given in Table 8.1. These scenarios were created for different reasons.

Parameter	Explanation	I	II	III
m_0/GeV	Common scalar mass at M_{GUT}	100	160	100
$m_{1/2}$/GeV	Common gaugino mass at M_{GUT}	200	200	200
A_0/GeV	Common trilinear coupling at M_{GUT}	0	600	-715
$\tan\beta$	Ratio of Higgs VEVs at EW scale	3	30	3
sign(μ)	Sign of SUSY Higgs mix. term	+	+	+

Table 8.1: Input parameters for the three mSUGRA benchmark scenarios

Scenario I implies that the lighter neutral higgs boson h_0 can be observed at LEP2, so strictly speaking, it is already excluded. Scenario II was created for the opposite reason: It can not be observed at LEP2, because of its high common scalar mass. Scenario III has been chosen to create a light stop that can be observed at future colliders. Normally, squarks are heavier than sleptons but because of the large negative A_0, the stop left-right mixing is so strong that it pushes the lighter stop to 133 GeV, compared to heavy stop with 491 GeV. Using the input parameters one can calculate all MSSM parameters by applying the MSSM RGEs. This has been done in [17, 18, 19], yielding the values in Table 8.2. These values are then used by us to obtain the neutralino/chargino and slepton properties.

Parameter	Explanation	I	II	III
M_1	U(1) Gaugino mass	78.7	78.0	79.5
M_2	SU(2) Gaugino mass	152	150	153
μ	SUSY Higgs mixing term	316	263	435
$m_{\tilde{e}_L,\tilde{\mu}_L}$	Left slepton SSB mass, 1st 2 gener.	171	212	171
$m_{\tilde{\tau}_L}$	Left stau SSB mass	171	189	171
$m_{\tilde{e}_R,\tilde{\mu}_R}$	Right slepton SSB mass, 1st 2 gener.	127	179	127
$m_{\tilde{\tau}_R}$	Right stau SSB mass	126	115	125
A_τ	τ tri-linear SSB coupling	-133	384	-847

Table 8.2: MSSM parameters at the electroweak scale according to the mSUGRA input parameters of Table 8.1. All values are given in GeV.

8.3.1 Neutralinos and charginos

The neutralino and chargino properties are listed in Table 8.3 (scenario I), 8.4 (scenario II) and 8.5 (scenario III). The gauge components of the neutralinos are given in terms of $(\tilde{B}, \tilde{W}^0, \tilde{H}_1^0, H_2^0)$, and those of the charginos in terms of $(\tilde{W}^+, \tilde{H}_1^+)(\tilde{W}^-, \tilde{H}_2^-)$. In all three cases, the lightest neutralino is bino-

Particle	Mass/GeV	Decay Channel	Br	Gauge components
$\tilde{\chi}_1^0$	71.9	stable		(.97, -.15, .19, -.10)
$\tilde{\chi}_2^0$	130.4	$\tilde{\chi}_1^0 \tau^+ \tau^-$	0.24	(.21, .92, -.27, .17)
		$\tilde{\chi}_1^0 l^+ l^-$	0.20	
$\tilde{\chi}_3^0$	319.8	$\tilde{\chi}_1^\pm W^\mp$	0.31	(-.05i, .08i, .70i, .71i)
$\tilde{\chi}_4^0$	348.2	$\tilde{\chi}_1^\pm W^\mp$	0.26	(.14, -.34, -.64, .67)
$\tilde{\chi}_1^+$	127.9	$\tilde{\chi}_1^0 \bar{d} u$	0.28	(.91, -.42)(.96, -.28)
		$\tilde{\chi}_1^0 \bar{s} c$	0.28	
		$\tilde{\chi}_1^0 l^+ \nu_l$	0.15	
$\tilde{\chi}_2^+$	345.5	$\tilde{\chi}_2^0 W^+$	0.29	(.42, .91)(.28, .96)

Table 8.3: Neutralino and chargino properties in scenario I

Particle	Mass/GeV	Decay Channel	Br	Gauge components
$\tilde{\chi}_1^0$	74.8	stable		(.97, -.08, .20, -.06)
$\tilde{\chi}_2^0$	133.0	$\tilde{\tau}_1^\pm \tau^\mp$	0.50	(.15, .91, -.34, .18)
$\tilde{\chi}_3^0$	272.8	$\tilde{\chi}_1^\pm W^\mp$	0.27	(-.09i, .13i, .69i, .71i)
		$\tilde{\chi}_1^0 Z^0$	0.28	
$\tilde{\chi}_4^0$	293.0	$\tilde{\chi}_1^\pm W^\mp$	0.26	(.14, -.39, -.61, .68)
$\tilde{\chi}_1^+$	132.4	$\tilde{\tau}^+ \nu_\tau$	1.00	(.86, -.51)(.96, -.27)
$\tilde{\chi}_2^+$	294.8	$\tilde{\chi}_2^0 W^+$	0.31	(.51, .86)(.27, .96)

Table 8.4: Neutralino and chargino properties in scenario II

like, and the second lightest wino-like. The gaugino sector is quite similar comparing the three scenarios, because the common gaugino mass at the GUT scale $m_{1/2}$ is equal for all scenarios (see Table 8.1). The higgsino sector is more varied due to the variation in $\tan\beta$ and μ.

Particle	Mass/GeV	Decay Channel	Br	Gauge components
$\tilde{\chi}_1^0$	75.3	stable		(.99, -.10, .12, -.06)
$\tilde{\chi}_2^0$	139.0	$\tilde{\tau}_1^{\pm}\tau^{\mp}$	0.42	(.13, .97, -.19, .11)
$\tilde{\chi}_3^0$	437.9	$\tilde{t}_1^{\pm}t^{\mp}$	0.25	(-.04i, .06i, .70i, .71i)
		$\tilde{\chi}_1^{\pm}W^{\mp}$	0.16	
$\tilde{\chi}_4^0$	456.1	$\tilde{t}_1^{\pm}t^{\mp}$	0.40	(.10, -.23, -.68, .69)
$\tilde{\chi}_1^+$	138.1	$\tilde{t}^+\bar{b}$	0.59	(.96, -.29)(.98, -.17)
		$\tilde{\tau}_1^+\nu_\tau$	0.39	
$\tilde{\chi}_2^+$	454.3	$\tilde{t}^+\bar{b}$	0.63	(.29, .96)(.17, .98)

Table 8.5: Neutralino and chargino properties in scenario III

8.3.2 Sleptons

We now come to the slepton sector of the mSUGRA constrained MSSM. Generically, the charged slepton (mass)^2 matrix is given by

$$\begin{pmatrix} m^2_{\tilde{e}_L} & 0 & 0 & 0 & 0 & 0 \\ 0 & m^2_{\tilde{\mu}_L} & 0 & 0 & 0 & 0 \\ 0 & 0 & m^2_{\tilde{\tau}_L} & 0 & 0 & m^2_{\tilde{\tau}_{LR}} \\ 0 & 0 & 0 & m^2_{\tilde{e}_R} & 0 & 0 \\ 0 & 0 & 0 & 0 & m^2_{\tilde{\mu}_R} & 0 \\ 0 & 0 & m^2_{\tilde{\tau}_{LR}} & 0 & 0 & m^2_{\tilde{\tau}_R} \end{pmatrix}, \tag{8.2}$$

so the first two generations do not mix and can be labelled with their respective gauge labels. Additionally, the two are degenerate in both the right- and left-handed sector. The only nonvanishing left-right mixing occurs between the two staus and can be characterized by a mixing angle $\phi_{\tilde{\tau}_{LR}}$. The two mass eigenstates $\tilde{\tau}_1, \tilde{\tau}_2$ are labelled according to their mass value, $m_{\tilde{\tau}_1} < m_{\tilde{\tau}_2}$. The sneutrino mass matrix, lacking left-right mixing is diagonal, and degenerate in the first two generations. The sneutrinos can thus be labelled with their respective gauge labels. The slepton properties for the three scenarios are listed in Table 8.6. Comparing the scenarios, we can see that the first and third one yield a similar slepton sector due to their equal common scalar masses m_0 of 100 GeV, differing only in the $\tilde{\tau}$ mixing which is larger for scenario III because of the large A_0. The slepton masses in the second scenario are generally higher because of the greater common scalar mass $m_0 = 160$ GeV and the large $\tan\beta$. On the other hand $\tilde{\tau}_1$ is very light due to the small right-stau SSB mass at the electroweak scale (see Table 8.2) and a large left-right mixing angle, that pushes the mass of the lighter stau further down.

	Scenario I		Scenario II		Scenario III	
	Mass	Width	Mass	Width	Mass	Width
$\tilde{e}_L^-$	176.1	0.51	217.2	1.03	176.1	0.42
$\tilde{\mu}_L^-$	176.1	0.51	217.2	1.03	176.1	0.42
$\tilde{\tau}_2^-$	176.9	0.52	210.0	0.84	178.9	0.46
$\tilde{e}_R^-$	132.9	0.31	184.3	0.61	132.9	0.29
$\tilde{\mu}_R^-$	132.9	0.31	184.3	0.61	132.9	0.29
$\tilde{\tau}_1^-$	131.0	0.30	94.8	0.06	127.2	0.25
$\tilde{\nu}_e$	161.0	0.42	202.0	0.93	161.0	0.31
$\tilde{\nu}_\mu$	161.0	0.42	202.0	0.93	161.0	0.31
$\tilde{\nu}_\tau$	161.0	0.42	177.7	0.57	161.0	0.29
$\phi_{\tilde{\tau}_{LR}}$	.136(7.8°)		.432(24.8°)		.269(15.4°)	

Table 8.6: Slepton properties in the mSUGRA scenarios I, II, III. Mass and width values are in GeV. $\phi_{\tilde{\tau}_{LR}}$ is the left-right mixing angle for the staus in rad (deg).

8.4 Minimal LFV for sneutrinos

We are now in a position to apply the mSUGRA scenarios to the LFV models. First, we use our minimal LFV model (section 3.1) for the sneutrinos to extend the MSSM. Throughout this section, we only use unpolarized beams and sum over all final helicities.

Using the minimal LFV model for the sneutrinos, we effectively have a two dimensional slepton (mass)^2 matrix, and the mixing can be characterized by a mixing angle ϕ and a mass difference δm (see (3.3)). δm is defined as the difference between the $\tilde{\nu}_\tau$ mass in the LFV model and the $\tilde{\nu}_\tau$ mass in the flavor conserving MSSM. This means both ϕ and δm measure the shift from the MSSM. For the sneutrino process it is necessary to perform the calculations with a mass dependent width for the $\tilde{\nu}_\tau$, because it strongly varies. In all three scenarios, the dominant decay channels are [17, 18, 19]

$$\begin{aligned} \tilde{\nu}_\tau \quad \rightarrow \quad & \tilde{\chi}_1^+ \tau^- \\ & \tilde{\chi}_1^0 \nu_\tau \\ & \tilde{\chi}_2^0 \nu_\tau, \end{aligned}$$

which can be easily calculated using our own amplitudes (the last two decays require the last vertex in section 4.2).

Figure 8.1 shows the total cross section as a function of δm for a fixed value of $\phi = \pi/4$. The grey curves are calculated with a constant $\tilde{\nu}_\tau$ decay width, $\Gamma_{\tilde{\nu}_\tau}(\delta m = 0)$, i.e. using the MSSM value. The black ones are calculated using a mass dependent width. For scenarios I,III the curves follows closely the expected behaviour, as described in section 5.2. Scenario II obviously differs from this because the MSSM already has a nonvanishing mass difference $m_{\tilde{e}} - m_{\tilde{\tau}} \approx 25$ GeV, so we are far away from the degeneracy kink. Because we are far away from the Z resonance, the dominant contributions are the t-channel graphs. The finite rise for large $|\delta m|$ comes from kinematical mass effects that were neglected in the analytical calculation of section 5.2. As already mentioned, the shape of the degeneracy kink is modified by loop contributions but the position and the large mass difference limit are unaffected.

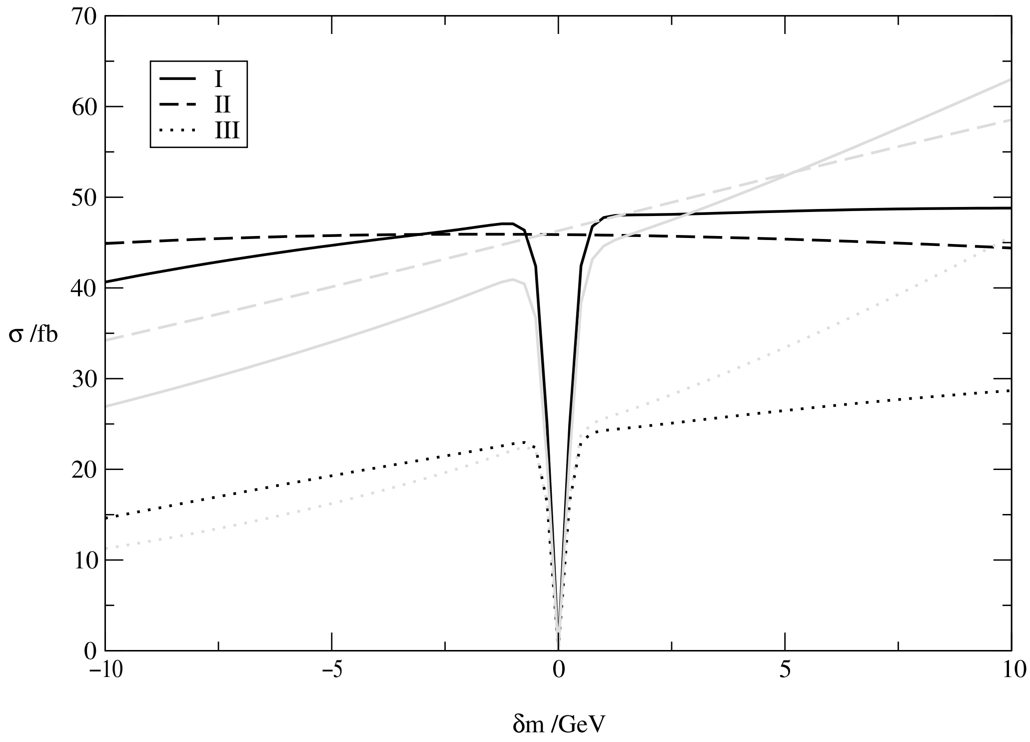

Figure 8.1: Total cross section as function of δm for $\phi = \pi/4$ ($\sqrt{s} = 500$ GeV). Grey: constant decay width, Black: mass dependent decay width

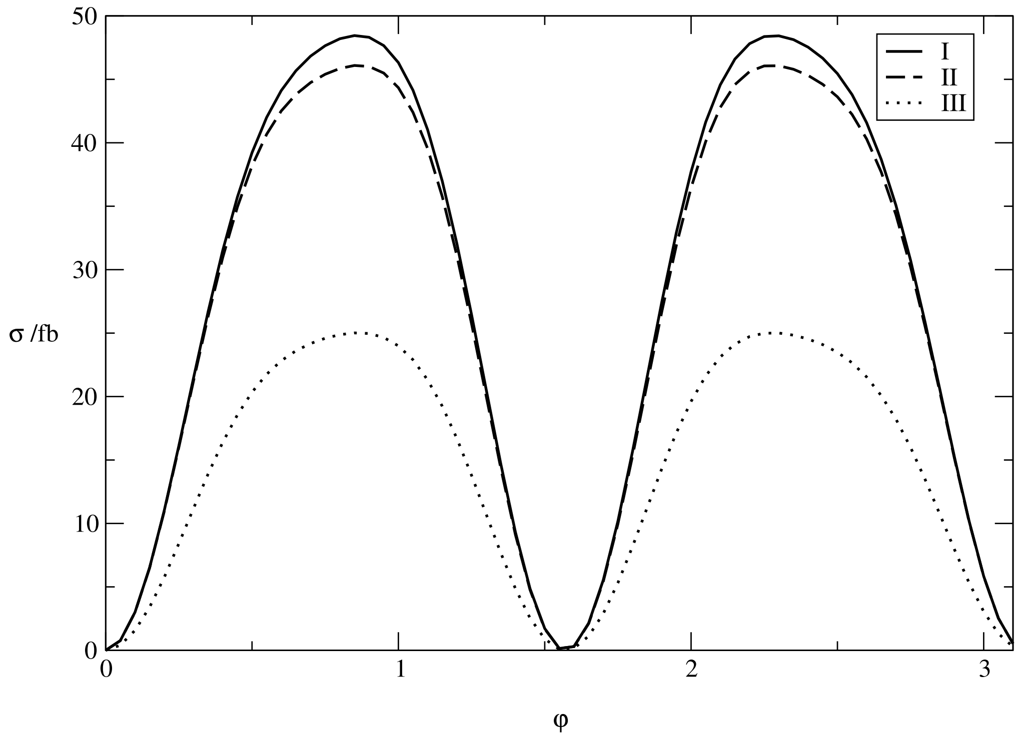

Figure 8.2: Total cross section as function of ϕ for $\delta m = 2$ GeV ($\sqrt{s} = 500$ GeV).

Figure 8.2 shows the total cross section as a function of the mixing angle ϕ for a fixed $\delta m = 2$ GeV. The curves follow more or less the expected behaviour of Figure 5.1, i.e. an approximate $\sin^2 2\phi$ dependence with higher order contributions around the maximal mixing with $\phi = \pi/4, 3\pi/4$. This also explains that the cross-section approximately just scales with the strength of the mixing.

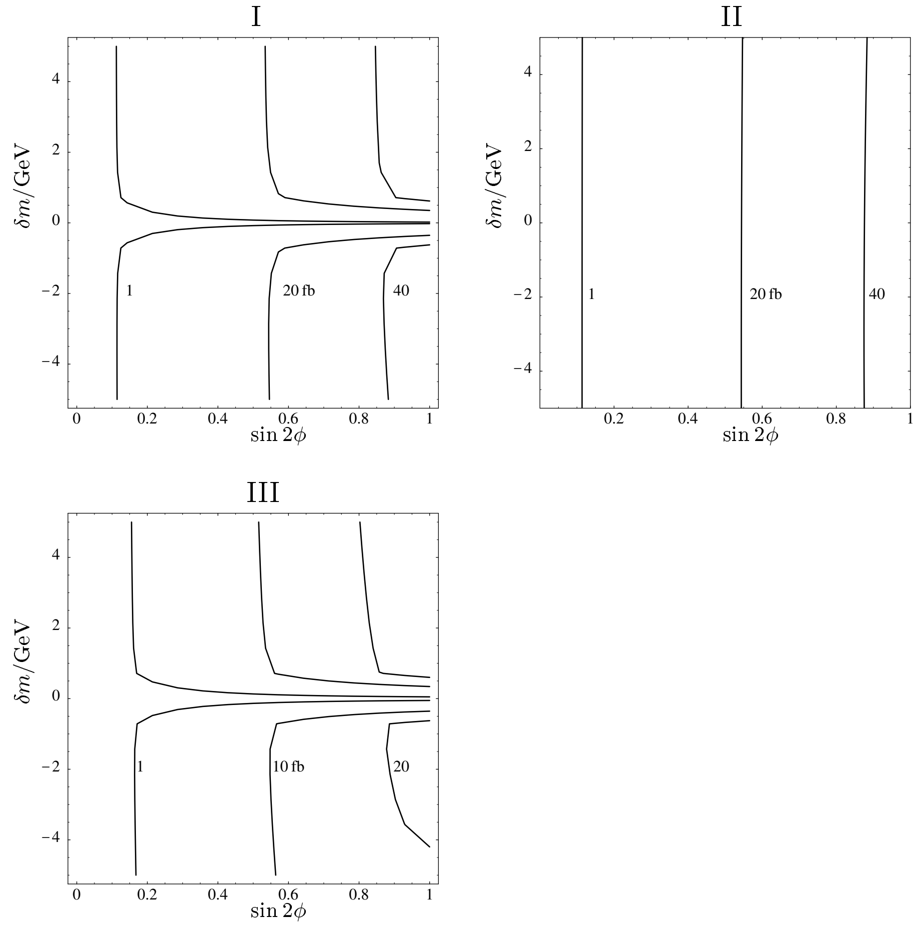

Figure 8.3: Total cross section as function of δm and $\sin 2\phi$ ($\sqrt{s} = 500$ GeV).

As a combination of both plots, Figure 8.3 shows the total cross section as a function of δm and $\sin 2\phi$ (because of the approximate $\sin^2 2\phi$ dependence). Such plots can be used to determine the parameter range $(\delta m, \phi)$ where the process can be observed experimentally. For scenario II the behaviour is quite trivial, being almost independent of δm in the observed range -5 GeV $< \delta m <$ 5 GeV.

8.5 Right-handed neutrino models

We now apply the three mSUGRA scenarios to the MSSM extensions ν_R and SU(5)ν_R. We always sum over final helicities.

8.5.1 Sneutrinos

We start with the easier sneutrino case. The corrections induced to the left-handed slepton sector are the same for both the ν_R and SU(5)ν_R (compare (3.8) with (3.23)), so we apply the three mSUGRA scenarios just to the ν_R model. Table 8.7 lists the sneutrino masses, widths and gauge components $(\tilde{\nu}_e, \tilde{\nu}_\mu, \tilde{\nu}_\tau)$. The mass eigenstates are not labelled according to their mass value but according to their resemblance to the gauge eigenstates, i.e. $\tilde{\nu}_1 \approx \tilde{\nu}_e$, $\tilde{\nu}_2 \approx \tilde{\nu}_\mu$, $\tilde{\nu}_3 \approx \tilde{\nu}_\tau$. Figure 8.4 shows the total cross-section (unpolarized) as a function of the beam energy. We can see that the third scenario yields the largest cross section due to its large lepton flavor mixing. The first scenario has a smaller cross-section because it is suppressed by the small mass differences, analogous to the minimal LFV model. Although we cosider $e - \tau$ mixing, the main contribution in scenarios I, III is a double mixing $e^+ \to \bar{\tilde{\nu}}_2 \to \tau^+$, because the relevant mixings are extremely large. The second scenario has the smallest cross-section due to its small flavor mixing of the first generation to both the second and the third generation, although

Particle	Mass/GeV	Width/Gev	Gauge components
		ν_RI	
$\tilde{\nu}_1$	160.98	0.42	(.71, .53, -.48)
$\tilde{\nu}_2$	160.91	0.42	(.71, .48, -.53)
$\tilde{\nu}_3$	159.35	0.42	(.05, .71, .71)
		ν_RII	
$\tilde{\nu}_1$	201.67	0.93	(.99, -.12, .02)
$\tilde{\nu}_2$	195.87	0.83	(.12, .94, -.32)
$\tilde{\nu}_3$	164.32	0.43	(.02, .31, .95)
		ν_RIII	
$\tilde{\nu}_1$	160.98	0.30	(.71, -.53, .48)
$\tilde{\nu}_2$	159.72	0.28	(.71, .48, -.53)
$\tilde{\nu}_3$	128.53	0.14	(.05, .71, .71)

Table 8.7: Sneutrino properties for ν_RI,ν_RII and ν_RIII

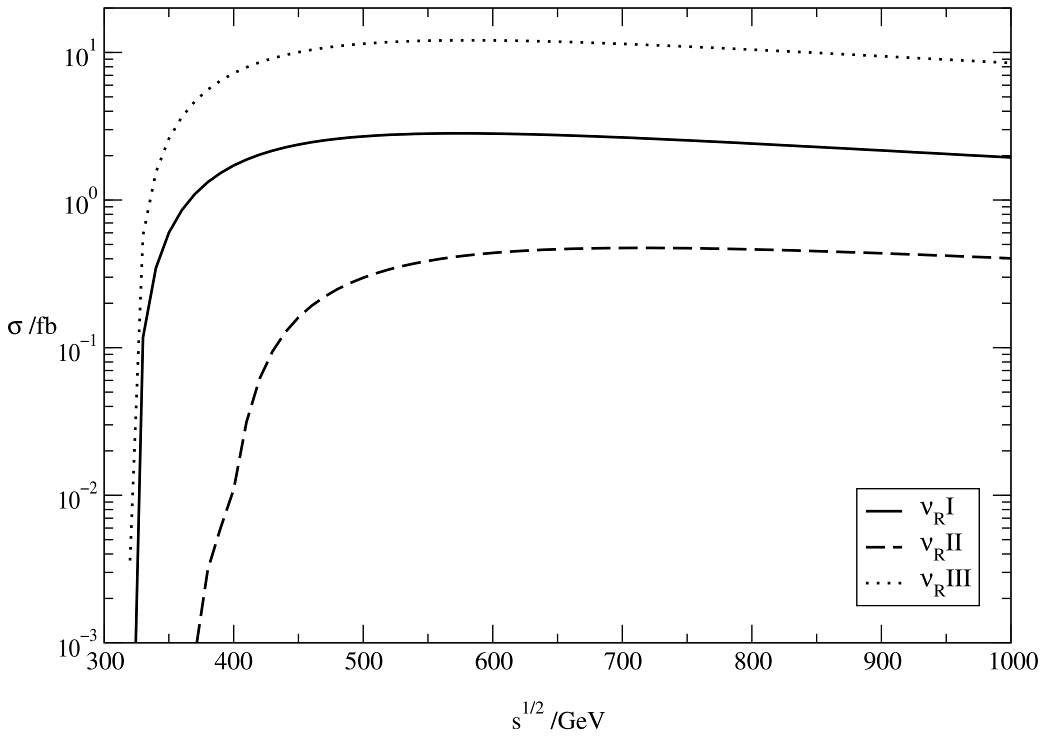

Figure 8.4: Energy dependence of the total cross section for $e^+e^- \to \tilde{\nu}_i\bar{\tilde{\nu}}_j \to e^-\tau^+\tilde{\chi}_1^+\tilde{\chi}_1^-$.

the mass differences are large. Because there are only left-handed sneutrinos, the dominant contribution comes from the $(-+)$ polarized t-channel, which is therefore about four times larger than the unpolarized cross-section. All other t-channel contributions are zero and the s-channel is energetically suppressed. The maximal values that can be reached with the estimated maximum NLC polarizations of $|P_-| = 0.8, |P_+| = 0.6$ [22], are

	ν_RI	ν_RII	ν_RIII
σ_{max}/fb	7.58	0.85	32.34

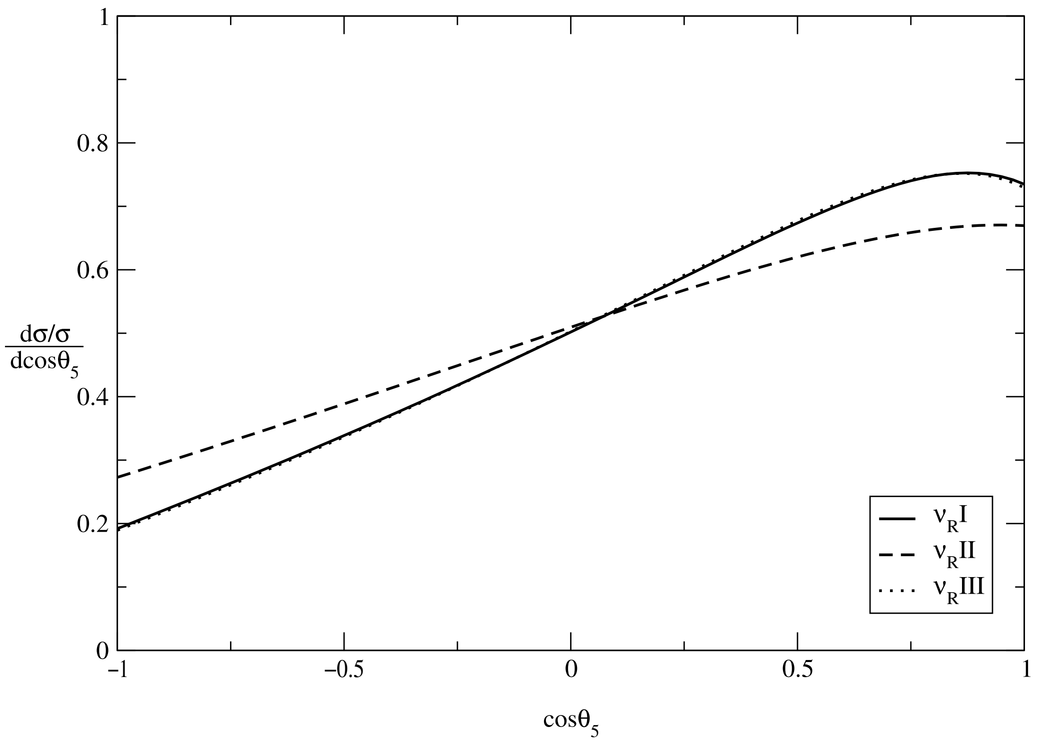

Figure 8.5: Angular distribution of the electron for $e^+e^- \rightarrow \tilde{\nu}_i\bar{\tilde{\nu}}_j \rightarrow e^-\tau^+\tilde{\chi}_1^+\tilde{\chi}_1^-$ at $\sqrt{s} = 500$ GeV, unpolarized

The angular distributions of the final leptons are influenced by two effects. First, by the angular distribution of the slepton production process, and second, by the boosted decay distributions of the leptons. In the dominant $(-+)$ case, the production distribution has a p-wave (total angular momentum $= 1$) t-channel dependence, so it vanishes at the beam pipe, $\cos\theta_3 = \pm 1$ (this can be easily read off the production amplitudes in section 6.3). This behaviour is smeared out by the decay distribution, effectively flattening the curve. This can be observed in Figures 8.5, 8.6, which show the normalized angular distribution of the final electron at $\sqrt{s} = 500, 800$ GeV, respectively (unpolarized). We see that the distribution is rather insensitive to the strength of the lepton flavor violation. Scenarios I and III are indistinguishable due to their practically identical mass spectrum of the first two mass eigenstates. The third mass eigenstate does not contribute due to the negligible flavor violation (see Table 8.7). The second scenario differs from the other scenarios through the larger sneutrino masses, which therefore have a smaller momentum. Hence, the decay distribution is less pronounced in the forward boost direction, flattening the curve even more.

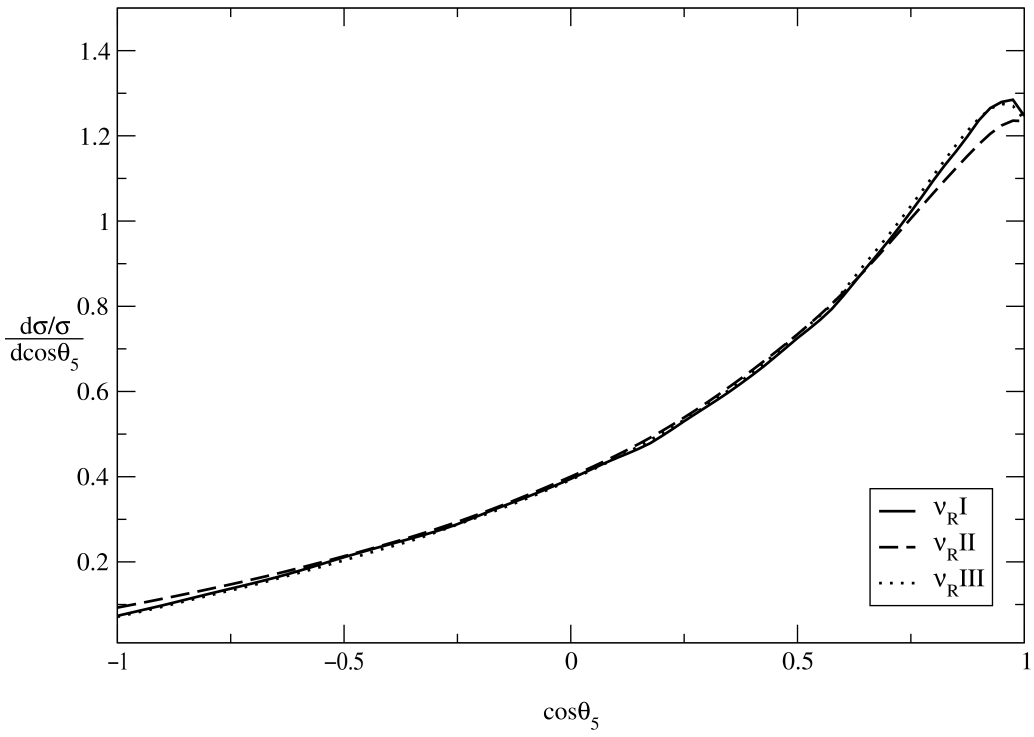

Figure 8.6: Angular distribution of the electron for $e^+e^- \to \tilde{\nu}_i\bar{\tilde{\nu}}_j \to e^-\tau^+\tilde{\chi}_1^+\tilde{\chi}_1^-$ at $\sqrt{s} = 800$ GeV, unpolarized

For $\sqrt{s} = 800$ GeV the distribution is more pronounced in the forward direction due to the t-channel dependence and the higher velocities of the decaying sneutrinos, leading to a pronounced peak in the forward boost direction. The difference between scenario II and the other two scenarios is reduced because mass effects get smaller for higher energies. In Figure 8.7 we also show the normalized angular distribution of the final tau at $\sqrt{s} = 500, 800$ GeV, respectively (unpolarized). The distribution is practically the same as the electron distribution, it is merely peaked in the backward direction. This is because both the propagating sneutrinos have the same momentum and almost the same velocity because the mass differences are small compared to the beam energy.

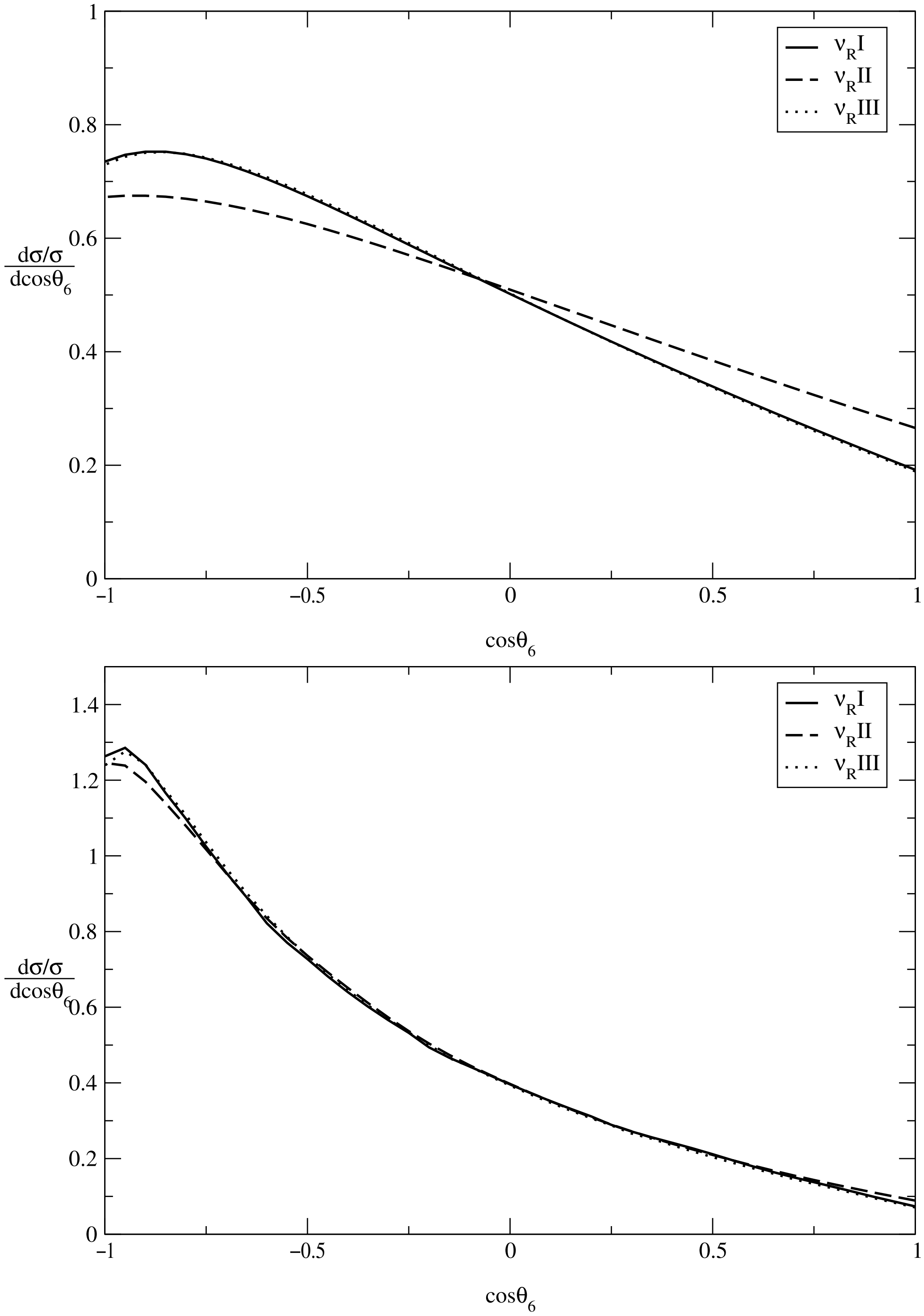

Figure 8.7: Angular distribution of the tau for $e^+e^- \to \tilde{\nu}_i\bar{\tilde{\nu}}_j \to e^-\tau^+\tilde{\chi}_1^+\tilde{\chi}_1^-$ at $\sqrt{s} = 500, 800$ GeV, unpolarized

8.5.2 Charged sleptons

We now apply the three scenarios to the right-handed neutrino models for the charged slepton case. Unfortunately the SU(5)ν_R corrections are so large for the second scenario, that one of the sleptons aquires such a small mass that it contradicts known limits [5] and would render our calculations inconsistent because the lightest neutralino is no longer the LSP. The case is even worse in the third scenario where the $\tilde{\tau}_R$ (mass)^2 entry becomes negative, implying that a charged slepton aquires a vacuum expectation value, breaking electromagnetism. The slepton masses, width and gauge components $(\tilde{e}_L, \tilde{\mu}_L, \tilde{\tau}_L, \tilde{e}_R, \tilde{\mu}_R, \tilde{\tau}_R)$ for the four remaining models ν_RI, ν_RII, ν_RIII, SU(5)ν_RI are given in Table 8.8. Again, the mass eigenstates are not labelled according to their mass values but according to their resemblance to the gauge eigenstates i.e. $\tilde{l}_1 \approx \tilde{e}_L, \tilde{l}_2 \approx \tilde{\mu}_L, .., \tilde{l}_6 \approx \tilde{\tau}_R$.

Particle	Mass/GeV	Width/GeV	Gauge components
	ν_RI		
$\tilde{l}_1^-$	176.12	0.51	(.99, -.04, -.06, .00, .00, .01)
$\tilde{l}_2^-$	174.96	0.51	(.07, .86, .50, .00, .00, -.07)
$\tilde{l}_3^-$	176.60	0.52	(.03, -.51, .85, .00, .00, -.12)
$\tilde{l}_4^-$	132.93	0.31	(.00, .00, .00, 1.0, .00, .00)
$\tilde{l}_5^-$	132.93	0.31	(.00, .00, .00, .00, 1.0, .00)
$\tilde{l}_6^-$	130.95	0.30	(.00, .01, .14, .00, .00, .99)
	ν_RII		
$\tilde{l}_1^-$	216.92	1.00	(.99, -.15, .06, .00, .00, -.02)
$\tilde{l}_2^-$	213.78	0.99	(.16, .82, -.51, .00, .00, .22)
$\tilde{l}_3^-$	198.32	0.75	(.04, .56, .73, .00, .00, -.40)
$\tilde{l}_4^-$	184.29	0.62	(.00, .00, .00, 1.0, .00, .00)
$\tilde{l}_5^-$	184.29	0.62	(.00, .00, .00, .00, 1.0, .00)
$\tilde{l}_6^-$	90.74	0.04	(.00, .04, .46, .00, .00, .89)
	ν_RIII		
$\tilde{l}_1^-$	175.44	0.39	(.96, .14, -.24, .00, .00, .07)
$\tilde{l}_2^-$	150.75	0.10	(.06, .74, .56, .00, .00, -.38)
$\tilde{l}_3^-$	177.26	0.30	(.28, -.64, .69, .00, .00, -.19)
$\tilde{l}_4^-$	132.93	0.30	(.00, .00, .00, 1.0, .00, .00)
$\tilde{l}_5^-$	132.93	0.30	(.00, .00, .00, .00, 1.0, .00)
$\tilde{l}_6^-$	124.62	0.23	(.01, .17, .39, .00, .00, .91)
	SU(5)ν_RI		
$\tilde{l}_1^-$	176.08	0.51	(.99, .05, -.15, .00, .00, .02)
$\tilde{l}_2^-$	173.59	0.47	(.06, .77, .63, .00, .00, -.06)
$\tilde{l}_3^-$	176.39	0.50	(.15, -.63, .76, .00, .00, -.07)
$\tilde{l}_4^-$	132.93	0.31	(.00, .00, .00, .99, .14, .00)
$\tilde{l}_5^-$	132.92	0.31	(.00, .00, .01, -.14, .99, .04)
$\tilde{l}_6^-$	105.73	0.14	(.00, .00, .10, .01, -.04, .99)

Table 8.8: Slepton properties for the models ν_RI, ν_RII, ν_RIII, SU(5)ν_RI

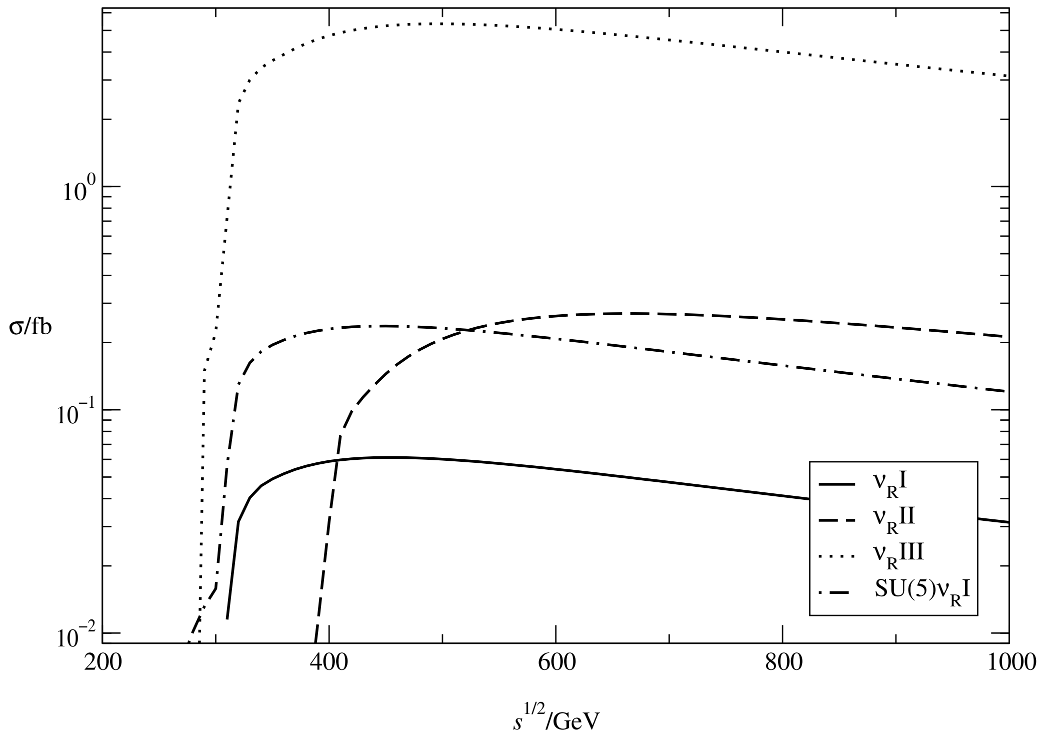

Figure 8.8: Energy dependence of the total cross section for $e^+e^- \to \tilde{l}_i^- \tilde{l}_j^+ \to e^-\tau^+\tilde{\chi}_1^0\tilde{\chi}_1^0$ (unpolarized)

In Figure 8.8 we show the total cross-section (unpolarized) as a function of the beam energy. Again, model ν_RIII yields the largest cross section because of the large $\tilde{e}_L\tilde{\tau}_L$-mixing. Model ν_RI yields the smallest cross sections, now because of both small off-diagonal mixing matrix elements and almost degenerate masses, $m_1 \approx m_3$ (see Table 8.8). This is the reason why the cross-section is vanishingly small compared to the sneutrino case. For the models ν_RII, ν_RIII, the sneutrino cross-sections are of the same order of magnitude as the charged slepton cross-sections, but slightly larger due to the stronger chargino couplings. The mixing in model ν_RII is almost the same as in ν_RI, but due to the bigger mass differences the cross section is not suppressed. SU(5)ν_RI yields a cross-section that is about four times larger than that of ν_RI, again because of larger mixing in the left-handed sector and a larger mass difference. The LFV induced to the right-handed sector is vanishingly small and does not seem to have a large direct impact.

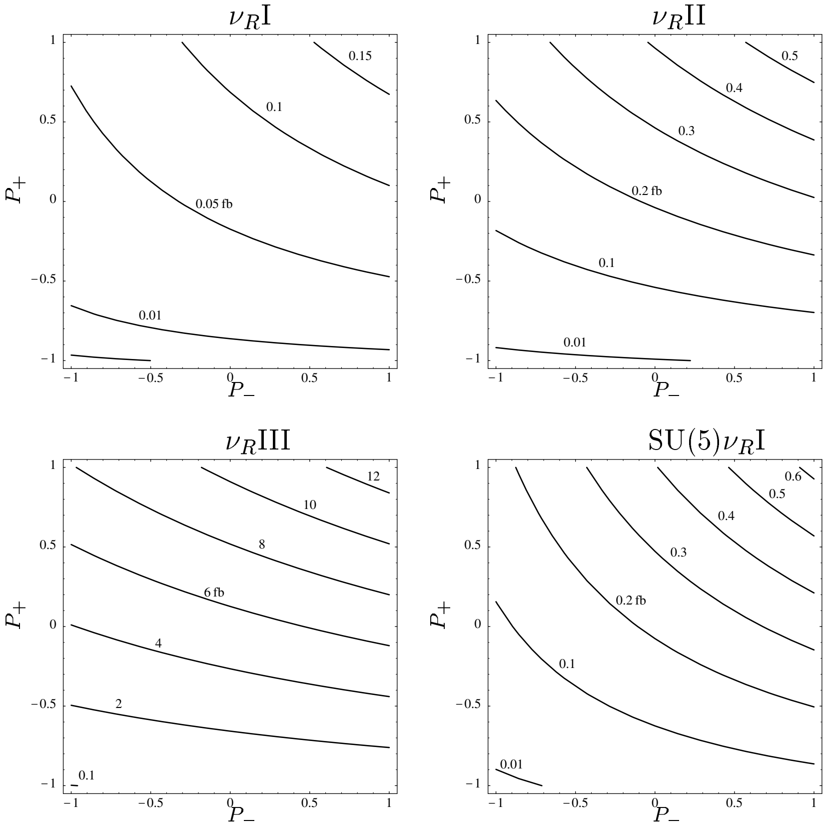

Figure 8.9: Polarization dependence of the total cross section for $e^+e^- \rightarrow \tilde{l}_i^- \tilde{l}_j^+ \rightarrow e^-\tau^+\tilde{\chi}_1^0\tilde{\chi}_1^0$ at $\sqrt{s} = 500$ GeV

In the charged slepton case, the polarization dependence has a richer structure than for the sneutrinos because both left- and right-handed charged sleptons can propagate. Figure 8.9 shows the total cross-section as a function of the electron (P_-) and positron (P_+) polarizations at $\sqrt{s} = 500$ GeV. Here, the maximum is reached for the (++) polarization. This is because the slepton flavor violation is induced to the left-handed sector, thus the positron, which is affected by the violation, must be right-handed. The electron, which is approximately not affected by lepton flavor violation, couples stronger with its right-handed part because the exchange of the lightest neutralino, which is bino-like, is the dominant contribution among the t-channel graphs. As can be read off the vertices in section 4.2, the right-handed coupling is stronger than the left-handed for a bino. Again, the s-channel contribution is vanishingly small.

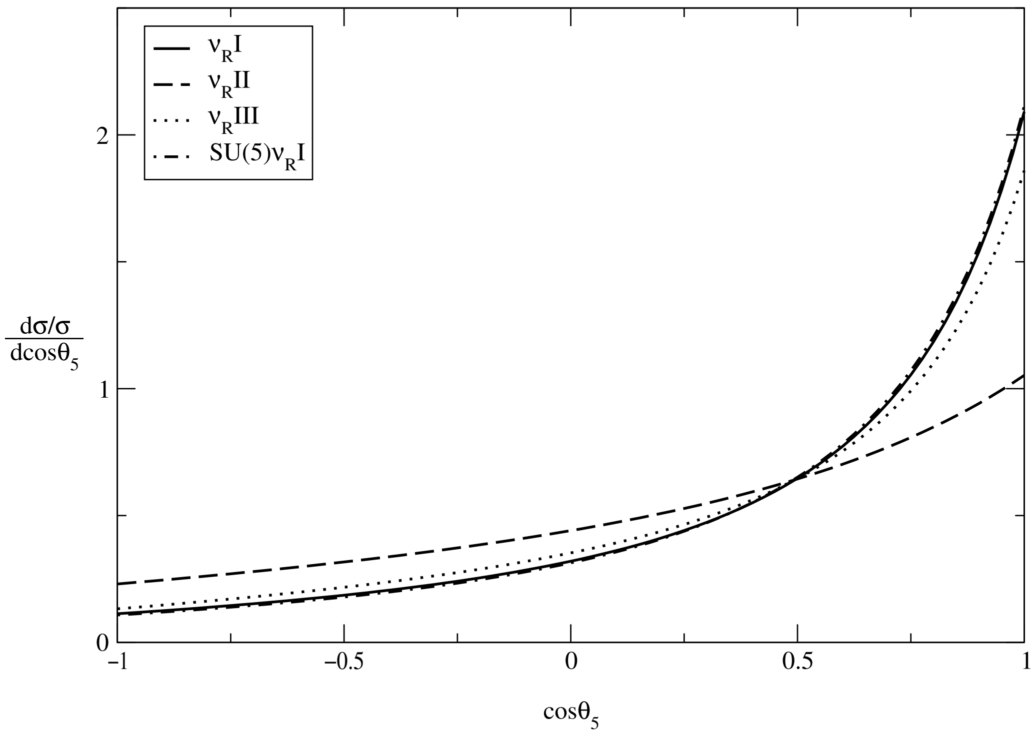

Figure 8.10: Angular distribution of the electron for $e^+e^- \rightarrow \tilde{l}_i^- \tilde{l}_j^+ \rightarrow e^-\tau^+\tilde{\chi}_1^0\tilde{\chi}_1^0$ at $\sqrt{s} = 500$ GeV, (unpolarized)

The maximal values that can be reached with the estimated maximum NLC polarizations of $|P_-| = 0.8, |P_+| = 0.6$, are

	ν_RI	ν_RII	ν_RIII	SU(5)ν_RI
σ_{max}/fb	0.13	0.43	10.08	0.47

Unlike the sneutrino case with a dominant $(-+)$ p-wave t-channel contribution, the dominant contribution in the slepton case is a s-wave. This means that we have a pure t-channel angular dependence, peaking in the forward direction. In Figures 8.10, 8.11 we show the normalized angular distribution of the final electron at $\sqrt{s} = 500, 800$ GeV, respectively (unpolarized). The models ν_RI, ν_RIII, SU(5)ν_RI are almost undistinguishable, because of the similar mass spectrum of the intermediate sleptons, thus leading to equal decay distributions. Again, ν_RII differs from this due to the higher slepton masses.

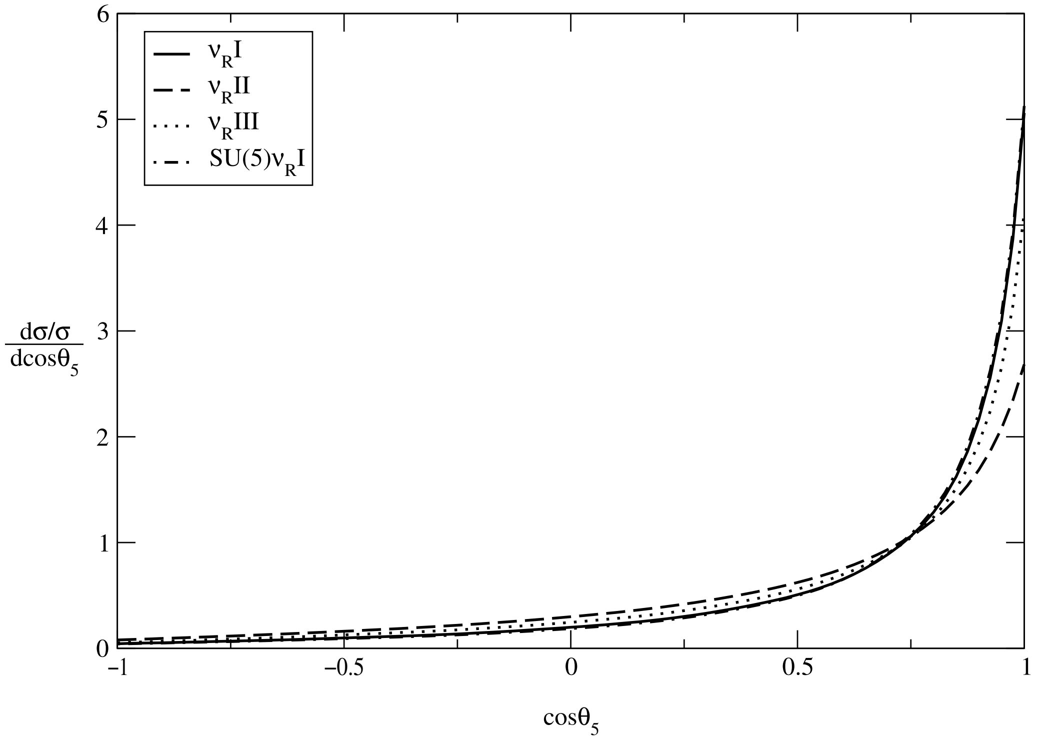

Figure 8.11: Angular distribution of the electron for $e^+e^- \to \tilde{l}_i^- \tilde{l}_j^+ \to e^-\tau^+\tilde{\chi}_1^0\tilde{\chi}_1^0$ at $\sqrt{s} = 800$ GeV, (unpolarized)

For higher energies, the forward peak gets sharper, and the model differences vanish even more. Unlike the sneutrino case, the distributions with respect to the final tau (Figure 8.12) are noticably flatter than those for the electron. This is because the heavier left-handed sleptons propagate in the LVF branch $e^+ \to \tilde{l}_j^+ \to \tau^+$ of the t-channel graphs, and therefore have a smaller velocity.

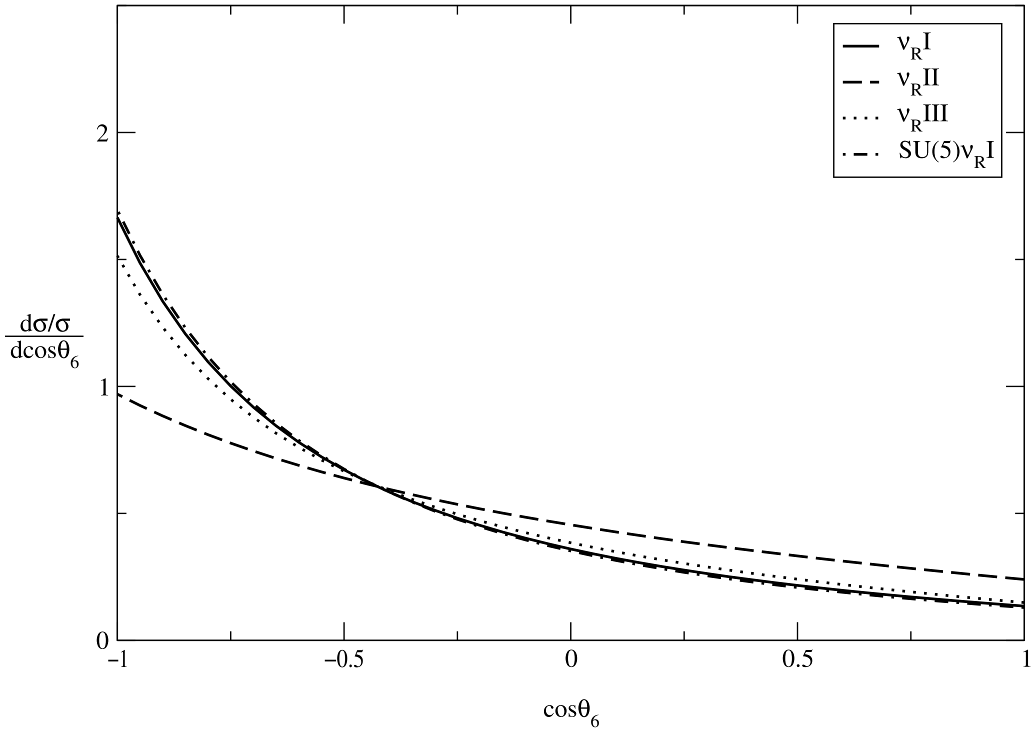

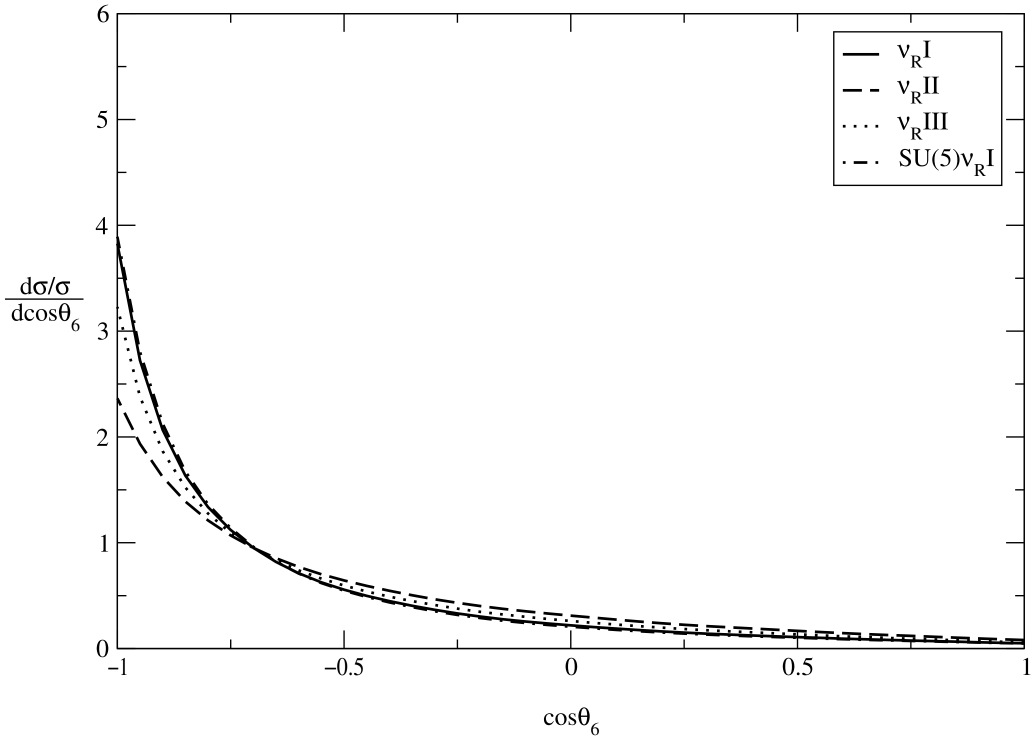

Figure 8.12: Angular distribution of the tau for $e^+e^- \to \tilde{l}_i^- \tilde{l}_j^+ \to e^-\tau^+\tilde{\chi}_1^0\tilde{\chi}_1^0$ at $\sqrt{s} = 500, 800$ GeV, (unpolarized)

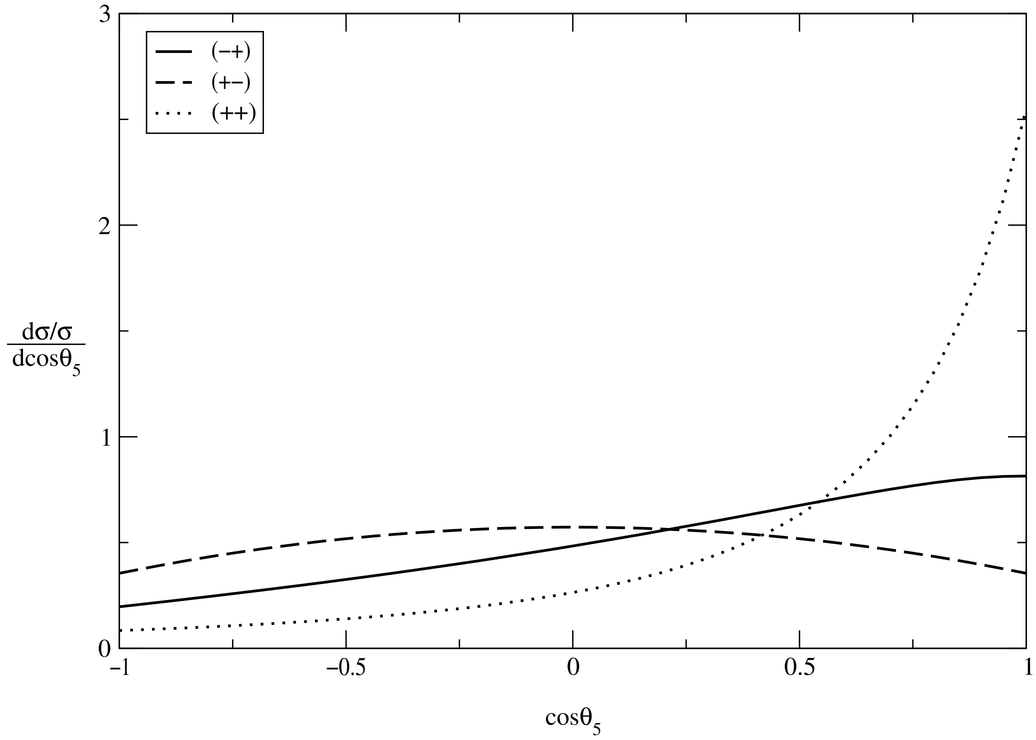

Figure 8.13: Angular distribution of the electron for $e^+e^- \rightarrow \tilde{l}_i^- \tilde{l}_j^+ \rightarrow e^-\tau^+\tilde{\chi}_1^0\tilde{\chi}_1^0$ in the model ν_RIII at $\sqrt{s} = 500$ GeV

As examples for distributions with polarized beams, we show in Figure 8.13 the normalized angular distribution of the final electron for the beam polarizations $(-+)$, $(+-)$ and $(++)$ for model ν_RIII. The integrated cross-sections are

$(-+)$	7.9 fb
$(+-)$	0.4 fb
$(++)$	13.0 fb.

$(-+)$ is primarily a p-wave, t-channel contribution. $(+-)$ is a small p-wave, s-channel contribution (here, the t-channel vanishes because the positron is left-handed $\rightarrow$ no LFV in the t-channel possible), and $(++)$ is the dominant s-wave, t-channel contribution. All other models have similar contributions. If the cross-sections are themselves large enough, one can dial through the different contributions and check their magnitude and distributions.

This way one can determine to which sector the LFV is induced. For our models this would yield the result that the lepton flavor violation occurs mainly in the left-handed sector.

Because the final neutralinos can not be detected it may be useful to examine the missing energy distribution, which is shown in Figure 8.14. The energy limits are almost equal in all models because they are determined by the masses of the outgoing lightest neutralinos which are similar in all three scenarios. The dependence is again governed by the mass spectrum of the propagating sleptons.

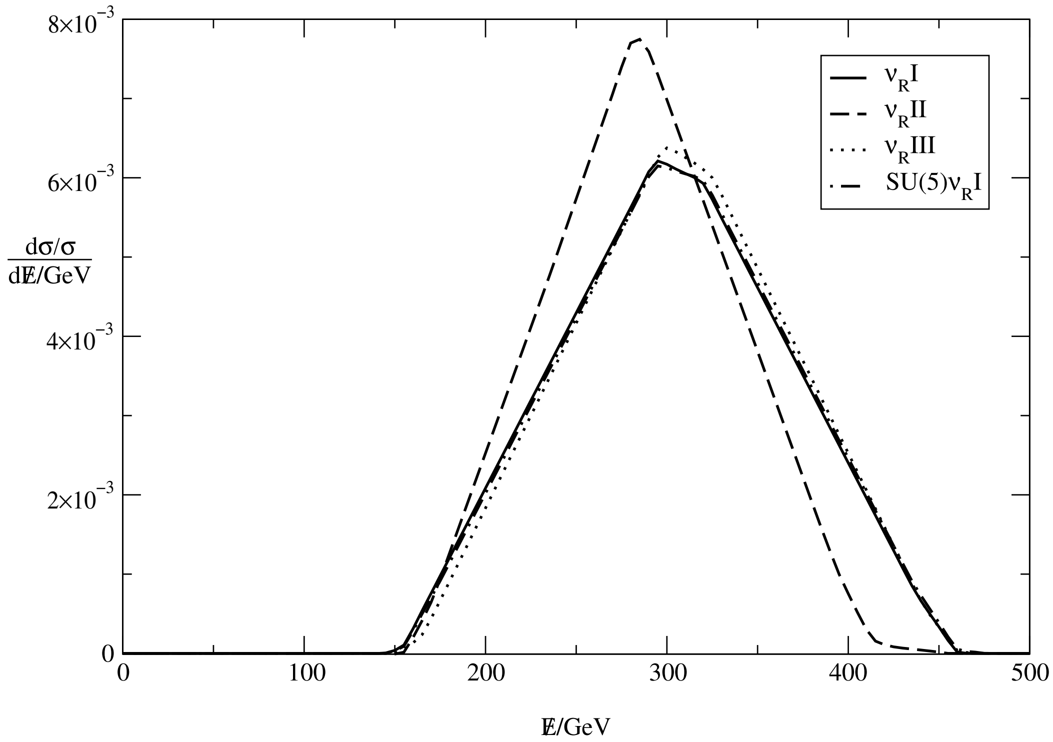

Figure 8.14: Missing energy distributions for $e^+e^- \to \tilde{l}_i^- \tilde{l}_j^+ \to e^- \tau^+ \tilde{\chi}_1^0 \tilde{\chi}_1^0$ at $\sqrt{s} = 500$ GeV, (unpolarized)

In section 9.2 we also show the transverse momentum distributions.

As a summary for both the sneutrino and charged slepton case we can say that distributions are rather unaffected by the strength of the mixing because the cross-section simply scales with $\sin^2 2\phi$ in the two-flavor mixing case (even for more than two flavors, there is one dominant mixing). The distributions are only affected by the mass spectrum of the propagating sleptons, and in the case of charged sleptons by the sector to which the flavor mixing is induced. The largest mixing for both sneutrinos and charged sleptons occurs for scenario III that is also responsible for a light stop, a consequence of the large negative trilinear coupling A_0.

Chapter 9

Background processes

9.1 Sneutrino production

In this case the background is quite complicated because the signal is also! Up to now we assumed that the charginos are in the observable final state, but looking at the Tables 8.3, 8.4 and 8.5 one can see that charginos are not stable and decay to scenario dependent final states. The possible signatures for each model together with their relative branching ratios and the estimated total cross-sections are given below. The possible Standard Model background

$e^+e^- \to$	$\sum \mathrm{Br}^2$	σ/fb (500 GeV)	σ/fb (800 GeV)
ν_RI			
τ^+e^-, 4 jets+ $\not{E}$	0.3	0.8	0.7
τ^+e^-l, 2 jets+ $\not{E}$	0.5	1.3	1.2
$\tau^+e^-l^+l^-+\not{E}$	0.2	0.5	0.5
ν_RII			
$\tau^+e^-\tau^+\tau^-+\not{E}$	1.0	0.3	0.5
ν_RIII			
τ^+e^-, 4 jets+ $\not{E}$	0.4	4.0	3.7
$\tau^+e^-\tau$, 2 jets+ $\not{E}$	0.5	5.3	4.8
$\tau^+e^-\tau^+\tau^-+\not{E}$	0.1	1.7	1.6

consists mainly of W^+W^-Z and $W^+W^-W^+W^-$ production with subsequent decays of the gauge bosons into hadronic and leptonic final states, imitating our signal. A treatment of these background processes is beyond the scope of this work.

9.2 Charged slepton production

In all our models, the lightest neutralino is also the lightest supersymmetric particle so it cannot decay due to R-parity conservation and can not be detected. Thus, the signature of our process is

$$e^+e^- \to \tau^+e^- + \not{E}, \tag{9.1}$$

where we assumed the τ to be an observable final particle. The most important Standard Model background with this signature is given by the process

$$e^+e^- \to \tau^+e^-\bar{\nu}_e\nu_\tau. \tag{9.2}$$

The possible lowest order Feynman graphs are shown on page 82. We use CompHEP to calculate the cross-section for this process. Because of the photon exchange in the graphs 2, 4, 6 we must exclude the phase space region for small electron scattering to avoid divergences. We do this by applying an angular cutoff $\cos\theta_5 < 0.98$, as well as $-0.98 < \cos\theta_5$ and thus exclude the beam pipe for the observation of the electron. Such a cut can be applied to some of the distributions of our signal process. In Figure 9.1 we show the angular distribution and in Figure 9.2 we show the transverse momentum distribution of both the signals and the Standard Model background (as error bars). In Table 9.1 we present the integrated cross sections for the signals and the background.

$\sqrt{s}$ at	ν_RI	ν_RII	ν_RIII	SU(5)ν_RI	Background
500 GeV	0.06	0.20	5.15	0.20	57.5
800 GeV	0.04	0.24	3.70	0.13	55.6

Table 9.1: Cross sections for our process in the various models and the Standard model background with the angular cut $|\cos\theta_5| < 0.98$ applied. All cross sections are in fb.

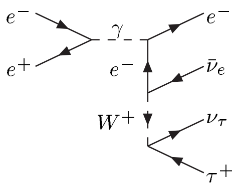

diagr.1

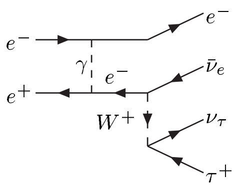

diagr.2

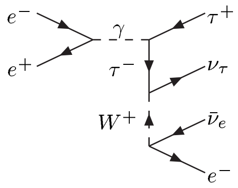

diagr.3

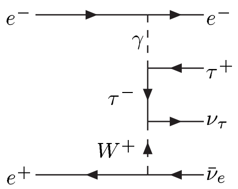

diagr.4

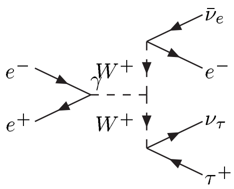

diagr.5

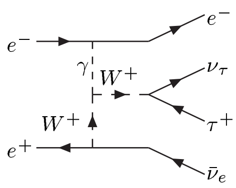

diagr.6

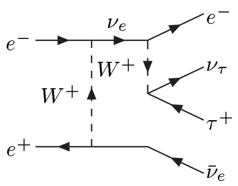

diagr.7

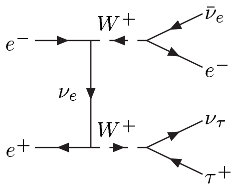

diagr.8

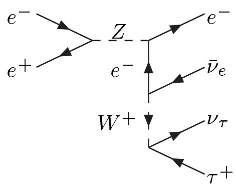

diagr.9

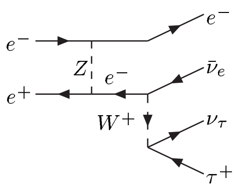

diagr.10

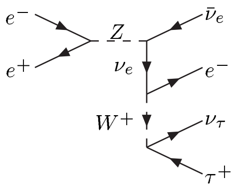

diagr.11

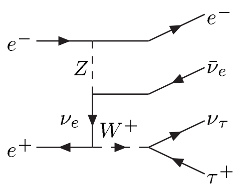

diagr.12

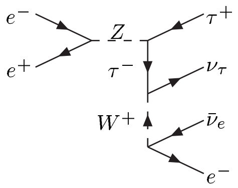

diagr.13

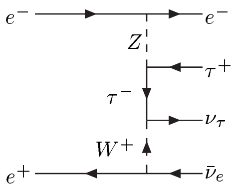

diagr.14

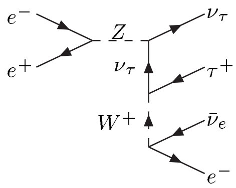

diagr.15

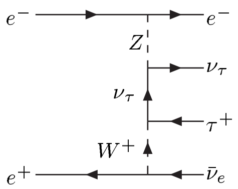

diagr.16

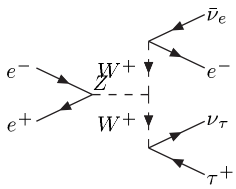

diagr.17

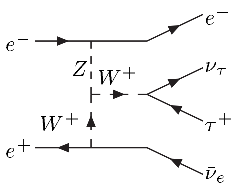

diagr.18

The angular distribution shows that we can enhance the signal by further cutting the forward direction at $\cos\theta_5 \approx 0.75 \equiv 41°$. The reason for the rather flat signal curves is, as already mentioned, the propagation of the massive sleptons in the intermediate state whose decays smear out the whole distribution.

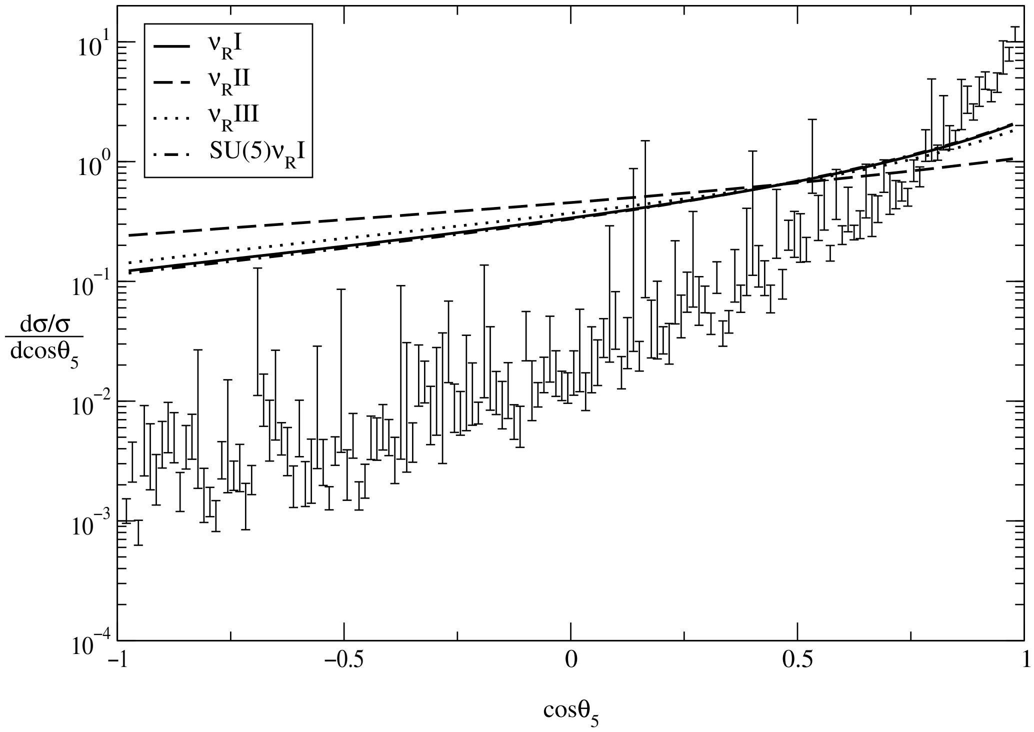

Figure 9.1: Angular distribution of the electron for $e^+e^- \to e^-\tau^+ + \not{E}$ at $\sqrt{s} = 500$, GeV (background: error bars), unpolarized

The transverse momentum distribution is not as useful as the angular distribution, regarding cuts. One can make a cut at $p_\perp < 175$ GeV, but the effect is not as large as for the angular distribution.

An example of a MSSM background is given by the lepton flavor conserving process

$$e^+e^- \to \tilde{\tau}^-_{L/R}\tilde{\tau}^+_{L/R} \to \tau^+\tau^-\tilde{\chi}^0_1\tilde{\chi}^0_1, \tag{9.3}$$

where the negative tau decays further into $e^-\bar{\nu}_e\nu_\tau$, thus imitating our signature. We can easily calculate its cross-section up to the tau decay, because it is just a special case of our general charged slepton process. The cross-section is about 50 fb in all three scenarios ($\sqrt{s} = 500$ GeV). Multiplying this with the branching ratio of the tau decay, $Br \approx 0.18$, this yields an approximate cross-section for the whole process of about 10 fb. The cross-section of the

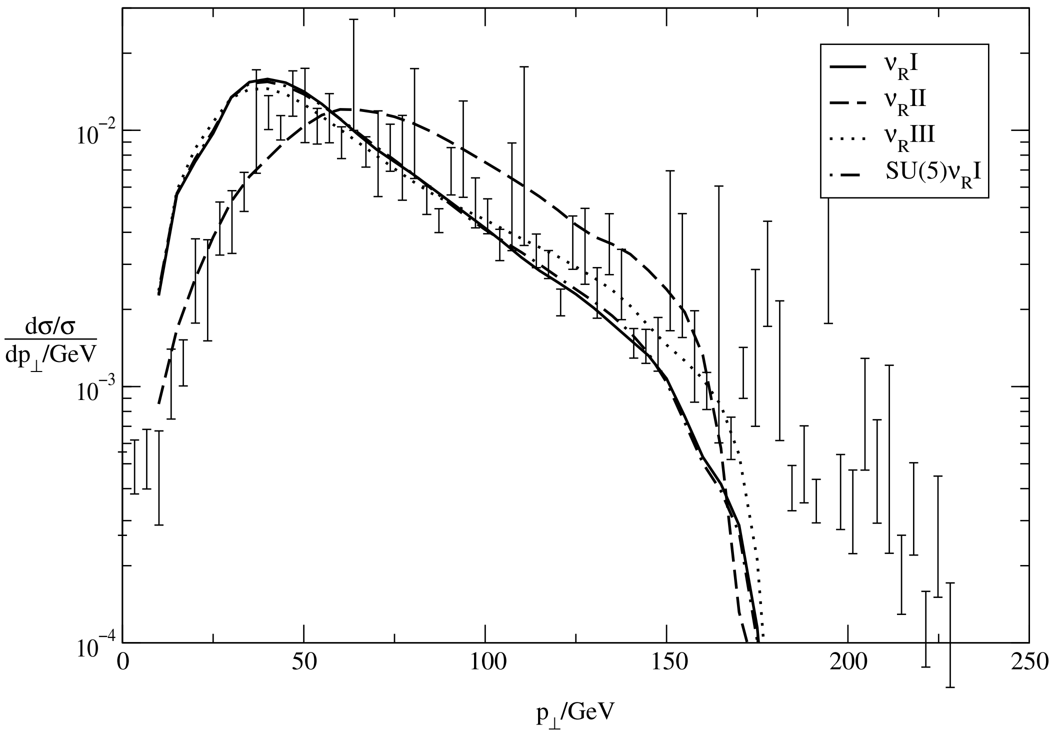

Figure 9.2: Transverse momentum distribution of the electron for $e^+e^- \to e^-\tau^+ + \not{E}$ at $\sqrt{s} = 500$ GeV, (background: error bars), unpolarized

lepton flavor conserving process is rather small because it can only occur in the s-channel. This also means that the angular distribution is quite different from the t-channel dominated signals. Another possibility to reduce the background is to shift the beam polarizations in the (++) direction favored by the signal. The s-channel of the background becomes zero for such a polarization.

Chapter 10

Summary

In this work, we have calculated two lepton flavor violating SUSY processes at an e^+e^- linear collider, namely the production of charged sleptons/sneutrinos with their subsequent decays into leptons and neutralinos/charginos.

We have introduced lepton flavor violation in two different ways. First, by manually changing the sneutrino mass matrix generating a simple two-flavor mixing model, and second, by using extensions of the MSSM that radiatively induce flavor-mixing terms in the slepton sector, namely MSSM+right-handed neutrinos and SU(5) SUSY GUT+right-handed neutrinos. In order to cope with the possibility of the proposed next linear collider to use polarized beams, we calculated the respective helicity amplitudes of the processes. This allows one to check the handedness of the produced sleptons and to determine whether the lepton flavor violation is induced to the left- and/or right-handed slepton sector.

For our numerical work, we applied our analytical results to two specific processes:

$$\begin{aligned} e^+e^- &\to \tilde{l}_i^- \tilde{l}_j^+ \to e^- \tau^+ \tilde{\chi}_1^0 \tilde{\chi}_1^0 \\ e^+e^- &\to \tilde{\nu}_i \bar{\tilde{\nu}}_j \to e^- \tau^+ \tilde{\chi}_1^+ \tilde{\chi}_1^- \end{aligned}$$

The numerical calculations were performed using three mSUGRA scenarios. The largest cross-sections (about 10 fb) for both the sneutrino and slepton case were found for the mSUGRA scenario that also generates a light stop. We studied possible background processes only very briefly. For the charged slepton production case we found that the Standard Model background is of the order of about 50 fb and could be reduced by an angular cut.

For the two-flavor LFV model for sneutrino mixing we found both analytically and numerically that the cross-section approximately scales with the strength of the flavor mixing, described by a mixing angle ϕ and is suppressed for small slepton mass differences. This can explain that the shape of the distributions we calculated for the realistic LFV models are unaffected by the strength of the flavor mixing, depending only on the mass spectrum of the sleptons. In the charged slepton case, on the other hand, the distributions do depend on to which sector (left or right) the lepton flavor violation is induced. Experimentally this can be observed by using polarized beams. Such measurements together with the study of other flavor combinations like $e - \mu$ or $\mu - \tau$ (at a muon collider) may shed light on the origins of lepton flavor violation and thus on the physics beyond the MSSM (if existing).

Acknowledgments

I am grateful to Prof. Dr. R. Rückl and Dr. Y. Shimizu for many helpful comments and discussions on this work. I am also indebted to my collaborator Andreas Redelbach for countless illuminating and inspiring conversations on the subject and for reading the final script.

Appendix A

Calculation of the narrow width propagator

Our starting point is the general "interferenced" propagator

$$A_{ik}(p^2) = \frac{1}{p^2 - m_i^2 + im_i\Gamma_i}\frac{1}{p^2 - m_k^2 - im_k\Gamma_k}. \tag{A.1}$$

We can easily write it in terms of the mean squared mass and the squared mass difference $\overline{m^2} = \frac{1}{2}(m_i^2 + m_k^2); \Delta m^2 = m_i^2 - m_k^2$:

$$A_{ik}(p^2) = \frac{1}{p^2 - \overline{m^2} - \frac{1}{2}\Delta m^2 + im_i\Gamma_i}\frac{1}{p^2 - \overline{m^2} + \frac{1}{2}\Delta m^2 - im_k\Gamma_k} \tag{A.2}$$

Using the abbreviations

$$\begin{aligned} z = p^2 - \overline{m^2}; \quad a = \frac{1}{2}\Delta m^2; \\ b_i = m_i\Gamma_i; \quad b_k = m_k\Gamma_k, \end{aligned}$$

we arrive at

$$\begin{aligned} & \frac{1}{(z-a+ib_i)(z+a-ib_k)} \\ = \quad & \frac{1}{2a - i(b_i+b_k)}\frac{(z+a-ib_k)-(z-a+ib_i)}{(z-a+ib_i)(z+a-ib_k)} \\ = \quad & \frac{1}{2a - i(b_i+b_k)}\left(\frac{1}{z-a+ib_i} - \frac{1}{z+a-ib_k}\right) \\ = \quad & \frac{1}{1+i\frac{2a}{b_i+b_k}}\frac{1}{b_i+b_k}\left(\frac{i(z-a)+b_i}{(z-a)^2+b_i^2} + \frac{-i(z+a)+b_k}{(z-a)^2+b_k^2}\right). \end{aligned}$$

Now we have the expression in the right form to use the following representation of the Dirac function [3]

$$\delta(t) = \lim_{\epsilon \to 0} \frac{\epsilon}{\pi(t^2 + \epsilon^2)}; \quad \epsilon > 0 \tag{A.3}$$

In our case, we have $b_i, b_k \to 0$ and by taking only the singular part, we get

$$\frac{1}{1 + i\frac{2a}{b_i + b_k}} \frac{1}{b_i + b_k} (\pi\delta(z - a) + \pi\delta(z + a)). \tag{A.4}$$

Resubstituting the physical variables, we arrive at the narrow-width approximated propagator

$$A_{ik}(p^2) = \frac{1}{1 + i\frac{\Delta m^2}{2\overline{m\Gamma}}} \frac{\pi}{2\overline{m\Gamma}} \left(\delta(p^2 - m_i^2) + \delta(p^2 - m_k^2)\right). \tag{A.5}$$

Appendix B

Boosting a massless particle

An active boost of the four momentum $p^* = (E^*, \vec{p}^*) \rightarrow p' = (E', \vec{p}')$ with the velocity $\vec{v}$ (in units of c) is given by ($\gamma = (1 - v^2)^{-1/2}$) [4]:

$$\begin{aligned} E' &= \gamma \left(E^* + \vec{v} \cdot \vec{p}^* \right) \\ \vec{p}' &= \vec{p}^* + \vec{v} \left(\gamma E^* + \frac{\gamma - 1}{v^2} \vec{v} \cdot \vec{p}^* \right) \end{aligned} \tag{B.1}$$

In our case, it is sufficient to consider a boost in the z-direction $\vec{v} = (0, 0, v)$ with the spatial momentum fixed in the x-z-plane. Now, the boost reads:

$$\begin{aligned} E' &= \gamma E^* + \gamma v p_z^* \\ p_z' &= \gamma v E^* + \gamma p_z^* \\ p_x' &= p_x^* \end{aligned} \tag{B.2}$$

In the limit of a massless particle, $E = |\vec{p}\,|$ and using

$$p_z = |\vec{p}\,| \cos\theta, \quad p_x = |\vec{p}\,| \sin\theta \text{ (in both frames)}, \tag{B.3}$$

we get

$$\begin{aligned} E' = |\vec{p}\,'| &= \gamma (E^* + v |\vec{p}^*| \cos\theta^*) \\ &= \gamma E^* (1 + v \cos\theta^*). \end{aligned} \tag{B.4}$$

To obtain E^* in terms of the primed variables we just have to make the reverse transformation, thus $E^* \leftrightarrow E', \theta^* \leftrightarrow \theta', v \rightarrow -v$:

$$E^* = \gamma E' (1 - v \cos\theta') \tag{B.5}$$

Analogously we obtain a relation between the polar angles alone,

$$\begin{aligned}
|\vec{p}'|\cos\theta' &= \gamma|\vec{p}^*|(v+\cos\theta^*) \\
&= |\vec{p}^*|\gamma(\cos\theta^*+v) \\
\Rightarrow \qquad & |\vec{p}^*|\gamma(1+v\cos\theta^*)\cos\theta' = |\vec{p}^*|\gamma(\cos\theta^*+v) \\
\Rightarrow \qquad & \cos\theta' = \frac{\cos\theta^*+v}{1+v\cos\theta^*}. \qquad \text{(B.6)}
\end{aligned}$$

Again, the reversed relation is obtained by $\theta' \leftrightarrow \theta^*$ and $v \to -v$:

$$\cos\theta^* = \frac{\cos\theta' - v}{1 - v\cos\theta'} \qquad \text{(B.7)}$$

Appendix C

Mathematical results

C.1 Spherical trigonometry

In our discussion of the decays we have to deal with three different directions:

1. The beam axis formed by the positive z-axis and defining the beam-pipe-frame (azimuths are defined with respect to the upper x-z-plane).

2. The direction of the decaying slepton given in the beam-pipe frame by (θ_3, ϕ_3) and itself defining the decay-pipe frame (primed variables), with the azimuth ϕ' defined with respect to upper half-plane formed by the beam- and decay-axes.

3. The direction of the final lepton. In the beam-pipe-frame: (θ_5, ϕ_5). In the decay-pipe-frame: (θ'_5, ϕ'_5)

Using spherical trigonometry [3], we can express (θ'_5, ϕ'_5) in terms of the actually measurable beam-pipe-angles (θ_5, ϕ_5):

$$\cos\theta'_5 = \cos\theta_5\cos\theta_3 + \sin\theta_5\sin\theta_3\cos(\phi_5 - \phi_3) \tag{C.1}$$

$$\sin\phi'_5 = \frac{\sin\theta_5}{\sin\theta'_5(\theta_5, \phi_5)}\sin(\phi_5 - \phi_3) \tag{C.2}$$

C.2 Integrals

Azimuthal angle integral [3], Mathematica

$$\int_0^{2\pi} \frac{d\phi}{(a - b\cos(\phi_0 - \phi))^2} = \frac{2\pi a}{(a-b)^{3/2}(a+b)^{3/2}} \tag{C.3}$$

Delta function

$$\int_a^b \delta(f(x))g(x)dx = \sum_i \frac{g(x_i)}{|f'(x_i)|}, \tag{C.4}$$

where x_i are first order zeros of $f(x)$ within (a, b): $f(x_i) = 0,\ a < x_i < b$

Appendix D

Use of CompHEP

For the background calculations, some decay width and to verify some of our numerical calculations, we use the software package CompHEP (version 33.22) [23], either with "Standard Model" or "MSSM". The relevant CompHEP-parameters are

CompHEP	Parameter
EE	EM coupling constant α_{EM}
SW	$\sin\theta_W$
MZ	Z-mass m_Z
Mt	τ-lepton mass m_τ
Mtop	top-quark mass m_t
hx	SUSY Higgs mix. term μ
tb	Higgs VEV's ratio $\tan\beta$
MG1	U(1) Gaugino mass M_1
MG2	SU(2) Gaugino mass M_2
Ml1,Ml2,Ml3	Left slepton SSB masses $m_{\tilde{e}_L}, m_{\tilde{\mu}_L}, m_{\tilde{\tau}_L}$
Mr1,Mr2,Mr3	Right slepton SSB masses $m_{\tilde{e}_R}, m_{\tilde{\mu}_R}, m_{\tilde{\tau}_R}$
ls3	τ trilinear SSB cplg. $A_\tau \frac{m_\tau}{v\cos\beta}$
MSne	e-sneutrino mass $m_{\tilde{\nu}_e}$
MSnmu	μ-sneutrino mass $m_{\tilde{\nu}_\mu}$
MSe1,MSe2	Left,Right selectron masses $m_{\tilde{e}_L}, m_{\tilde{e}_R}$
MSmu1,MSmu2	Left,Right smuon masses $m_{\tilde{\mu}_L}, m_{\tilde{\mu}_R}$

Bibliography

[1] Quang Ho-Kim, Pham Xuan Yem, *Elementary Particles and their interactions*. Springer Verlag Berlin, Heidelberg 1998.

[2] David Griffiths, *Introduction to Elementary Particles*. John Wiley & Sons, Inc., New York 1987.

[3] E. Zeidler (publ.), *Teubner-Taschenbuch der Mathematik*. B.G. Teubner Stuttgart, Leipzig 1996.

[4] Hubert Goenner, *Einführung in die spezielle und allgemeine Relativitätstheorie* . Spektrum Akademischer Verlag, 1996.

[5] DELPHI collaboration, CERN-EP/2000-088.

[6] K. Kolodziej, M. Zralek, Phys. Rev. **D 43** (1991) 3619

[7] E. Kh. Akhmedov, hep-ph/0001264

[8] N. Arkani-Hamed, J. L. Feng, L. J. Hall, Hsian-Chia Cheng, Nucl. Phys. **B 505** (1997)

[9] Howard E. Haber, Nucl. Phys. **B** Proc. Suppl.: 62 (1998)

[10] Yuval Grossman, Howard E. Haber, Phys. Rev. Lett.: 78 (1997) 3438

[11] Y. Shimizu, Unpublished note, 2000

[12] Stephen P. Martin, hep-ph/9709356

[13] J. Hisano, M. M. Nojiri, Y. Shimizu, M. Tanaka, Phys. Rev. **D 60** (1999) 5508

[14] John F. Gunion, Howard E. Haber, Nucl. Phys. **B 272** (1986) 1

[15] Gudrid Mortgaat-Pick, *Doktorarbeit*, Universität Würzburg (1999)

[16] Gudrid Mortgaat-Pick, *Diplomarbeit*, Universität Würzburg (1996)

[17] S. Ambrosanio, G. A. Blair, P. M. Zerwas, http://wwwhephy.oeaw.ac.at/susy/lcws.html (1998)

[18] S. Ambrosanio, G. A. Blair, P. M. Zerwas, http://wwwhephy.oeaw.ac.at/susy/lcws.html (1998)

[19] S. Ambrosanio, G. A. Blair, P. M. Zerwas, http://wwwhephy.oeaw.ac.at/susy/lcws.html (1998)

[20] H. E. Haber, G.L. Kane, Phys. Rep. **117** (1998) 75

[21] H. Pilkuhn, *The Interactions of Hadrons*, North-Holland Publishing Company, Amsterdam 1967

[22] http://wwwhephy.oeaw.ac.at/susy/lcws.html

[23] A. Pukhov et. al, hep-ph/9908288, 1999 (Version 33)

[24] John Ellis, hep-ph/0008334

Erklärung

Hiermit versichere ich, daß ich die vorliegende Arbeit selbständig verfaßt und keine anderen als die angegebenen Hilfsmittel verwendet habe.

Würzburg, 2. November 2000

Frank Deppisch